FRICTION MECHANISMS IN HYDRAULIC CONVEYING AT HIGH SOLIDS CONCENTRATION

by

Nigel Pearson Brown, B.Sc(Eng) ACGI

A thesis submitted for the degree of Doctor of Philosophy of the University of London and for the Diploma of Membership of the Imperial College.

Chemical Engineering
and
Chemical Technology

March, 1980

ABSTRACT

Experimental results obtained from the horizontal and vertical rising flow of high solids concentration sand-water mixtures in a 25.4 mm (1.0 in.) pipeline are presented. Three closely graded sands were studied at *in situ* concentrations slightly below the freely settled value. The frictional hydraulic losses under pipeline operating conditions are around 0.75 m water/m pipeline at grain sizes of approximately 700 μm. The losses are approximately half for vertical rising flow at the same velocity. To obtain a better understanding of the frictional mechanisms involved the flow of the two phase systems are interpreted using mathematical models.

The horizontal results are analysed using a two-layer approach. This assumes a gravity bed of solids moving *en bloc* along the bottom of the pipe, and a clear water-way above. This assumption has been highly satisfactory for low velocities up to about 1.5 m/s. At high velocities it is shown that particle-particle interaction accounts for the non-Newtonian nature of the flow.

Vertical rising flow has been analysed with an annular model. This model postulates the use of a Magnus type force driving the particles toward the pipe axis and a dispersive force providing an equilibrium component. These forces give rise to a varying concentration gradient across the flow field in the vicinity of the pipe wall. It has also been shown that this analysis reconciles the mixture density correction to the clear fluid losses previously used to estimate frictional energy loss for such mixtures.

The development of these models to describe the flow conditions leads to more confident scale-up of small scale results.

ACKNOWLEDGEMENTS

I sincerely wish to thank Prof. Cliff Shook, Dr. Ken Wilson and Dr. Michael Streat for their assistance and guidance. The unfailing help of Mr. Brian Bennett has been gratefully appreciated, without his practical and academic expertise much of this work would have been formidable. My thanks are also due to all the academic staff in the Department of Chemical Engineering who were always willing to give helpful advice.

I should also like to thank Mr. Dick Wood for his assistance with the electronics, Mr. Terry Stephenson and his staff in the engineering workshop and Mr. Colin Smith and Mr. Ken Grose in the glass workshop.

Thanks are also due to Ms. Caroline Pether and Ms. Peggy Browett and their predecessors in the Egerton Hinchley Library for bibliographical assistance.

The financial support of the Science Research Council is gratefully acknowledged.

CONTENTS

ABSTRACT

ACKNOWLEDGEMENTS

CONTENTS

LIST OF FIGURES

LIST OF TABLES

1. HYDRAULIC CONVEYING - an Introduction 1

2. EXPERIMENTAL WORK

2.1 Description of pilot plant 4

2.2 Measurements 11

2.2.1 Frictional pressure gradient 12

2.2.1.1 Introduction 12

2.2.1.2 Calibration procedure 14

2.2.1.3 Results 14

2.2.2 In situ solids concentration 15

2.2.2.1 Introduction 15

2.2.2.2 Theory of measurement 15

2.2.2.3 Calibration procedure 17

2.2.2.4 Results 18

2.2.3 Delivered solids concentration 22

2.2.3.1 Introduction 22

2.2.3.2 Continuous measurement 22

2.2.3.3 Calibration procedure 22

2.2.3.4 Results 23

2.2.3.5 Sampling device 23

2.2.4 Superficial slurry velocity 25

2.2.4.1 Introduction 25

2.2.4.2 Calibration procedure 25

2.2.4.3 Results 25

2.2.5 Instrumentation 25

2.3 Experimental techniques in operating the pilot plant 28

3. HORIZONTAL FLOW

3.1 Introduction 30

3.2 General considerations 30
3.2.1 Types of flow pattern 30
3.2.2 Pipeline operating velocity 33
3.2.3 Prediction of operating velocity 34
3.2.4 Methods for estimating head loss 35
3.3 Description of experimental results 39
3.4 Theoretical flow model 41
3.4.1 The two-layer approach 41
3.4.2 Sliding bed-load 41
3.4.3 Development of the two-layer model 42
3.4.4 Computational procedure 49
3.5 Comparison of the analysis with experimental results 50
3.5.1 Sensitivity analysis on the model 50
3.5.2 Low velocity results 54
3.5.3 High velocity results 56
3.5.4 The pseudo-homogeneous correction 59
3.5.5 Comparison with results from another laboratory 61

4. VERTICAL RISING FLOW
4.1 Introduction 78
4.2 The work of earlier investigators 79
4.3 Description of experimental results 83
4.4 Theoretical flow model 85
4.4.1 The dispersive force 85
4.4.2 The Magnus force 89
4.4.3 Computational procedure 92
4.4.3.1 High velocity results 92
4.4.3.2 Low velocity results 93
4.5 Comparison of the analysis with experimental results 95
4.5.1 Low velocity results 95
4.5.2 High velocity results 96

5. CONCLUSIONS
5.1 Horizontal flow 109
5.2 Vertical rising flow 109
5.3 General conclusions 110

NOMENCLATURE 111

REFERENCES 118

APPENDIX 1

A1 Physical properties of the sands 128

A1.1 Particle size 128

A1.2 Particle density 128

A1.3 Limiting volumetric solids concentration 128

A1.4 Fall velocity 129

A1.5 Angle of repose 129

A1.6 Coefficient of friction 129

APPENDIX 2

A2 Regression constants for the measuring devices 134

LIST OF FIGURES

Figure		Page
2.1	Flow diagram of the hydraulic transport pilot plant	5
2.2	Photographs giving a general view of a pilot plant	6
2.3	Detailed drawing of the transport line	8
2.4	Detail of the piping joint in the visible flow section	9
2.5	Photograph of the visible flow section with the photographic box in position	10
2.6	Section through a pressure tapping plate	12
2.7	Photograph of a pressure tapping point	13
2.8	Photograph of a pressure tapping point with flange alignment jig in position	13
2.9	Photograph of the calibration set-up for the gamma photon density gauge	17
2.10	Calibration results for horizontal density gauge	19
2.11	Calibration results for vertical density gauge	20
2.12	Photographs of the total flow sampler	24
2.13	Block diagram of the instrumentation	26
3.1	The experimental points describing the hydraulic characteristic of the fine sand in horizontal flow	63
3.2	The experimental points describing the hydraulic characteristic of the medium sand in horizontal flow	64
3.3	The experimental points describing the hydraulic characteristic of the coarse sand in horizontal flow	65
3.4	Overlay of the experimental points describing the hydraulic characteristic of all three sands	66

3.5	The horizontal and vertical in situ and delivered solids concentration as functions of mean velocity for the fine sand	67
3.6	The horizontal and vertical in situ and delivered solids concentration as functions of mean velocity for the medium sand	68
3.7	The horizontal and vertical in situ and delivered solids concentration as functions of mean velocity for the coarse sand	69
3.8	Defining figure for the bed-load component	44
3.9	Defining figures for the two-layer model	43
3.10	Results of the two-layer analysis overlaid on the experimental points for the fine sand	70
3.11	Results of the two-layer analysis overlaid on the experimental points for the medium sand	71
3.12	Results of the two-layer analysis overlaid on the experimental points for the coarse sand	72
3.13	Photograph of the flow pattern of coarse sand at a mean velocity around 0.5 m/s (reproduced actual size)	55
3.14	Photograph of the flow pattern of coarse sand at a mean velocity around 2.5 m/s (reproduced actual size)	56
3.15	Results of the modified two-layer analysis for fine sand overlaid on the experimental points	73
3.16	Results of the modified two-layer analysis for medium sand overlaid on the experimental points	74
3.17	Results of the modified two-layer analysis for coarse sand overlaid on the experimental points	75
3.18	Results of the modified two-layer analysis for -5/16 in. + 4 BSS gravel from Reference 68	76
3.19	In situ solids concentration as a function of mean velocity for the -5/16 in. + 4 BSS gravel, plotted from Reference 68	77

4.1	The experimental points describing the hydraulic characteristic of the fine sand in vertical rising flow	98
4.2	The experimental points describing the hydraulic characteristic of the medium sand in vertical rising flow	99
4.3	The experimental points describing the hydraulic characteristic of the coarse sand in vertical rising flow	100
4.4	Overlay of the experimental points describing the hydraulic characteristics of all three sands in vertical rising flow	101
4.5	The experimental and calculated frictional losses for the fine sand	102
4.6	The experimental and calculated frictional losses for the medium sand	103
4.7	The experimental and calculated frictional losses for the coarse sand	104
4.8	Schematic representation of the stresses in vertical rising flow near the pipe wall	88
4.9	Schematic representation of the forces on a particle in a steep fluid velocity gradient	90
4.10	Schematic representation of the velocity and solids concentration profiles in vertical rising flow near the pipe wall	91
4.11	Predicted frictional loss (broken line) for iron-ore (S = 4.5) of the same diameter as the coarse sand	105
4.12	Predicted total loss overlaid on the experimental points for the fine sand	106
4.13	Predicted total loss overlaid on the experimental points for the medium sand	107

4.14 Predicted total loss overlaid on the experimental points for the coarse sand 108

A1.1 Photograph of the three sands 130

A1.2 Sieve analysis for the three sands 131

A1.3 Photograph of the apparatus used to measure the angle of repose 132

LIST OF TABLES

Table		Page
2.1	Gamma photon attenuation coefficients for sand and water	21
3.1	The difference between the total head loss and that attributable to the bed-load at various velocities	58
A 1.1	Physical properties of the sands	133
A 2.1	Regression constants detained from the calibration of the measuring devices	134

1. HYDRAULIC CONVEYING - an Introduction

The hydraulic transportation of solids in pipelines has many advantages over more conventional methods of materials handling both in horizontal and vertical conveying. The use of the term horizontal in describing such installations is somewhat misleading as very few industrial lines are truly horizontal, the term merely implies that the line is longer than any change in elevation.

In recent years there has been much interest in long distance horizontal hydraulic transportation, and many systems have been built and successfully operated as well as several new projects which are in the planning and development stage. Wasp et al. (76) give details of a selection of commercial slurry pipelines, and show that a large throughput of solids can be achieved using a relatively small diameter pipe. In instances where there is no established transport network, for example where mineral deposits are to be exploited in remote or rugged terrain, hydraulic conveying can provide a reasonably low capital cost transportation system. A pipeline does not have to contour the land, since it does not have to follow shallow gradients, and in fact the lie of the land can be an advantage especially regarding syphoning.

All the long distance pipelines operating to date pre-crush the solids so that the slurry is transported as a suspension of fine particles at velocities high enough to prevent settling out of the solids. Specially designed reciprocating or centrifugal pumps are employed to pump such slurries. The type of pump selected will depend to a large extent upon maximum particle size of the slurry and the pressure head that has to be developed. A compromise has to be struck between low line pressures with multiple pumping stations or higher line pressures with fewer intermediate stations. The economics associated with the siting of pump stations are complex.

Aggregates used in the building industry, such as sands and gravels are usually required for use unbroken. Coarse particles are best transported hydraulically as a sliding bed of solids in the pipeline as uneconomic fluid velocities would be required for suspension. Problems are encountered when large particle size solids are required to pass through the pump. Only relatively low concentrations can be

pumped using inefficient pumps with large clearances between the impeller and the case. This makes the operating costs less attractive.

Many of the problems associated with conventional hydraulic conveying of large particles can be overcome by using a pressurised lock hopper to feed the solids into the pipeline at relatively high concentration. This technique is often referred to as dense-phase flow. Transporting solids at high concentration saves on the quantity of carrier fluid needed, also a much lower transport velocity can be used for the same throughput of solids compared to that needed at lower concentrations. Pressurised hoppers were first used for high concentration conveying at Imperial College, subsequently larger lines have been used at Warren Spring Laboratory. This technique is necessarily intermittant in operation but several units can be sequenced to obtain steady flow. Proprietary pipe and chamber feeders are now industrially available (61,62). This type of device is best suited to feeding solids into relatively short distance pipelines since the pressure loss along the line tends to be somewhat elevated at high solids concentrations. The use of these feeding devices and direct pumping mentioned earlier are also applicable to vertical hydraulic hoisting.

There are numerous examples of hydraulic hoisting installations in current use throughout the world (44). The hoisting of materials from mines offers many advantages. The capacity of mining shafts can be increased more economically by installing hydraulic hoisting systems rather than sinking new shafts (42). Hydraulic hoisting could never totally replace existing shafts as these are necessary for both ventilation and access for personnel and machinery. The mining of coal and its transportation to the surface has been carried out completely by hydraulic techniques (43). Whilst the idea is simple in principle the technical problems of integrating the necessary equipment are vast, but not insurmountable.

The hydraulic transport of solids in pipes is by no means a new technique, though much of the design knowledge that is presently available is empirical. There is a need for a better physical understanding of the flow of such mixtures. Selection of the operating velocity and estimation of the pressure loss in the line under operating conditions are central to any pipeline design.

This information may be obtained from pilot-plant work, using exactly the same conditions as those to be experienced in the commercial line or by less certain methods of scaling up results obtained using small diameter pipes. For preliminary work it is most useful to have a mathematical model to help predict the necessary parameters before adopting more costly experimental work. Such mathematical analyses are proposed here for both, true horizontal and vertical rising flow. Whilst they are strictly only applicable to high concentration conveying most of the principles are nevertheless general. In order to assess the behaviour and worth of such models accurate experimental results are necessary.

2. EXPERIMENTAL WORK

The hydraulic characterisation of a slurry involves the measurement of the mean velocity dependence on the pressure loss, and on the *in situ* and delivered solids concentration. Three closely sized sands have been characterised in a 26.15 mm diameter steel pipeline incorporated in a pilot plant facility. The mean particle diameters of the sands were 320 and 680 μm and 1.7 mm, a full specification of the sands is given in Appendix 1.

2.1 Description of pilot plant

The hydraulic transport pilot plant was designed by R.A. Bantin and specifications of the major items of plant are given elsewhere by Televantos (68). A flow diagram of the facility is presented in Figure 2.1. The instrumentation on the plant is interfaced to a digital computer to facilitate data handling. Figure 2.2 gives a general view of the pilot plant facility.

The operation of the pilot plant is essentially batch-wise and once the plant is loaded with sand all material handling is performed hydraulically. A distinct advantage of this lock hopper discharge system is that as only clear water is pumped, no special slurry pumps are needed. Two Worthington Simpson vortex pumps arranged in parallel give a maximum slurry velocity of just over 3 m/s. The water flowrate can be controlled by either a digital flow control valve, installed downstream of the pumps or using a by-pass around the pumps.

The feed and receiving lock hoppers used in this system have included cone angles of 60 and 90 degrees respectively. Under flooded conditions with the materials investigated it is probable that the feed hopper is mass-flow (39), hence material in contact with the hopper wall is moving and radial flow is highly probable (8). For the case of funnel-flow a *rat hole* tends to form in the hopper with the bulk of the discharge material being drawn down from the vortex of the hopper. Both lock hoppers are of similar dimensions, the volume of the 90 degree hopper is 1.43 m^3. The receiving hopper was

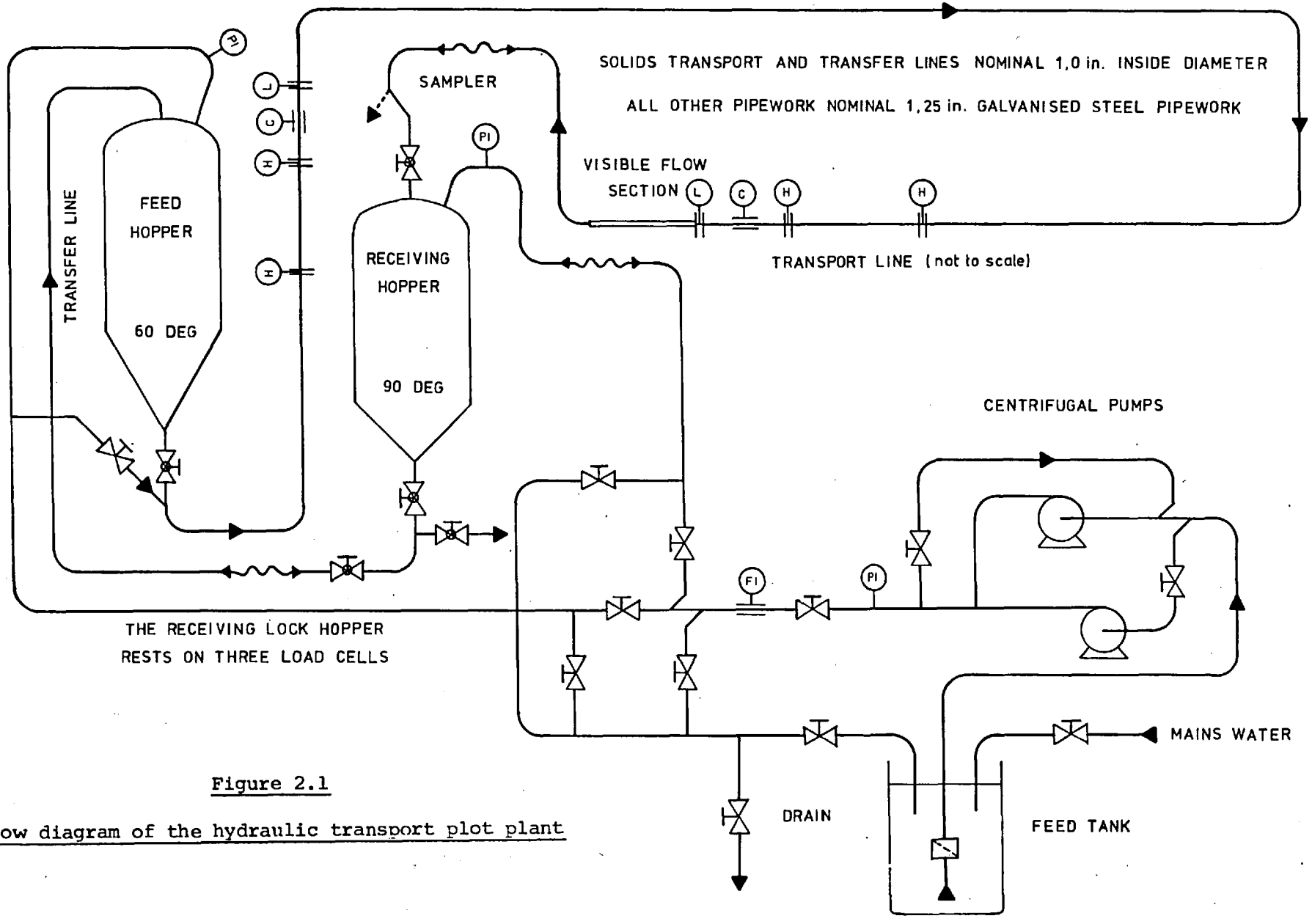


Figure 2.1

Flow diagram of the hydraulic transport plot plant



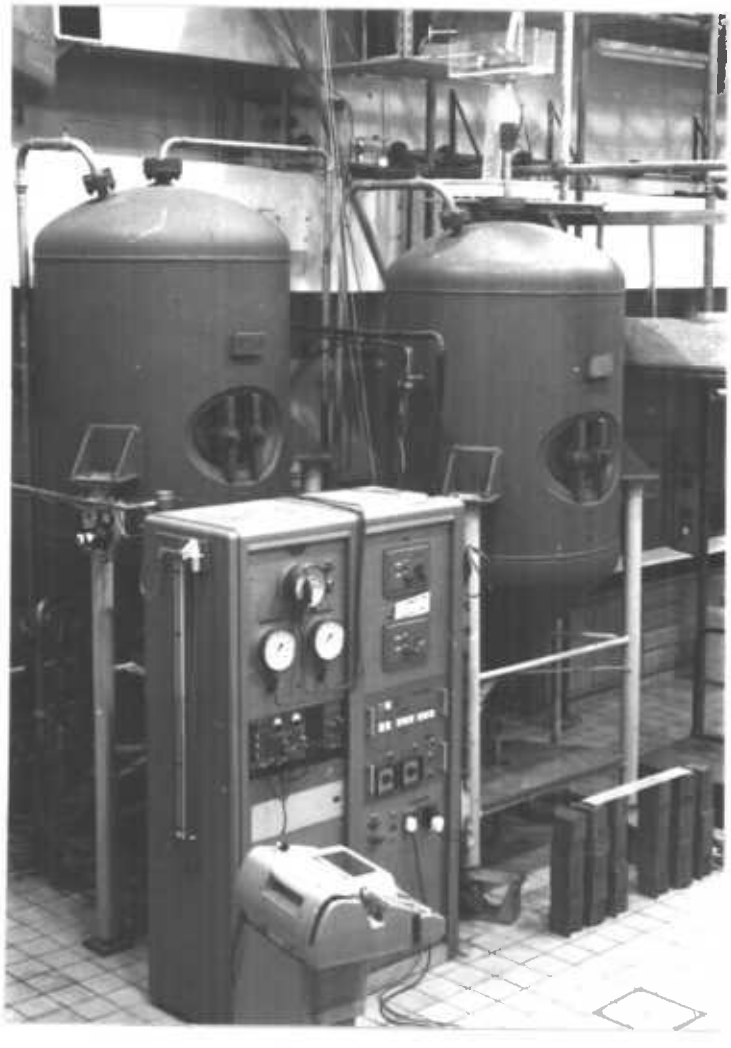


Figure 2.2

Photographs giving a general view of a pilot plant

charged with just under a tonne of dry material for each material under investigation.

The solids transport line is constructed of galvanised water pipe of nominal bore 25.4 mm (1 in) mounted on a vertical laboratory wall as depicted in Figure 2.3. The total length of line is about 21 metres. The sections of pipeline are joined with raised face flanges. Unfortunately these had been skimmed flat in an attempt to reduce internal flow obstruction due to poor alignment. This was unnecessary and later caused problems with leakage. This was cured by using a silicon rubber compound to seat new gaskets. As commercial grade pipe was used the inside diameter is not constant. A representative number of sections of pipework were removed from the flow circuit and their diameter established by a volumetric technique. A mean diameter of 26.15 mm ± 0.5 mm has been used as a representative figure. All the bends are of standard 90 degree design with a radius of curvature to pipe diameter ratio of 3. From experimental runs with water the transport line can be regarded as a commercially smooth pipe.

In order to pump solids around the transport line clear water is pumped onto the settled solids in the feed hopper. The sand is discharged into the line with a concentration characteristic of the hopper geometry and physical properties of the solids. The concentration was independent of velocity in the case of the larger sands -- the fine sand showed a small dependence upon slurry velocity. The rate of discharge of the solids into the line is independent of the head of material in the hopper except when the hopper is nearly empty, implying that the discharge is controlled by conditions at the orifice. The slurry can be diluted by feeding water into the line at the hopper exit, but concentration is not a variable readily controlled under batch conditions. Recirculating loops are more suited for lower concentration work. The receiving hopper acts as a solid-liquid separator giving insignificant particle carryover even using fine sand at high velocities. The feed water is discharged to drain since sand particles passing into the pump suction ports would have disastrous effects on the graphite sealing faces. When all the sand has been transported the valve arrange-

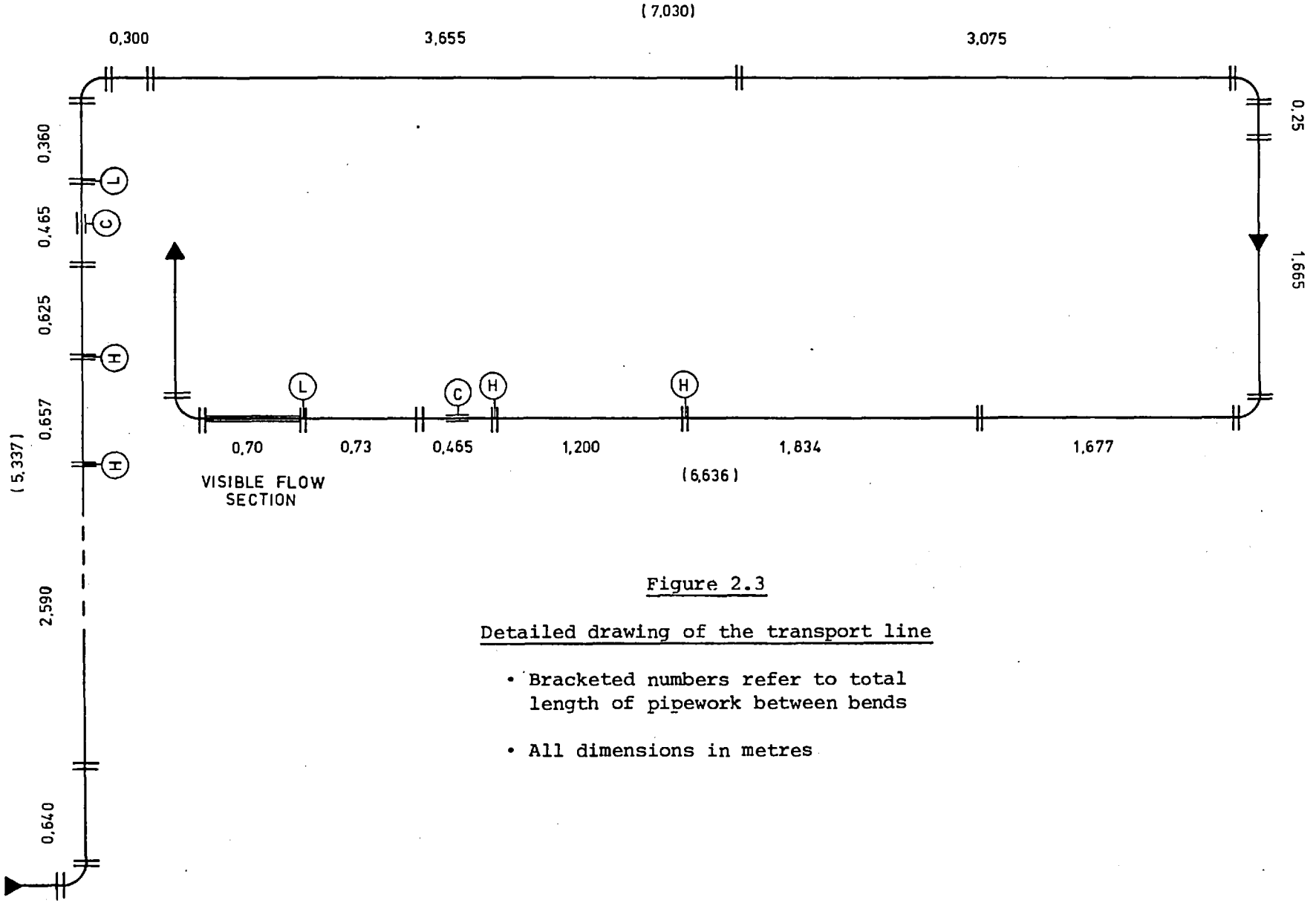


Figure 2.3

Detailed drawing of the transport line

- Bracketed numbers refer to total length of pipework between bends
- All dimensions in metres

ment allows clear water to be fed to the receiving hopper in order to transfer the sand back to the feed hopper.

A visible flow section was installed into the horizontal line after the final pressure tapping. Each end of a 700 mm length of conically flanged Quickfit Visible Flow industrial glass pipe is joined to a modified pipe flange as shown in Figure 2.4, this enables the glass section to be incorporated directly into the flow circuit.

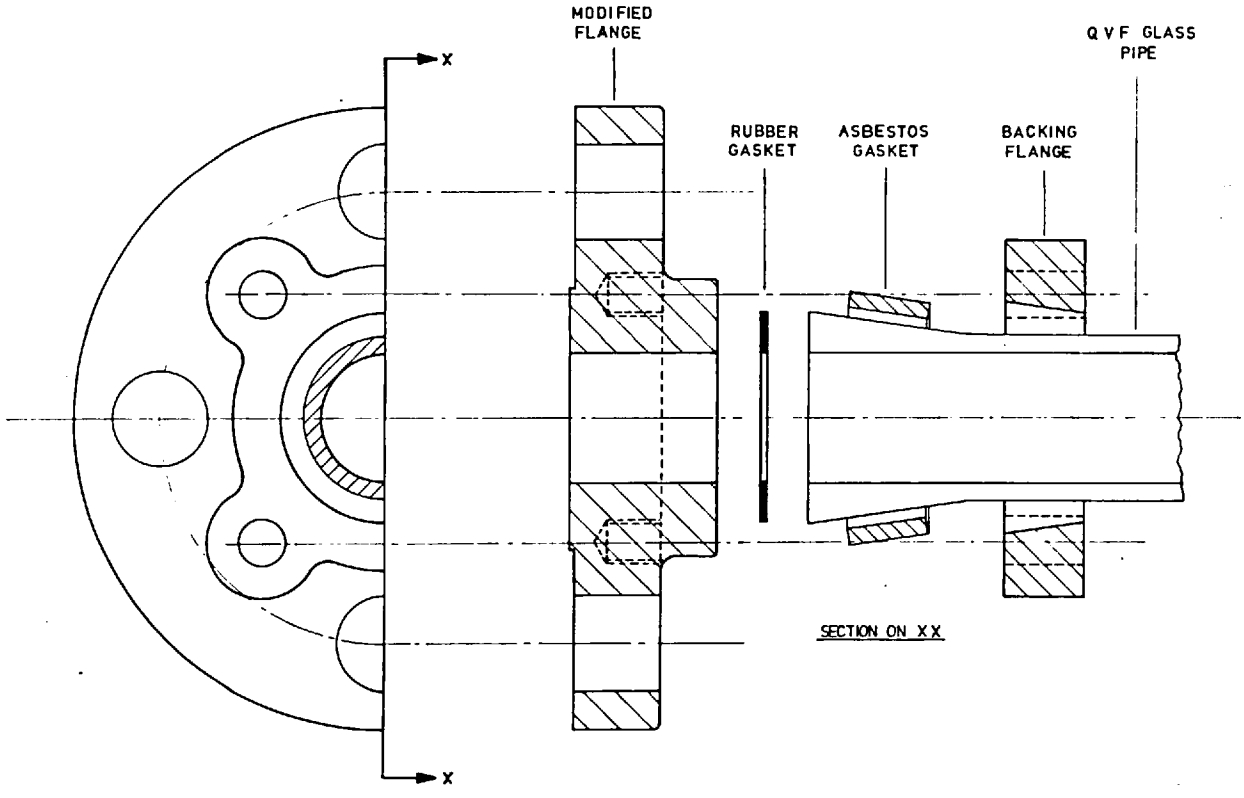


Figure 2.4

Detail of the piping joint in the visible flow section

Care had to be exercised to ensure that the steel lines were properly aligned before tightening the 4 securing bolts. Reflection from the curved surface of the glass pipe tended to obscure the flowing slurry. A perspex box with a glass front window was built to enclose a 200 mm length of glass line as shown in Figure 2.5. By filling the box with glycerol, which has the same refracture index as borosilicate glass, the pipe wall was in effect rendered invisible, thus observation of the slurry was greatly improved.

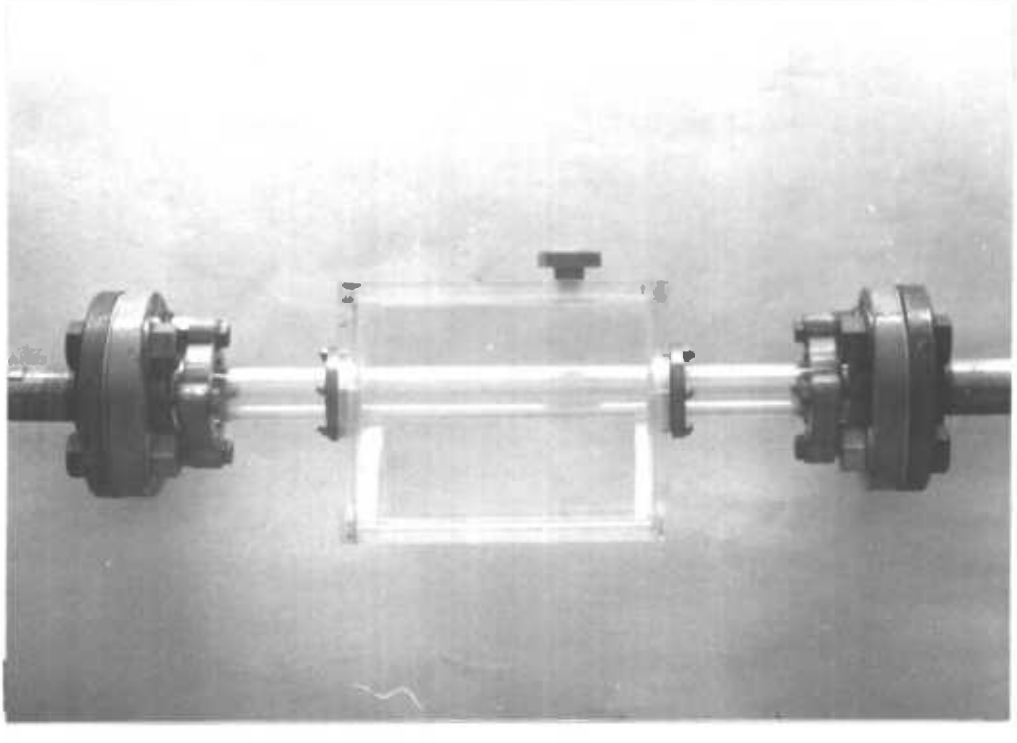


Figure 2.5

Photograph of the visible flow section with the photographic box in position

2.2 Measurements

The vertical rising and lower horizontal sections of pipework are fitted with pressure tapping points. Devices to measure the *in situ* or transport concentration were installed in the same lengths of pipework as the pressure measurements were made. The delivered or input solids concentration and superficial slurry velocity were also measured.

2.2.1 Frictional pressure gradient

2.2.1.1 Introduction

The frictional energy loss, expressed as a hydraulic gradient, is obtained by making two pressure measurements over a straight section of pipework, using a differential strain gauge transducer.

The tapping points are located well downstream of any bends and are in regions of linear pressure drop. A qualitative experimental investigation was undertaken to verify this. The pressure loss was measured over intervals of approximately 1.5 m downstream from the bends in the vertical and horizontal sections of pipework. It was found that the length of pipework needed to obtain reproducible pressure gradients was somewhat greater than the 50 pipe diameters often quoted for single phase Newtonian fluids. The use of a common low pressure tapping point (see Figure 2.3) was settled upon arbitrarily after making a further investigation to check that the upstream bend was not unduly influencing the pressure measurements. This was accomplished by using a common high tapping point; no discernible difference in pressure drop was noticed for this change in configuration over the slurry velocity range 0.2 to 3.2 m/s.

Pressure measurements were made in the vertical rising and horizontal sections. The vertical down-coming section was too short to allow reliable measurements to be made. As sufficient transducers were available two measurements were made in each section. The agreement between them was exceptionally good in both cases. Pressure drops over the longer sections were measured by transducers with a range of ± 1.4 bar while over the shorter sections ± 1.0 bar devices were used.

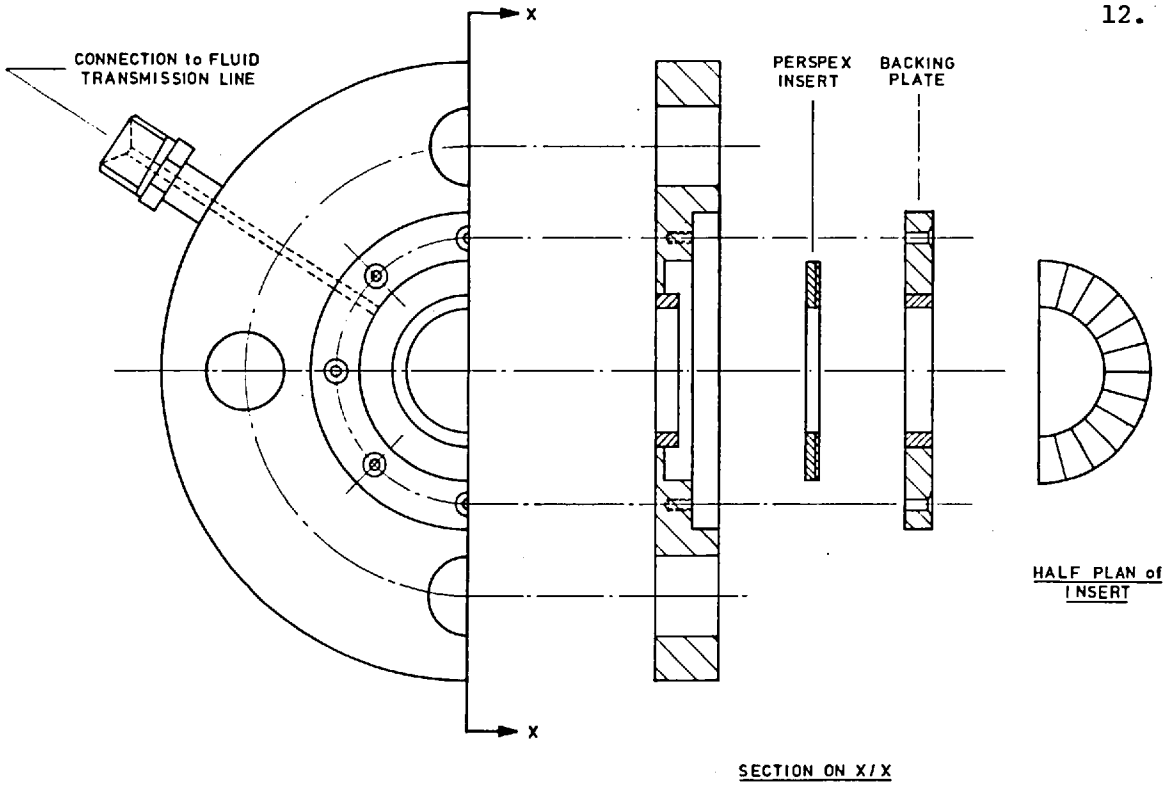


Figure 2.6

Section through a pressure tapping plate

Liquid continuity is maintained at the pressure tapping points using circumferential holes in the pipe wall. The holes are radial slots cut into a perspex disc which is inserted into a mild steel tapping plate. Figure 2.6 shows an exploded section through a tapping plate. The perspex discs replace porous polythene inserts previously used which suffered badly from clogging with fine particles and rust. The tapping plate is incorporated into the pipework by sandwiching it between two flanges as shown in Figure 2.7. It is essential to align the flanges and tapping plates as accurately as possible to reduce local internal losses. This was not easy to accomplish by eye, as often the tapping plates and flanges were of different external diameter. A simple but effective jig was clamped around the assembly when tightening up the flange bolts to ensure a well aligned flow area. This jig is shown in position in Figure 2.8. The tapping plates were connected to the transducers by water filled lines which could be back flushed with filtered mains water.

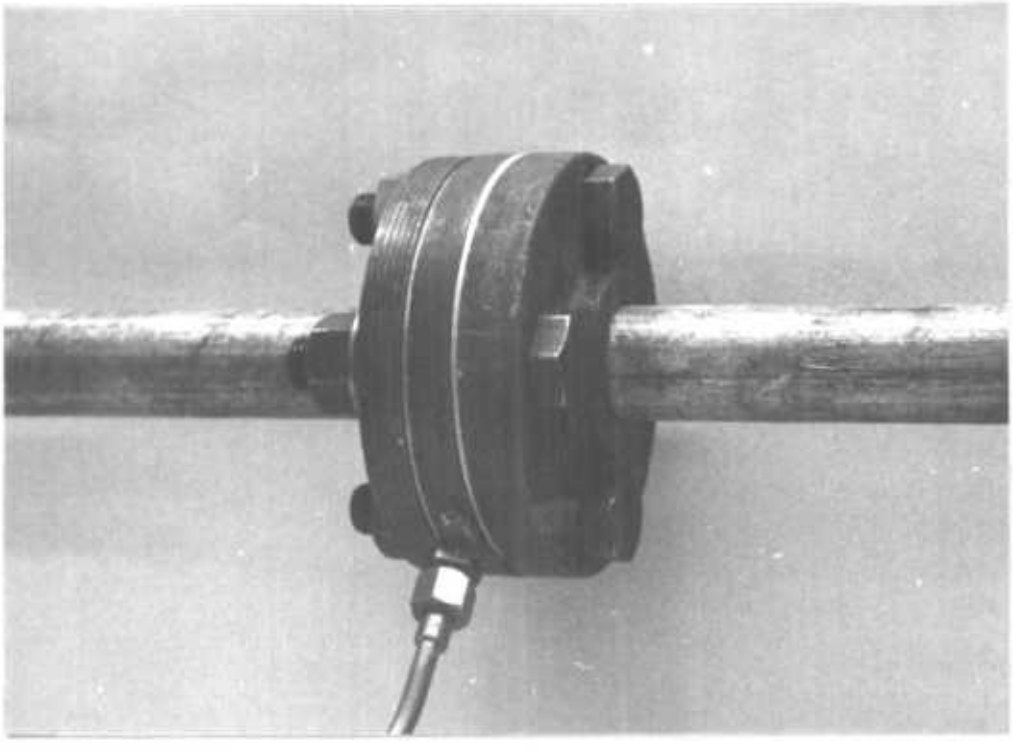


Figure 2.7

Photograph of a pressure tapping point

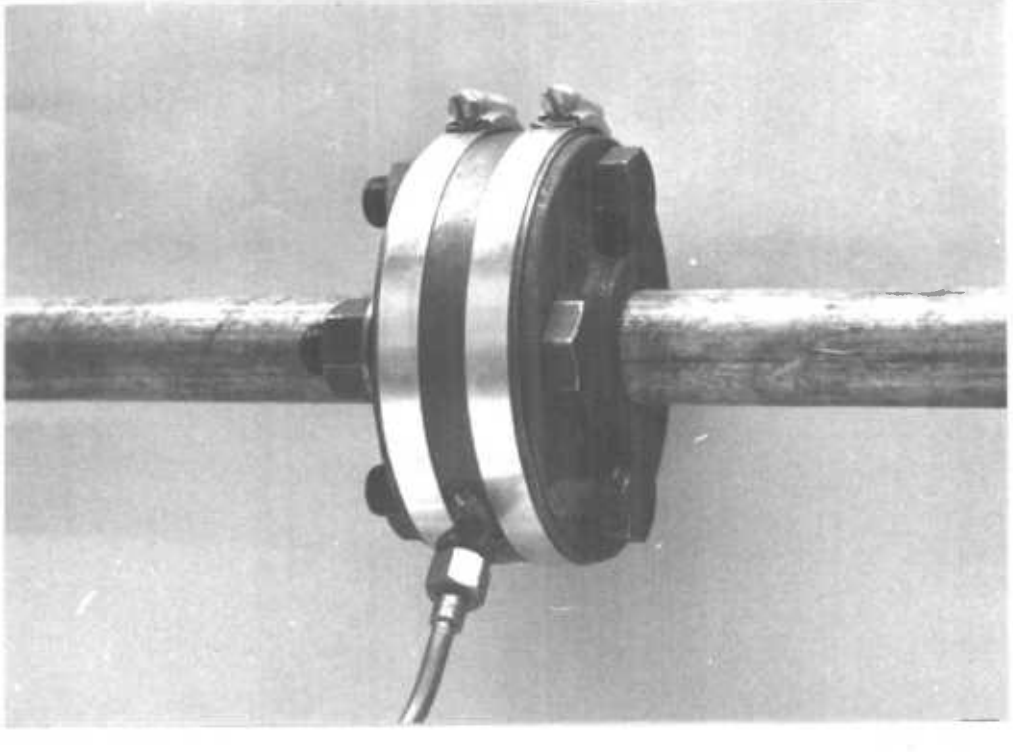


Figure 2.8

Photograph of a pressure tapping point with flange alignment jig in position

A rotameter was installed in the back flush water supply line. Any decrease in flowrate of the back flushing water gave indication of fouling in the tapping holes. Dissolved air in the water presented problems as bubbles formed in the lines when the flow was throttled by a valve. A low pressure supply was installed to flush out any air. This worked most satisfactorily. As a direct check on the computer output a tetrabromoethane and water manometer was used in parallel with several transducers in turn to confirm the hydraulic gradient during the recommissioning of the pilot plant.

2.2.1.2 Calibration Procedure

With the transmission lines disconnected, regulated compressed air was supplied to the high pressure side of the transducer, while the other side was open to the atmosphere, (the high pressure side was selected so that increasing the pressure on the limb gave a positive electrical response). The air pressure was measured by an open mercury manometer. While readings were being taken the manometer and transducer were isolated from the supply air line to avoid small fluctuations in pressure from disturbing the device.

2.2.1.3 Results

The strain gauge devices gave a linear calibration with pressure according to the relation:

$$P = A + BX_k; \quad 1 \leqslant k \leqslant 4 \qquad (2.1)$$

The pressure P is evaluated using the parameter X_k which has a numerical value proportional to the electrical output signal from device k. The slope of this relation is a characteristic of the device and is given in Appendix 2. During recalibration over the two year experimental period the value of B, for each device did not change by more than 1%, this fluctuation is attributable to experimental error during the calibration procedure.

2.2.2 In situ solids concentration

2.2.2.1 Introduction

The *in situ* solids concentration is measured by a gamma photon attenuation device. The solids concentration obtained by this means is necessarily both space and time averaged.

Nuclear devices of this type have several drawbacks for industrial use. The half-life of the isotope and drift in the electronics calls for frequent recalibration. The measurement is not instantaneous. as it requires a finite integration period to evaluate the radiation intensity. For experimental use these disadvantages can be sufficiently minimised to make these devices an attractive research tool.

The half-life of the Cesium 137 isotope used in the concentration gauges is 30 years, so that the countrate will only diminish by a few percent over the experimental period. The detectors consist of a scintillation crystal optically coupled to the end window of a photo multiplier tube; the pulses are amplified and discriminated from noise before being counted. The H T voltage applied to the photo multiplier detector has to be selected so that counting on the photo peak of the isotope (0.662 MeV) is on the plateau region of the detector characteristic. The plateau was found to be well defined and about 200 V wide. The H T was set to the mid-point of this region. A major consideration concerning the accuracy of the concentration measurement is the integration period. In 1973 the effective activity of the two sources were 102 mCi and 575 mCi, and in order to obtain an accuracy better than 5% in the solids concentration the standard deviation of the count rate had to be better than 0.5%. This criterion, when applied to the lower activity source leads to an integration period of 15 s.

2.2.2.2 Theory of measurement

A composite absorbing medium located between a narrowly collimated source of monoenergetic gamma photons can be treated as n individual layers of material, each of thickness x_k. The ratio of the transmitted to incident radiation is given by:

$$\frac{I}{I_o} = \prod_{k=1}^{n} \exp - (x_k \mu_k) \qquad (2.2)$$

where μ_k is the linear attenuation coefficient of the material. Applying this directly to the case of a slurry of concentration C in a pipe of internal diameter D, with a wall thickness x_w, the transmitted intensity of radiation is given by:

$$I_m = I_o \exp - (2 x_w \mu_w + DC \mu_p + D (1-C) \mu_f) \qquad (2.3)$$

This includes contributions due to absorption in the pipe wall, and in the solid and fluid phases. For an empty pipe the absorption in the air will be negligible in comparison with that due to the walls, the transmitted radiation is given by:

$$I_e = I_o \exp - (2x_w \mu_w)$$

When the pipe is full of water the transmitted radiation is:

$$I_f = I_o \exp - (2x_w \mu_w + D\mu_f) \qquad (2.4)$$

using the previous result, Equation 2.3 reduces to:

$$I_f = I_e \exp - (\mu_f D)$$

This expression allows Equation 2.2 to be simplified to:

$$I_m = I_e \exp - (DC \mu_p + D (1 - C) \mu_f) \qquad (2.5)$$

Taking natural logarithms and substituting for the pipe diameter from Equation 2.5 the final expression is obtained.

$$\ln \frac{I_m}{I_e} \Big/ \ln \frac{I_f}{I_e} = 1 + C \left(\frac{\mu_p}{\mu_f} - 1 \right) \qquad (2.6)$$

The solids concentration C is in linear relation to a function of radiation intensity.

2.2.2.3 Calibration procedure

Both devices had to be separately calibrated since the sources were of different activity. Calibration was performed by evaluating the lefthand side of Equation 2.6 for a given concentration of sand filling the apparatus. A distributor containing a fine mesh was fitted to the bottom of the removable section of pipework containing the concentration gauge, and a sight tube fitted to the top. This arrangement is shown in Figure 2.9. A high solids concentration is achieved by consolidating the bed of sand by gently tapping the apparatus. For concentrations below the freely settled value the sand was fluidised. The apparatus was calibrated for volume with water so that when a slurry was present

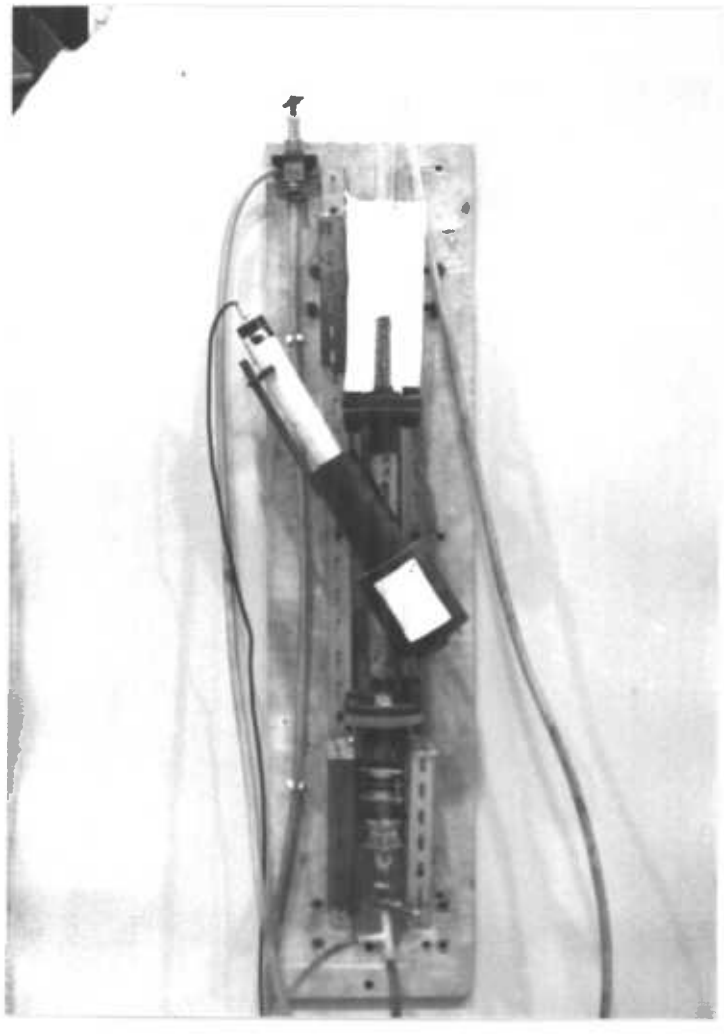


Figure 2.9

Photograph of the calibration set-up for the gamma photon density gauge

the stable height of solids could be directly interpreted as a solids concentration. This procedure required both devices to be calibrated vertically, but as the average diametral concentration is measured in both cases this does not impose any error.

2.2.2.4 Results

The results of the calibration of both devices for all 3 sands are shown in Figures 2.10 and 2.11. They are linear in all cases. There is a slight change in slope with particle size which may be partially explained by the half-life as experiments were performed in increasing sand size over a period of two years. The increased scatter on the coarse sand at high concentration is due to increased difficulty in obtaining a reproducible uniform concentration in the apparatus, for this reason it would appear inadvisable to increase the particle diameter further. The slope of the lines may be directly compared with the theoretical prediction.

Published values of attenuation coefficients (3) are available for sand of relative density 2.2 and water. The linear attenuation coefficients are proportional to absorber density so the necessary correction is readily made for the sand used in the experiments. The linear attenuation coefficient is also slightly dependent upon the gamma photon energy, a small extrapolation is made to account for this. The values of the published data and corrected values of the linear attenuation coefficients are given in Table 2.1. Using these values to evaluate the slope of the calibration relation, (Equation 2.6) the values are found to agree to within 5% of those measured experimentally.

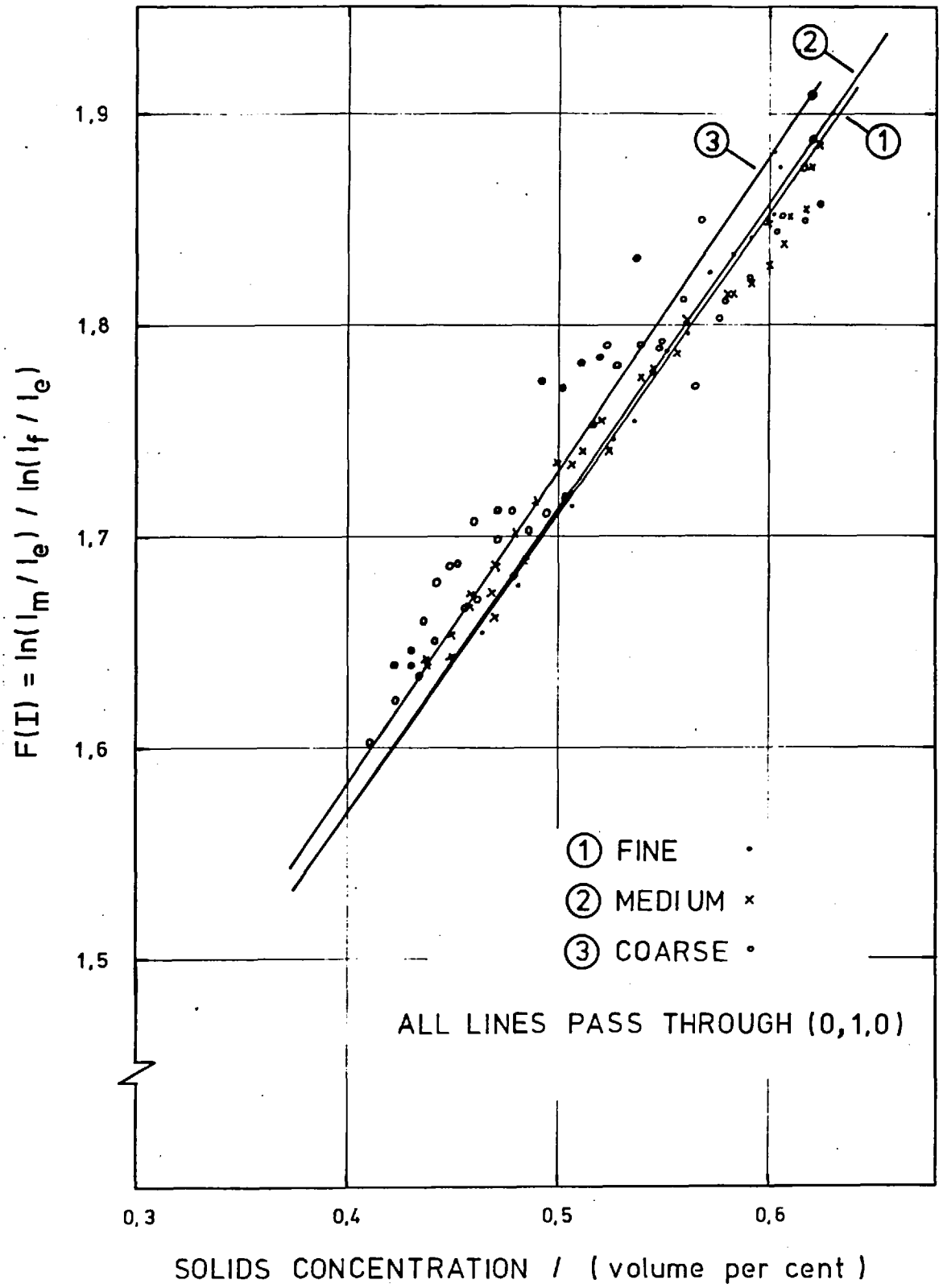


Figure 2.10

Calibration results for the horizontal density gauge

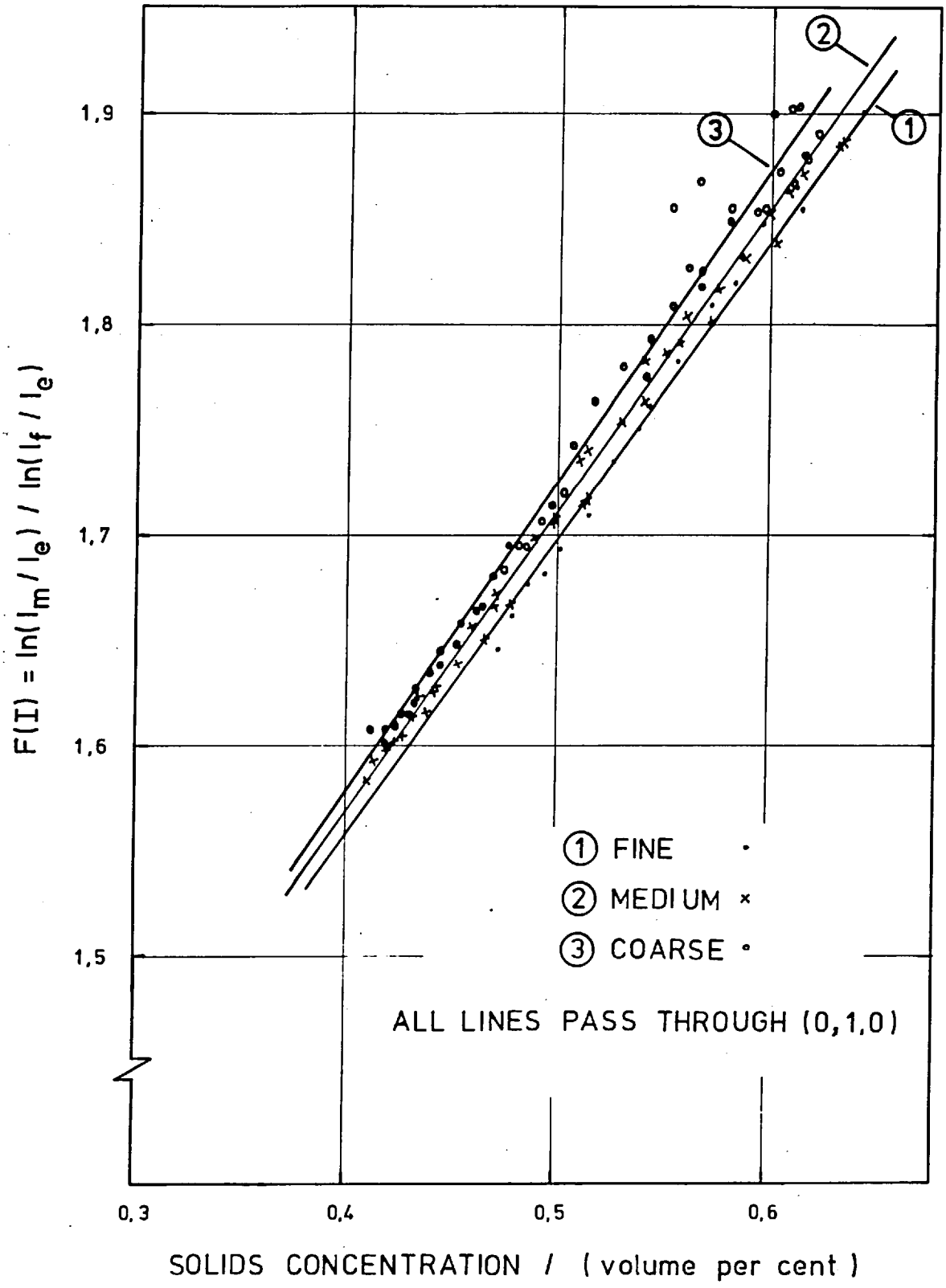


Figure 2.11

Calibration results for the vertical density gauge

TABLE 2.1

GAMMA PROTON ATTENUATION COEFFICIENTS FOR SAND AND WATER (From Ref. 38)

MATERIAL	DENSITY / 10^3 kg/m^3	LINEAR ATTENUATION COEFFICIENT / (cm^{-1})		
		1 MeV	3 MeV	0.662 MeV
SAND	2.2	0.140	0.0825	0.1776
	2.65	-	-	0.1803
WATER	1.0	0.0706	0.0396	0.0759

2.2.3 Delivered solids concentration

2.2.3.1 Introduction

Two methods exist on the pilot plant for measuring the delivered solids concentration. A sliding plate sampling device which is suitable for use below about 2 m/s can be used to remove a total. flow sample of slurry. The change in weight of the receiving hopper and the liquid feed rate can also be used to give a continuous reading of the delivered solids concentration.

2.2.3.2 Continuous measurement

The 90 degree receiving lock hopper is isolated from the rest of the system by flexible hoses. This allows the mass of the hopper to be recorded by three load cells. The total capacity of these is 6 tonnes with a resolution better than 0.5 kg. In order to obtain high accuracy in the delivered concentration a sufficient mass of sand must be recorded. At high velocities this method is particularly satisfactory as a large mass of sand is transported in a relatively short time, however, at low velocities run times would become arduously long. For this reason a sampling device is used below about 2 m/s.

By considering an overall mass balance over the hopper the rate of change of total mass ΔW with time can be used with the fluid flow rate L_v into the feed hopper to calculate a delivered concentration.

$$C_d = \frac{\Delta W}{\Delta t} \quad \frac{1}{L_v \ (\rho_p - \rho_f)} \tag{2.7}$$

The solids throughput may also be obtained by considering the definition of C_d:

$$S_v = L_v \ C_d/(1 - C_d) \tag{2.8}$$

2.2.3.3 Calibration procedure

The load cells were calibrated by loading up to 0.5 tonnes of lead shielding bricks onto a platform below the hopper, the computer algorithm summed the electrical output signals. This sum was found

to be a linear function of mass added, as is to be expected with strain gauge transducers. The signal did not alter by more than 0.1% for an uneven distribution of 20% of the maximum calibration load. This shows that the transducers were evenly matched and likely to give consistent results.

2.2.3.4 Results

The calibration for the devices is presented below:

$$W = A + B\ (X_6 + X_7 + X_8) \qquad (2.9)$$

The total mass of the hopper W is a linear function of the summed electrical outputs from the transducers. The slope of the calibration relation is a characteristic of the device. Similar reproducibility in the value of the slope B was encountered with the load cells as was experienced with the pressure transducers. The values of A and B are given in Appendix 2.

2.2.3.5 Sampling device

A pneumatically operated sliding plate sampling device was constructed from 18-8 stainless steel to enable a total flow sample of the slurry to be taken.

Figure 2.12 shows the sampler mounted above the receiving hopper. Normally the slurry flows straight through the sampler and into the hopper. When a sample is required the flexible delivery pipe is moved above the sample port by a pneumatic ram. The sample is collected in a clear plastic 2,000 cm^3 measuring cylinder.

Initial problems were encountered when air could reach the stationary slurry in the main flow line while a sample was being taken, causing the slurry to partially drain. This resulted in a total system blockage when normal flow was resumed. Flooding the sliding faces with water prevented air entrainment and helped lubricate the machined faces during changeover. In the design of a sampler of this type it is important that the exit of the slurry is not restricted at any time. This requires that the exit ports

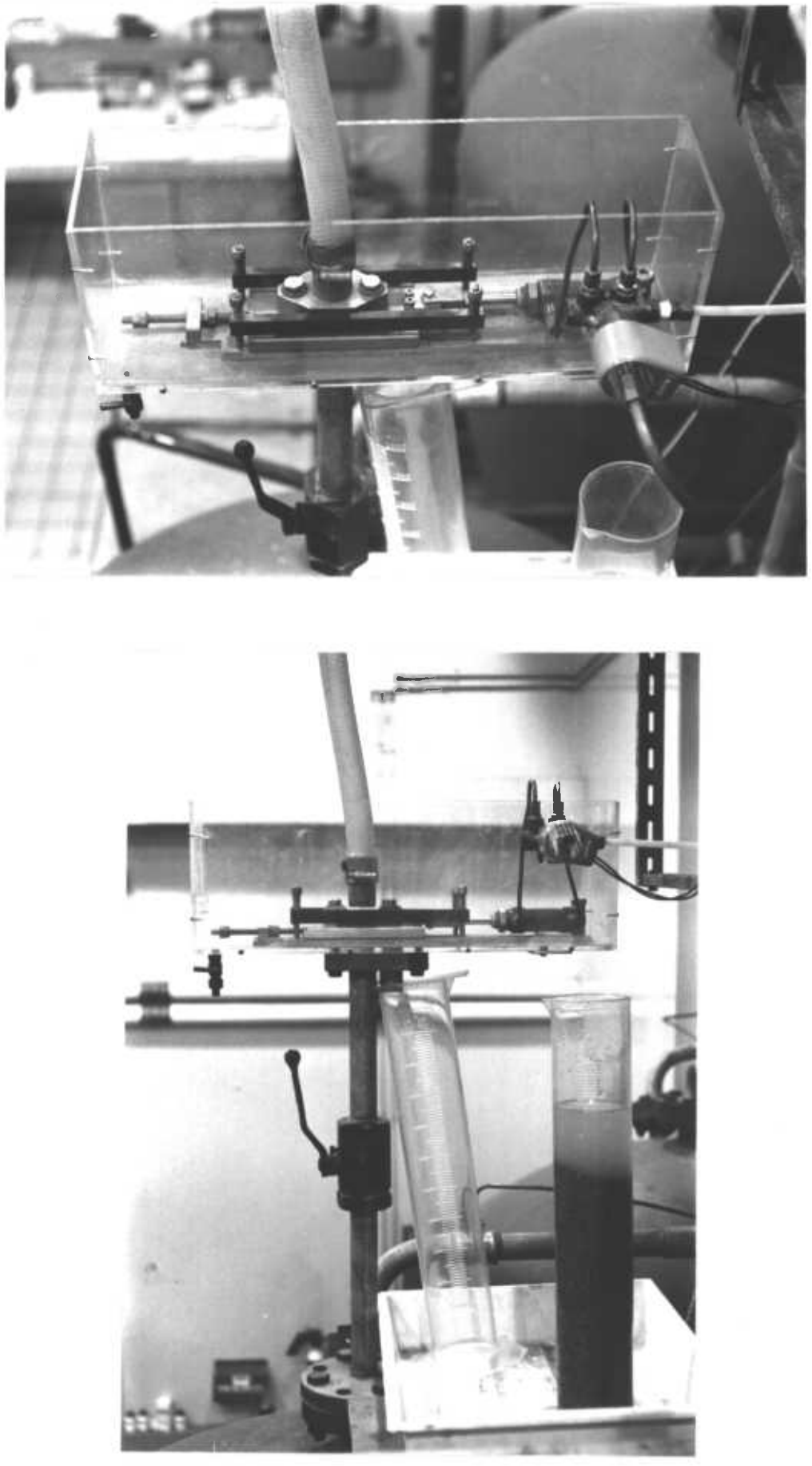


Figure 2.12

Photographs of the total flow sampler

are as close together as possible while leaving a sufficient amount of metal to make a seal after extended use has caused wear. In practice it was found necessary to surface grind the sliding faces every time a new sand was loaded.

The 25 mm pneumatic ram, when operated at 4 bar, produced a fast changeover in both directions.

From a knowledge of the total mass W and volume V of the sample the delivered solids concentration C_d can be evaluated using:

$$C_d = (\frac{W}{V} - \rho_f)/(\rho_p - \rho_f) \qquad (2.10)$$

Agreement between the two methods of obtaining the delivered solids concentration was exceptionally good, generally better than 0.2%.

2.2.4 Superficial slurry velocity

2.2.4.1 Introduction

The most direct method of obtaining the superficial slurry velocity is by measuring the volumetric flowrate of water to the feed hopper. This is accomplished by a turbine flowmeter fitted with flow straightening sections of pipework.

2.2.4.2 Calibration procedure

Calibration of the flowmeter was performed by pumping water from the weighed feed tank through the flowmeter to drain.

2.2.4.3 Results

The frequency of the pulsed output was found to be directly proportional to the water flowrate and in excellent agreement with the calibration supplied by the manufacturer. The value of the regression constant is given in Appendix 2.

2.2.5 Instrumentation

The instrumentation on the pilot plant is interfaced to a Digital Equipment Corporation PDP8/e computer, following the block layout shown in Figure 2.13.

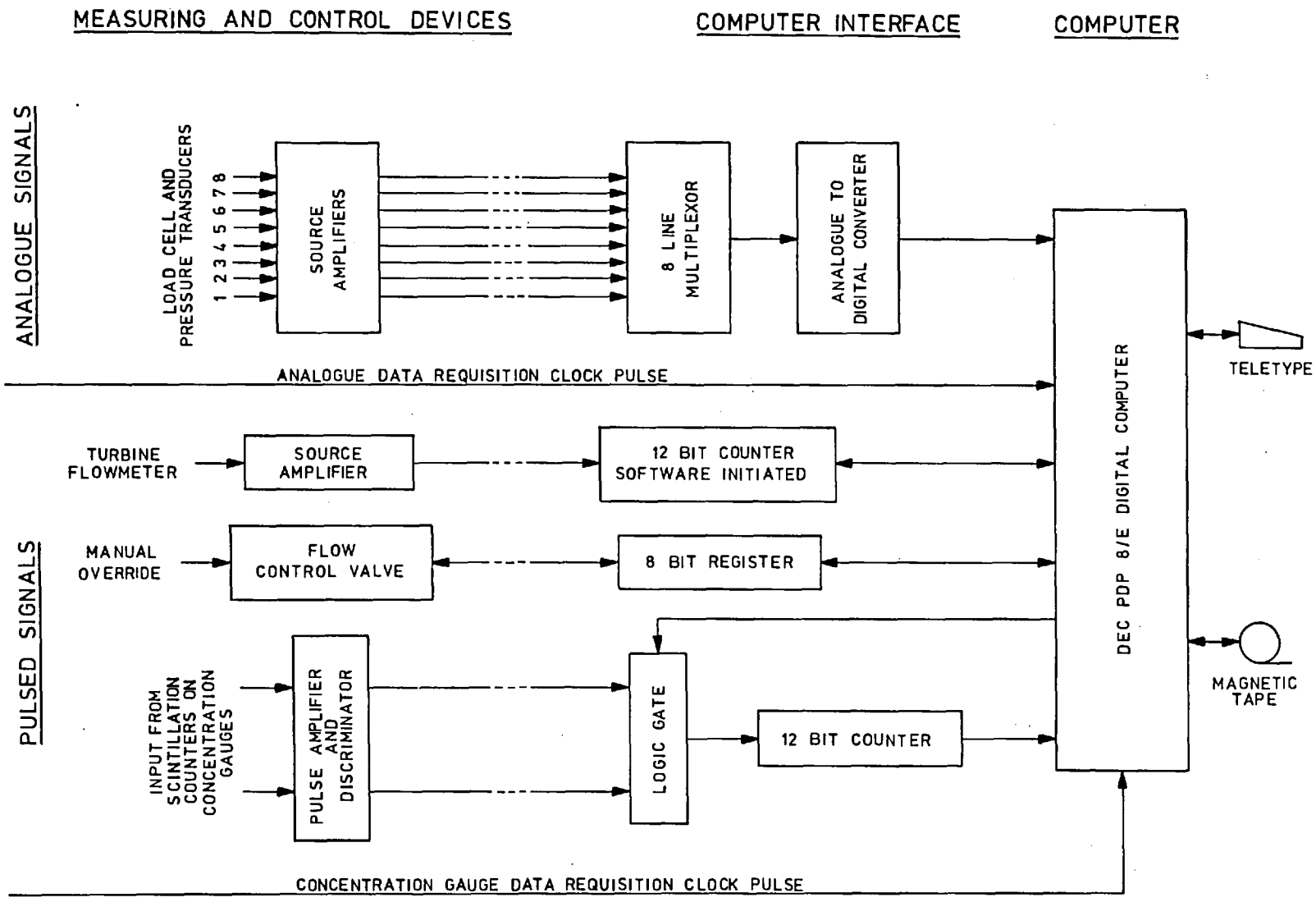


Figure 2.13

Block diagram of the instrumentation

The output signals from all the measuring instruments are amplified close to the source before being transferred to the computer interface. This is necessary to reduce noise on the signals, as the computer is situated in an adjacent laboratory. Two process timers are used to initialise the reading of the measuring devices. The inline concentration gauges are read alternately. The reading of the analogue devices is essentially instantaneous, typically 5μs is needed to address each device, perform an analogue to digital conversion on the signal and store the value. A one second integration period is used to evaluate the pulse frequency from the flowmeter. The digital flow valve can be controlled manually or by software. As the flow from the hoppers was quite steady no control routine was needed. In order to obtain meaningful data from the instrumentation, software routines had to be written.

It is necessary to have two basic routines, one to help perform the calibration of the equipment and the other to use the calibration values to print out useful parameters while the plant is running. Both routines were written in a real time assembler language with flexibility of operation as a major consideration.

The calibration routine allows any device to be selected and read with the option of performing a curve fit to the stored values and the corresponding physically measured quantities. This gives the necessary regression constants to be used by the data logging routine. This second routine essentially performs two operations, it reads the devices and writes out the measured quantities. When a device requires servicing the device is addressed and read and the output value is sequentially stored. While no device requires servicing, the routine accesses the stored data and uses the regression constants together with other data to print out hydraulic gradient, concentrations and the mean slurry velocity. At the end of a run the average of any set or sets of output are calculated, this essentially does away with the need for any off-line computation.

2.3 Experimental techniques in operation of the pilot plant

The *in situ* concentration devices must be adjusted for any drift by making any slight adjustment necessary to the H T voltage to make the clear water value agree with that used during calibration. Before an experimental run started it was advisable to back flush the tapping plates with low pressure water. Once a plate started to become blocked mains water (at about 2 bar) could be used to try to unblock it, though this did not always resolve the situation and it was often necessary to remove the plate and clean out the slots. It was of utmost importance when using the mains supply to isolate the transducers as sufficient pressure was available to overstrain the devices, if incorrectly applied.

With the line full of water (the concentration devices could be used to confirm this) and no flow in the transport line, the static output of the pressure transducers was typed into the computer routine. The weight of the hopper could not be offset in a similar manner as the slurry flowing into it produced an additional weight recorded by the load cells. This would remain constant as long as the velocity stayed the same and would not affect the results, as only a difference in the hopper weight was needed for calculation purposes.

The water pressure needed to force the slurry into the transport line was always higher than that needed to maintain steady flow. For the fine sand a peak pressure of 12 bar was often needed to initiate transport, the running hopper pressure was dependent upon velocity, a typical value at 1.5 m/s would be about 4 bar. The over-pressure decreased markedly with increasing particle size. It was also noticed that a marginally lower pressure was required to pump from the smaller angle hopper. For fine particles it is most probable (37) that fluid drag upon the particles is highly significant for flow in the vicinity of the discharge orifice. The discharge velocity from the hopper was observed to be independent of the solids head in the hopper, except when the hopper was very nearly empty. Steady slurry flow was therefore obtained by pumping clear water at a steady throughput to the top of the discharge hopper. This observation is in accord with the hopper being designated as mass-flow.

The initial charge of sand in the system was sufficient to give long run times, especially if several runs at different velocity were combined together. It was often possible to get up to 4 runs from one charge of the hopper. As a large over-pressure was needed it was better to start out at high velocity and make measurements by decreasing the velocity for each successive run, noting the position of the valves to avoid repetition. Except for very low velocities (below about 0.5 m/s) the bypass valve was found the most satisfactory means of controlling the slurry velocity.

With the data logging routine running output over a 4 minute period was collected when conditions became stable. In the middle of this period a sample of the slurry was taken together with a visual record of the horizontal flow in the visible flow section. In order to minimise disturbance to the flow as the exit conditions are changed during sampling, the volume of slurry taken was restricted to approximately 1,400 cm^3 when the velocity is below about 1 m/s. At higher velocities up to 2,000 cm^3 of slurry was removed. A plastic plate was held on the top of the measuring cylinder to prevent splashes of slurry from escaping.

At the end of an experimental run it was necessary to transfer the sand back to the feed hopper.

3. HORIZONTAL FLOW

3.1 Introduction

The frictional energy loss exhibited in the horizontal flow of solid-liquid mixtures has complex causes. To some extent a simplification can be made if the solid particles are fine enough (approximately 50 μm or less) so that the sedimentation rate of the bulk slurry is not excessively fast. These suspensions can be treated as single-phase homogeneous fluids, and can be characterised by viscometric parameters. Cheng (15,16) has shown that many industrial slurries can be described by a viscous Bingham plastic flow curve. The rheological properties can be used for full-scale design, or alternatively, correlations can be obtained from pilot scale work and used directly for scale-up without reference to rheological characterisation.

Solid-liquid mixtures which show a marked tendency to settle under conditions of no-flow are showing distinct two-phase behaviour. These mixtures can exhibit a complex range of recognisable flow patterns depending upon the physical properties of the solid and carrier fluid, and the mixture velocity and concentration. When the velocity of a mixture capable of settling is reduced the solids settle out into a sliding bed in the bottom of the pipe. Further reduction in velocity will cause the bed to become stationary.

3.2 General considerations

3.2.1 Types of flow pattern

The motion of solid particles over stationary and moving beds of the same granular material have been extensively investigated by Bagnold (5) and Francis (29). The bed grains, upon exceeding a certain size and mass, can be observed to jump up into the moving fluid stream as if they were acted upon by some momentary impulse at the bed surface. The particle then follows a smooth downward trajectory to the bed under the influence of gravity. Francis has shown by careful experimentation that this phenomenon of particle *saltation* can exist in the absence of fluid turbulence and must, therefore, be due to a separate dynamic process from that of transport in suspension by the internal eddy motions of

a turbulent fluid. It has been further shown that the forward motion of saltating grains is opposed by a frictional force of the same order as the immersed weight of solids, the friction coefficient being approximated by the angle of internal friction of the solids in the granular bed. This is perhaps not surprising since the saltation arises solely from momentary particle - particle contact. Saltating particles are, therefore, associated with the gravity bed of solids in the pipe and are included in the bed-load.

Upon increasing the stream velocity the shear stresses on the bed surface are increased, entering a range of stress where elongated dunes or ripples form on the bed surface. The downstream face of these dunes have a greater slope than the face opposing the flow. Particles are eroded and since they cannot be supported by the fluid, are re-deposited on the bed. The effect of these mobile grains is to increase the height of the dunes to such a point that the wall stresses overcome the driving force on the bed, this results in the bed gradually decelerating to a momentary halt. The restriction in the waterway above the stationary dunes causes the fluid shear stress to increase to such a value as to reinstate movement of the bed. Conditions at the surface are potentially unstable, and the bed as a whole moves in a series of unsteady jerks.

As the velocity of the slurry is increased particles begin to be supported when the random succession of upward impulses imparted upon the particles by the eddies of fluid turbulence exceed gravitational attraction. Suspended solids can, therefore, be distinguished from bed-load as the particles remain out of contact with the bed for an indefinite time depending upon the essentially random nature of turbulence. Bagnold (5) notes that a critical bed shear stress is necessary to initiate turbulent suspension, its value being dependent upon grain size. A distinctly asymmetric solids concentration profile exists across the pipe in what tends to be referred to as the *heterogeneous* flow régime. Durand & Condolios (21) report solids concentration profiles invariant of mean velocity for sand of average size 2.04 mm, however, for somewhat finer sand (0.18 mm) the still skew profiles became velocity dependent. It is interesting to note that the concentration profiles for the finer sand intersect at a common fraction of the pipe diameter.

The effect of increasing the mixture velocity is generally to make the concentration profile attain greater uniformity through the pipe. Gamma photon attenuation devices can be used to obtain position averaged concentrations along a chord. Grimley (33) showed a marked flattening of the concentration profile at high velocities, these measurements were backed up by some elegant experimental work in which the local concentration was measured directly without disturbing the flow by counting the particles in a small volume of the pipe. Local concentrations may also be obtained by the cross correlation of systematic gamma photon attenuation scans through a pipe (54).

True homogeneous flow occurs when there is uniform solids concentration across any radial section of the pipe. At some high velocity the solids concentration profile may approach the velocity profile of the fluid. Soo & Regalbuto (66) found that this was the case for a glass ballotini-air system.

The aforementioned description holds for reasonably closely graded, naturally rounded granular particles of up to about 500 μm transported in fluids like water. At velocities below about 0.5 m/s the finest sand showed the tendency to form unsteady dunes, whereas the coarser sands formed a steadily moving bed. This is reflected in the smaller spread in the experimental values of the hydraulic gradient exhibited by the coarser sands. This is clearly seen in Figure 3.4 and in the photograph of the flow of coarse sand at low velocity in Figure 3.13. It is unlikely that any industrial application using coarse particles would utilise suspended flow as the energy consumption resulting from the high fluid velocity would be prohibitive. In most practical applications the solid particles are not closely sized, under these conditions the coarser particles would travel as bed-load with the finer particles carried in suspension above. Distinction between the different flow regimes is difficult to observe due to the complexity of the behaviour of flow as one flow pattern tends to blend into the next. Substantial reduction in energy loss in a certain velocity range has been reported (36) for slurries comprising coarse particles transported in a heavy medium, such as clay. Kazanskij (41) reports that the reduction in frictional loss occurs only when the slurry is transported with substantial

bed-load. At higher velocities when suspension occurs the added fines tend to increase the pressure loss above that for the coarse material alone. The admixture of the fine particles to the carrier fluid can show significant non-Newtonian properties.

The mechanism by which momentum is transmitted to the pipe wall is highly dependent upon the flow régime of the slurry. For this reason many authors (30, 32) assign special designations to the changes in the nature of the flow pattern. The exact velocities at which these changes in flow pattern occur are difficult to locate as they are generally based upon visual observation in a transparent section of pipeline, where the flow is often notoriously merky. Only recently has the use of electrical probes (27) mounted in the pipe wall given a reproducible method of estimating the onset of changes in flow behaviour by reducing the element of human interpretation.

3.2.2 Pipeline operating velocity

A major part of pipeline design involves the selection of the operating velocity for the slurry and the estimation of the line pressure loss. Much contention exists in the literature regarding the *design velocity* for a pipeline conveying granular material. Too low a velocity results in the solids forming a stationary deposit in the pipe, resulting in line blockage. This lower limiting velocity has been referred to as the limit-deposit velocity by Sinclair (65) or, the velocity at the limit to the stationary bed zone (79). The first definition has been used to describe the velocity at which the first grains form a stationary deposit on the bottom of the pipe as the slurry velocity is reduced. The second refers to the conditions necessary to initiate the movement of a stationary deposit in the pipe. A minimum in the hydraulic gradient is closely associated with the above phenomena. The velocity occurring at this minimum is often loosely referred to as the *critical velocity*. The term is more aptly applied to non-Newtonian suspension of fine particles which often exhibit a change in rheological character in the form of a laminar-turbulent transition. Settling suspensions are sometimes referred to as being in *turbulent flow*, such a statement is meaningless unless justification for the flow régime is given -- criterion used for single-phase Newtonian flow cannot be applied

to a distinctly two-phase situation. Determining the velocity at minimum energy loss does not require observation of the flow pattern as it can be deduced from the hydraulic characteristic of the slurry, but in many instances the minimum is difficult to locate as the curve is very shallow. This short cut inspires the choice of the *critical velocity* as an operating point for the pipeline. Whilst this velocity often gives satisfactory design it is not certain that the velocity is always equal to or higher than the velocity at which a sliding-bed occurs. Most industrial pipelines are operated without deposition, but there is no reason why a sliding-bed of solids cannot be permitted, as long as the flow pattern is stable. If wear in the pipeline is highly dependent upon velocity, operating with a moving-bed may be a necessary economic criterion. From a practical viewpoint large pressure fluctuations are often present in well stratified flow which will tend to reduce the experimental accuracy in the region of the minimum energy loss.

3.2.3 Prediction of operating velocity

The literature contains a wealth of correlations for predicting the *operating velocity* from particle and pipe properties and the solids concentration. Weidenroth (77) assessed sixteen such relations by systematically altering the independent variables. He found a wide variation in the velocities predicted by the equations. The deviation in the prediction was very much smaller for fine sands in small pipes than for coarse sands in large pipes. This result perhaps reflects the fact that most correlations were developed from experimental work in small diameter lines. Carlton & Cheng (12) made a comparison of 50 correlations and found that the design velocity V could be expressed in the form of a power law:

$$V = K\ C^p\ D^q\ d^r\ (S - 1)^s \qquad (3.1)$$

The values of the indicies p, q, r and s are summarised in Table 1 of the above reference.

The velocities predicted from the correlations were compared with two working commercial iron ore lines. For the smaller diameter

line (24 mm) the relation under-predicted by about 30%, whilst for a larger diameter line (53 mm) the average over-prediction was around 120%. In both cases cited the agreement is poor. Carlton & Cheng found that most correlations include only particle size and density among the particle parameters, quite ignoring the fact that suspension will depend on other factors such as particle diameter, particle size distribution and shape; this arises from the difficulty in describing these parameters for use in mathematical formulations.

Correlations of experimental data, often based upon a dimensional analysis approach, are a convenient way of obtaining design equations with the minimum of analytical work. Satisfactory results can usually be obtained from data correlations only when they are applied to situations similar to those under which they were developed. Misleading results are often obtained when such correlations are indiscriminately used outside the range of variables for which they were developed. It is improbable that a single empirical correlation could be developed to cover all practical ranges of variables. Correlations inherently give little insight into the basic physical mechanisms, and no indication is given of ways in which the performance can be improved or the accuracy of prediction readily assessed.

By considering a force balance on a gravity deposit of particles in a pipe Wilson has developed a *physically-based* model to predict the limit to the stationary deposit zone (81). He presents his results in the form of nomograms which are readily applicable to slurries of particles greater than 150 μm in which the particle size distribution is not too diverse. The nomograms should prove particularly useful during design calculations for preliminary feasibility studies. The results of his analysis appear to be in good accord with experimental and commercial pipeline experience.

3.2.4 Methods for estimating head loss

A further important part of the design of a solids pipeline system involves the estimation of head differences under various conditions of flow. Whilst transient and line restart conditions must be

considered to deal with system malfunction or unplanned shut-down, by far the most important economic aspect involves the estimation of the pressure loss in the line under steady operating conditions.

Early investigators hoped to find a universally applicable formula that would accurately describe the energy loss in the complex heterogeneous flow régime where contact load and suspended load are both present. An empirical formula which has gained widespread recognition and use as a design tool is that due to Durand & Condolios (21, 22).

Perhaps realising the limitations imposed by adopting a correlation approach to the collation of experimental results, Durand and his co-workers performed large scale experiments in pipelines up to 580 mm in diameter conveying closely sized sands and gravels up to 25 mm. Durand & Condolios, like earlier workers, assumed that the relative increase in head loss above that of the carrier fluid alone $(i_t - i_o)/i_o$, which is attributed to the presence of the solids, is proportional to the volumetric solids concentration C.

$$\frac{i_t - i_o}{i_o} = \phi\, C \qquad (3.2)$$

They also proposed that when the solids were sufficiently large the relative excess hydraulic gradient was independent of particle size. This led to the inclusion of the particle drag coefficient C_D with other independent variables in the term ψ:

$$\psi = \frac{U^2\, C_D^{\frac{1}{2}}}{g\, D\, (S-1)} \qquad (3.3)$$

Using the parameters ϕ and ψ they found that their experimental results could be correlated by the expression:

$$\phi = K\, \psi^n \qquad (3.4)$$

using a value of K = 81 and n = - 1.5.

In the years following the publication of the final equation numerous investigators have proposed alternate values for K and n (13, 88).

Newitt et al. (48, 50) recognised that the flow pattern would have an effect on the mechanism of energy dissipation. They derived three semi-theoretical equations to describe the hydraulic characteristics of slurries flowing in a sliding-bed, fully homogeneous and the intermediate, heterogeneous régimes. These equations were tested against experimental results obtained from closely graded materials in a 25.4 mm (1.0 in) recirculating test loop. They found that slurries comprising coarser materials could be described by their equation for sliding-bed flow:

$$i_t - i_o = C_d \; K \; (S - 1) \qquad (3.5)$$

whilst results for finer materials were found to agree reasonably well with their equation for the heterogeneous flow régime.

$$i_t - i_o = C_d \; i_o \; K \; (S - 1) \; \frac{w}{U} \; \frac{Dg}{U^2} \qquad (3.6)$$

In both equations the value of the relevant constant K was obtained from a plot of the experimental results. The scope of the experiments was extended to cover mixtures of sands to produce wider particle size distributions. The inclusion of finer particles was found to alter the flow pattern so that sliding-bed transport occurred with *homogeneous* suspension. They found that the equations developed for closely graded sands could not be used with the same certainty for the wide size range slurries.

By the late 1960's there were a large number of relations for the prediction of head loss to be found in the technical literature. Zandi & Govatos (89) gathered over 2,500 items of data from numerous sources and after satisfying themselves that there was no deposition, used the remaining data to compare various equations. They found that only the Durand and Newitt equations, mentioned above, approached a satisfactory fit to the data. Using the experimental results to obtain a plot of ϕ as a function of ψ, as suggested by the Durand approach, it can be clearly seen (81, Figure 1) that whilst there is a rough correlation between the variables the points are widely scattered. This was often attributed to experimental error, or error introduced into the calculations when i_t and i_o have similar numerical values as is often the case.

Babcock (1, 2) questioned both the grouping of the variables in the Durand equation and the assumptions it was based upon. Having carefully performed experiments with closely graded materials Babcock was confident that he had reduced errors associated with the experimental work and the arithmetic operations upon the results. His results were internally consistent within each set; in attaining this he hoped to remove the scatter previously attributed to poor experimental technique. However, Babcock's results did not correlate at all well with the Durand variables. Upon closer examination he found that the relative increase in head loss was proportional to the volumetric solids concentration only when a sliding-bed of solids was established in the pipe. For conditions intermediate between the homogeneous suspension and sliding-bed régime the excess head loss may or may not be proportional to the volumetric solids concentration depending upon the particle size, concentration and velocity. He also found that the incremental head loss was only independent of particle size within the sliding-bed régime. Other investigators, Hayden & Stelson (34), Fowkes & Wancheck (28) and Schriek (64) have made comparisons with the Durand approach, and all indicate significant discrepancies in the prediction of experimental results -- these differences generally fall well outside the range attributable to experimental error.

Although it has now been shown that a substantial body of experimental evidence exists that cannot be reconciled with the Durand approach of correlating experimental data, many investigators still use it -- often with the intention of scaling up pilot-plant results.

Rose & Duckworth (58) performed a systematic dimensional analysis on the case of non-deposit flow in an attempt to develop generalised equations for the transport of solids in both liquids and gases. Their final correlation includes the same significant variables used by others, though the functional relationships are presented in a different form. The functional dependence of the groups in the analysis were tested with a wide variety of available data and found to give reasonable agreement.

The design methods considered so far have been based on experiments performed with closely sized materials. Commercial slurries tend to be of broad size distribution, and even at high velocities there is a tendency towards an asymmetric concentration profile through the pipe, because a substantial amount of contact-load may be present. Wasp et al. (75) describe an empirical method for calculating the pressure gradient in such a situation. By dividing the solids grading curve into a number of equal fractions and assuming that the flow is *turbulent* they obtain a solids distribution through the pipe. The variation of solids concentration within the pipe is used to determine the degree to which each fraction is transported *homogeneously* by rheological mechanisms or *heterogeneously* in accordance with a modified Durand equation. The total pressure drop is obtained by summing the two contributions. This method appears to give good results where there is a substantial amount of fine material in the grading curve.

The methods adopted by Wilson to describe the behaviour of settling slurries have already been touched upon in the previous section. His analysis is important as it considers the *global* physical mechanisms involved. Numerous techniques have been presented to describe the behaviour of slurries by taking into account local fluid and particle behaviour -- analysis of this type often result in lengthy and deeply involved mathematical operations involving the position history of the particles. The outcome of such a detailed approach is often difficult to apply to realistic problems. Wilson's analysis was originally developed to describe predominantly contact-load transport, subsequent development has allowed for the inclusion of turbulently suspended solids (80). Perhaps the single most important contribution arose from the postulate that the particles in a gravity bed of solids exert a hydrostatic type of stress distribution at the pipe wall.

3.3 Description of experimental results

The hydraulic characteristics of the three sands tested by the writer are presented in Figures 3.1, 3.2 and 3.3 and overlaid on Figure 3.4 for comparison. The ordinate of these Figures is

manometric gradient, namely the pressure loss measured by the differential pressure transducers, the abscissa is superficial mixture velocity. The *in situ* volumetric solids concentration is slightly dependent upon velocity as can be seen in Figures 3.5, 3.6 and 3.7. The value is around 47.5% for the two finer sands while the value for the coarsest material is around 43%, both some what lower than the freely settled value. The delivered solids concentration was invarient with velocity for the two coarser materials (See Figures 3.6 and 3.7) whilst a slight dependence upon velocity could be detected in Figure 3.5 for the case of the finest sand. The two finer sands were fed into the system at around 46% solids by volume, whilst the coarse material was fed at about 41% solids.

For all three sands the pressure loss is substantially higher than that for the flow of an equal discharge of clear water, which is depicted by the straight line on the right in the aforementioned Figures.

As the flow velocity is decreased from around 3 m/s the hydraulic losses become more dependent on particle size until at about 1 m/s no further reduction is obtained. The hydraulic losses attain asymptotic values, which are distinctly dependent upon particle size. The velocity at the *knee* of the curves roughly coincides with the visual observation that the solids concentration is becoming increasingly higher in the lower part of the pipe. Certainly below 0.9 m/s, for all three sands investigated, the solids were transported predominantly as bed-load, with a narrow, particle lean, water-way above. Experimentation was halted as the motion of the bed became extremely unstable upon progressively reducing the velocity, and conditions pertaining to a stationary bed were imminent. Due to the layout of the pipe run it cannot be ascertained with certainty whether the limiting condition occurred in the horizontal or vertical sections. As the solids concentration was higher for all three sands in the vertical rising section, it is felt that *jamming* of the solids in this section of pipework led to the condition of no flow.

3.4 Theoretical flow model

3.4.1 The two-layer approach

It is proposed to interpret these experimental results with an *idealised* two-layer stratified model, in which the moving bed deposit and water-way are considered separately. This concept of a two-layer approach has been investigated by several workers. Carstens (14) has proposed that *heterogeneous* flow can be described in this manner, but his theoretical investigation assumed negligible solids transport by bed-load. Kao & Wood (40) used essentially a two-layer model to interpret their results in connection with the conditions necessary to initiate resuspension of a stationary deposit of solids in a pipe. Unlike Wilson they did not consider the bed moving *en bloc* at any stage during erosion of the bed. Wilson et al. (83) have shown that the flow of high concentration slurries can be reconciled with a bed-slip mechanism. Televantos et al. (69) have recently published a model, which is conceptually similar to that of Wilson; however, their findings need further investigation.

In order to develop a two-layer model certain assumptions must be made with regard to the velocity profiles. Televantos (68) has shown that for high concentration conveying of coarse particles, assuming the velocity profile to be invariant through each layer may be a not unreasonable assumption.

3.4.2 Sliding bed-load

The wall stresses due to a moving bed of solids in a pipe are central to the two-layer analysis. For the case of a gravity bed of granular material in a pipe, Wilson has reasoned that the total normal stress at the pipe wall σ_p is not constant over the area of the deposit, but depends upon the submerged weight of the granular bed. This dependence is of a similar form to the hydrostatic pressure distribution exhibited by a fluid.

$$\frac{d\sigma_p}{dx} = C_2 \, g \, (\rho_p - \rho_f) \qquad (3.7)$$

Here C_2 is the *actual* volumetric solids concentration of the bed and the vertical co-ordinate x is defined in Figure 3.8.

Wilson justified this approach through an examination of the stresses within the granular bed, but concluded that a rigorous solution to the stress analysis of the non-cohesive granular bed forming the deposit in the pipe may not be readily attainable (78).

With reference to Figure 3.8, which defines the gravity deposit in terms of the half angle β, it can be seen that the depth of the deposit, x can be expressed in terms of the angular co-ordinate θ, measured in radians:

$$x = \frac{D}{2} (\cos \theta - \cos \beta)$$

The variation of normal stress with the angular co-ordinate can then be expressed as:

$$\frac{d\sigma_p}{d\theta} = -C_2 \frac{D}{2} g (\rho_p - \rho_f) \sin \theta \qquad (3.8)$$

The normal stress at a point on the pipe wall, defined by θ, can be obtained by integrating the above expression, to obtain:

$$(\sigma_p)_\theta = C_2 \frac{D}{2} g (\rho_p - \rho_f) (\cos \theta - \cos \beta) \qquad (3.9)$$

Summing the normal stress contributions over the total area of pipe occupied by the deposit allows the estimation of the total normal force F_n, exerted by the deposit at the pipe wall:

$$F_n = C_2 \frac{D^2}{2} g (\rho_p - \rho_f) (\sin \beta - \beta \cos \beta) \qquad (3.10)$$

3.4.3 Development of the two-layer model

From the geometry of the system, defined in Figures 3.8 and 3.9 the following expressions can be deduced:

$$A = A_1 + A_2 \qquad (3.11)$$

$$A_2 = D^2 (\beta - \sin \beta \cos \beta)/4 \qquad (3.12)$$

$$S_1 = D (\pi - \beta) \qquad (3.13)$$

$$S_2 = D\beta \qquad (3.14)$$

$$S_{1,2} = D \sin \beta \qquad (3.15)$$

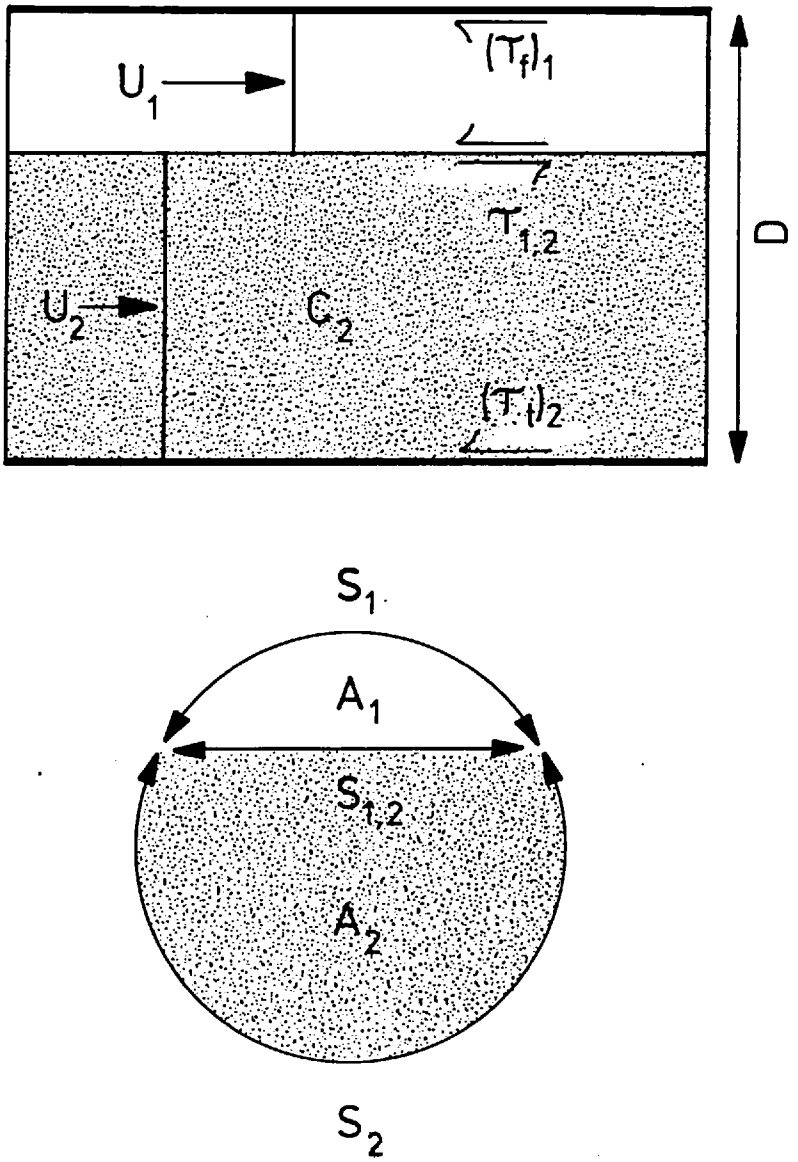


Figure 3.9

Defining figures for the two-layer model

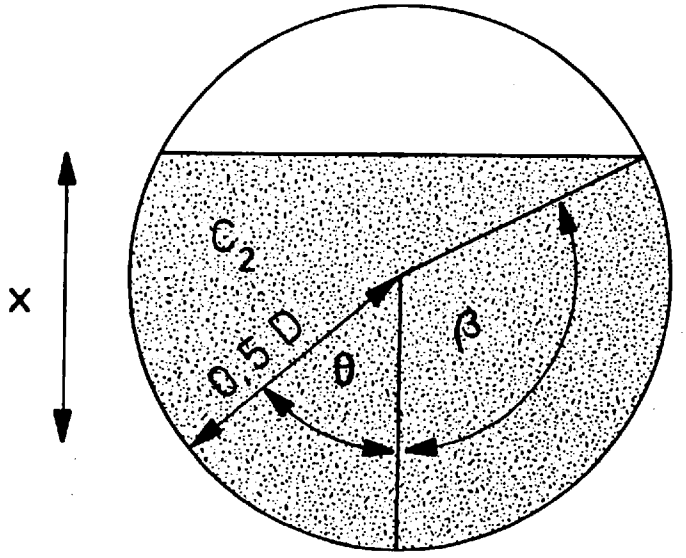


Figure 3.8

Defining figure for the bed-load component

The application of a momentum balance to the stratified system defined by Figures 3.8 and 3.9 under the conditions of fully developed flow where the linear frictional pressure drop is i_f, requires that the following be satisfied:

$$0 = i_f \; g \; \rho_f - (\tau_1 \; S_1 + \tau_{1,2} \; S_{1,2})/A_1 \qquad (3.16)$$

$$0 = i_f \; g \; \rho_f + (\tau_{1,2} \; S_{1,2} - \bar{\tau}_2 \; S_2)/A_2 \qquad (3.17)$$

The upper layer, defined by subscript 1, is assumed particle free, whilst the lower layer, defined by subscript 2, contains a moving gravity bed of particles, conditions at the interface are designated by the double subscript. Conservation of fluid and particles requires that:

$$AU_m = A_1 \; U_1 + A_2 \; U_2 \qquad (3.18)$$

where, U_m is the mean slurry velocity and:

$$A_2 \; U_2 = A_2 \; C_2 \; (u_p)_2 + A_2 \; (1 - C_2) \; (u_f)_2 \qquad (3.19)$$

For computational purposes it is convenient to define the volumetric solids concentration in the bed as C_2, this will be slightly larger than the bed concentration assuming no interphase slip defined as C_b:

$$C_b \; U_2 = C_2 \; (u_p)_2 \qquad (3.20)$$

The actual bed concentration is related to the measured *in situ* spatial concentration C by:

$$A_2 \; C_2 = A \; C \qquad (3.21)$$

and the delivered concentration C_d by:

$$A_2 \; C_2 \; (u_p)_2 = A \; C_d \; U_m \qquad (3.22)$$

The fluid shear stress at the pipe wall in the upper layer $(\tau_f)_1$ can be defined using the usual single phase relation:

$$(\tau_f)_1 = f \; U_1^2 \; \rho_f/2 \qquad (3.23)$$

for a smooth pipe containing turbulent fluid flow the Fanning friction factor f can be evaluated by:

$$f = 0.046 \; Re^{-0.2} \qquad (3.24)$$

The characteristic length needed for the evaluation of the Reynolds number Re, is usually taken as the pipe diameter. As the flow area is typically non-circular in this application an estimate of the equivalent diameter D_e has to be made through the usual relation:

$$D_e = 4 \; A_1/(S_1 + S_{1,2}) \qquad (3.25)$$

where S is a wetted perimeter.

The average total shear stress at the wall in the lower layer $(\bar{\tau}_t)_2$ will contain fluid and particle components:

$$(\bar{\tau}_t)_2 = (\tau_f)_2 + (\bar{\tau}_p)_2 \qquad (3.26)$$

The particulate component itself arises from two processes. The normal force at the pipe wall, due to the bed of particles, F_n has been considered earlier, the resulting shear stress is obtained by multiplication of this force by the coefficient of friction μ_p, between the particles and the wall. A further contribution arises from the conversion of the fluid shear stress arising at the interface. Bagnold (4, p. 242) has found that at particle concentrations prevailing immediately over granular beds less than 1% of the shear stress is maintained by the intergranular fluid, the remainder is maintained by solid transmitted stress. The maximum ratio of intergranular shear to intergranular pressure that a cohesionless granular material can withstand is given by tan ϕ, where ϕ is the internal angle of friction. As the bed is considered to be in *limiting* equilibrium, stresses arising at the interface are transmitted through the bed to the wall. The resulting stress is given by the second contribution in Equation 3.27.

$$(\bar{\tau}_p)_2 = C_2 \frac{D^2}{2} g (\rho_s - \rho_f) (\sin \beta - \beta \cos \beta) \mu_p / S_2 + \mu_p \tau_{1,2} / \tan \phi \qquad (3.27)$$

The specification of the fluid boundary shear stress associated with the lower layer is rather more difficult. A relation similar to Equation 3.23 is proposed, the specification of the characteristic length to be used in obtaining the Reynolds number has a pronounced effect on the model, and a discussion of this will be left to a later section.

The sign associated with the interfacial shear stress arises as the upper layer of fluid is assumed to be travelling at a higher velocity than that of the bed of solids. Televantos (68) made approximate measurements of the velocity in such a stratified system and verified that this assumption is indeed true. The shear stress can be determined by considering the velocity as that relative to the two layers.

$$\tau_{1,2} = f_{1,2} (U_1 - U_2)^2 / 2 \qquad (3.28)$$

From a cursory inspection it would seem reasonable to assign fluid and particle components to the interfacial shear stress in the lower layer. When the nature of this interface is considered such an approach may not be necessary. The action of the fluid shear stress will tend to dilate the surface of the bed in the vicinity of the topmost grains. As the boundary would appear rough it would seem most likely that the force on the fluid, under these conditions, would be small in comparison to that experienced by the mobile particles. The value of the friction factor used in this study is that obtained from an experimentally derived relation due to Nikuradse (51) for sand roughened pipes where he assigned the value of k equal to the sand grain diameter. In these experiments the sand was adhered to the pipe wall with varnish and it is probable that the grains were at least half submerged in varnish. Yalin (87) has suggested that for flow over naturally rough sand boundaries the value of k should be 2d.

$$f_{1,2} = \left[4 \log_{10}\left(\frac{D}{2k}\right) + 3.48\right]^{-2} \qquad (3.29)$$

The pressure gradient along the pipe will cause a small flow of fluid through the interstices of the bed. Whilst the fluid flow rate is quite small, and usually neglected, the forces exerted by this interstitial flow are significant and together with the interfacial shear force they constitute the driving force on the bed. An analysis of the fluid flow in the lower layer can be obtained by recognising that the momentum balance on the lower layer is in fact the sum of two such equations, one for the fluid and one for the particles. Adopting a technique used by Wallis (74) to describe the forces, these two momentum balances are:

$$0 = i_f \rho_f g A_2(1 - C_2) + (F_f)_p + (F_f)_w \qquad (3.30)$$

$$0 = i_f \rho_f g A_2 C_2 + (F_p)_f + (F_p)_w \qquad (3.31)$$

Here, $(F_f)_w$ and $(F_p)_w$ are wall drag forces on the fluid and particles, and $(F_f)_p$ and $(F_p)_f$ are the drag forces of the fluid on the particles and the particles on the fluid. The mutual

hydrodynamic drag between the phases must be of equal magnitude and opposite sign.

$$(F_f)_p + (F_p)_f = 0 \tag{3.32}$$

Taking note of the comments below Equation 3.28 the components acting on the wall are:

$$(F_f)_w = - (\bar{\tau}_f)_2 \; S_2 \tag{3.33}$$

$$(F_p)_w = \tau_{1,2} \; S_{1,2} - (\bar{\tau}_p)_2 \; S_2 \tag{3.34}$$

The frictional pressure drop through a granular porous mass of particles in contact can be represented by the Ergun Equation (18, p. 9).

$$i_f \; \rho_f \; g = 150 \; \frac{C_2^{\,2}}{(1-C_2)^2} \; \frac{\mu_f \; u_f}{d^2} + 1.75 \; \frac{C_2}{(1-C_2)} \; \frac{u_f |u_f| \rho_f}{d} \tag{3.35}$$

This equation is a statement of the drag force on the fluid by the solid particles, per unit volume of fluid phase, in terms of the interstitial fluid velocity u_f, when the particle velocity is zero. This arises by virtue of Equation 3.30 as fluid wall effects can be neglected in comparison to drag effects in the bulk flow. This force is really dependent upon the relative velocity u_r of the two phases:

$$u_r = (u_f)_2 - (u_p)_2 \tag{3.36}$$

and not only upon u_f. When $u_p \neq 0$ Equation 3.35 can still be used provided u_f is replaced by u_r.

$$(F_f)_p = A_2 \left[150 \; \frac{C_2^{\,2}}{(1-C_2)} \; \frac{\mu_f \; u_r}{d^2} + 1.75 \; C_2 \; \frac{u_r |u_r| \rho_f}{d} \right] \tag{3.37}$$

(The use of the absolute value of u_f is included in the above equations in order that information should not be lost in the event of a negative sign).

3.4.4 Computational procedure

The two-layer model described in the previous section was used to interpret the experimental results obtained from the horizontal section of pipework in the pilot plant.

The physical properties of the carrier fluid and the three sands are given in Appendix 1. The mean slurry velocity delivered and actual bed concentrations are taken as the main input variables for the computational scheme. The equations describing the model are solved using an iterative technique to locate the interface between the two layers. For a given bed concentration the measured *in situ* solids concentration can give a fairly good estimate of the depth of the bed of solids described by the half angle β, hence a sensible range of values can be prescribed for the search region of this variable. With a value assigned to the angle β the geometry of the system can be obtained using Equations 3.11 through to 3.15. A first estimate of the bed concentration C_b, is taken to be C_2. With a knowledge of the mean slurry velocity and the delivered solids concentration, the mean velocities of the two layers can be calculated. This enables the shear stresses to be calculated so that the value of the drag force on the fluid by the particles can be obtained by eliminating the pressure drop term between Equations 3.30 and 3.31, and the complementary force on the particles using Equation 3.32.

$$(F_f)_p = C_2 \ (\tau_f)_2 \ S_2 + (1 - C_2) \ \tau_{1,2} \ S_{1,2} - (1-C_2) \ (\bar{\tau}_p)_2 \ S_2 \qquad (3.38)$$

This expression together with Equation 3.37 forms an iterative loop to enable the relative velocity u_r to be calculated. The value of u_r was found to always lie within the range $0 < u_r < 0.1 \ U_2$. The value of u_r calculated by this means can then be used to obtain a further estimate of C_b from:

$$C_b = C_2 \ U_2 - u_r \ (1 - C_2) \ / U_2 \qquad (3.39)$$

This value of C_b is returned to the iteration scheme until satisfactory convergence is obtained. Using currently calculated values

of the parameters the force balances on the two layers (Equations 3.16 and 3.17) are evaluated. The difference in numerical value between these two equations will not be equal to zero unless the chosen value of β is correct. The sign associated with the difference in the numerical value of the two equations and the range of the angle assigned to β are used in an overall iterative loop to determine the value of β consistent with the input values of C_d, C_2 and U_m. When the value of the difference between the force balance equations approaches a small fraction of the *slowest* function (Equation 3.17) the value of the hydraulic gradient is obtained from this equation. The iterative calculations can be repeated with new values of C_2 and U_m. For convenience the overall computational scheme is handled by a computer algorithm. From the output the hydraulic gradient predicted by the model was obtained such that the mean velocity and both concentrations were in agreement with the experimentally measured values. In this manner the solid lines were obtained in Figures 3.10 to 3.12.

3.5 Comparison of the analysis with experimental results

3.5.1 Sensitivity analysis of the model

The two-layer model has proven to be particularly satisfactory for the analysis of the low velocity results, namely the almost horizontal part of the hydraulic characteristic below about 1 m/s. The results of this analysis are overlaid using a solid line on the experimental results in Figures 3.10 to 3.12. It can be seen from these Figures that predictions of this model do not describe very well the losses at higher velocities. Here an alternative approach will be discussed.

It is worth while performing a sensitivity analysis on variables used in the two-layer model to see which are significant in effecting its performance. From this a better insight can be obtained into which frictional mechanisms are responsible for the total energy loss for this particular model of the system.

As mentioned in the preceding section the model is used to predict the location of the interface between the two layers. With a bed concentration taken to be around the freely settled value, it can

be shown from the spatial *in situ* concentration measurements for the two finer sands that the value of the interface should be around 2.4 radians (135 Deg.). The predictions from the model were found to agree well with this. The value of β for the coarsest sand, which was fed more dilutely into the system, was found to be around 2.18 radians (125 Deg.) and was also in good agreement. These calculations agree with the visual observation that the pipe appeared over 4/5ths full of solids for the finer two sands and a little below this figure for the coarse sand (see Figure 3.13).

The effect of the clear-water friction factor, associated with the upper layer, did not have a pronounced effect on the results, because in this case the waterway area is small. For the analysis of lower concentration flows this variable could be appreciably more significant. The choice of d or 2d as the characteristic length for the evaluation of the interfacial friction factor was not crucial. Variables associated with the bed-deposit have been found to have a more significant effect on the predictions from the model, in particular those parameters associated with the wall shear stresses. Both the value of the coefficient of friction between the particles and the pipe wall, and that of the fluid friction factor at the wall will be considered in detail, as both of these have a considerable effect on the model.

For a granular material there are two distinct frictional systems to be considered, one relating to internal resistance to shear and the other to shear at the wall.

When relative motion occurs within a granular mass, frictional forces are set up. The simplest frictional model postulates a linear relation between direct normal stress σ and tangential shear stress τ, the proportionality constant being the internal coefficient of friction. The angle ϕ is often referred to as the internal angle of friction.

$$\tau = \sigma \tan \phi \qquad (3.40)$$

The frictional resistance to shear in granular materials is more complex than between solid bodies, since it is associated with both rolling and sliding motions of the particles. For most cohesionless granular solids of natural shape and surface texture the angle of internal friction differs little from 30 deg. whether measured in water or air, though this value is slightly dependent upon normal stress (57). Altering the value of ϕ by 5 degrees either side of this value did not have a significant effect on the model's predictions.

The frictional resistance set up when a bed of solids moves *en bloc* relative to a flat surface is of the same form as Equation 3.40 except that the constant of proportionality between the stresses is termed the coefficient of sliding friction, designated here as μ_p. The value of this coefficient is dependent upon the number of grain contacts per unit area, and the type and surface texture of material forming the solid surface. In general it is found that the value of μ_p is independent of velocity, but some contention upon this point seems to exist (69) especially when the phenomena of the *stick slip* is experienced.

The coefficient of friction between the particles and the wall has a pronounced effect on the predictions from the two-layer model. The value of μ_p essentially locates the hydraulic characteristic vertically on the i_f, U_m plot. The effect of increasing the value of μ_p, as will be seen from Equation 3.27, is to increase the frictional gradient. From a design standpoint the value assigned to the friction coefficient is of great importance. The literature contains a limited amount of information on this parameter and no single systematic investigation appears to have been carried out. Several methods are available for its measurement. Wilson (78) suggests a method of estimating the value using a tilting tube containing a bed of particles which is a direct pipeline analogy to the normal dynamic case used in mechanics. However, the method appears not to be very reproducible. The most direct method of measurement uses a shear box -- a well developed piece of apparatus used in experimental investigations into the mechanics of soils (67, 72). This apparatus is well suited to measuring both frictional coefficients. Whilst designed to measure the internal coefficient of friction the apparatus can

be readily modified to measure the coefficient of sliding friction of a sand mass against a plane surface by replacing the lower part of the shear box with a specimen of the material against which the sand mass is to be sheared.

Butterfield & Andraws (9) measured the coefficient of friction for a dry sand against perspex, glass and steel surfaces by plotting the stresses in Equation 3.40. They found that the surface material and also the porosity of the sand, had some effect on the coefficient of friction. Their results show clearly that the static coefficient of friction, obtained at the onset of motion, is larger than the kinetic value obtained during subsequent slow motion. Rowe (60) made a systematic study of the effect of particle size on the angle of sliding friction ($= \tan^{-1}\mu_p$). He reports a variation of 1 degree in the angle of friction for normal stresses in the range 14 to 890 kN/m^2 (2 to 100 lbf/in^2) when flooded sands were sheared over a flat quartz surface. Rowe found that the dependence of the angle of friction on particle diameter could be described by:

$$\mu_p = \tan (22.4 - 5.3 \log d) \qquad (3.41)$$

provided that $0.02 \leq d \leq 2$ where d is measured in mm and the argument in Equation 3.41 is measured in degrees. Also working with a flooded mass of sand Cumoliŏglu (19) reports a variation of the friction coefficient with sand porosity, surface material, particle shape and normal stress. In an attempt to reproduce shear experiments under the normal stress conditions commonly encountered in bed-deposit flow in pipe lines, he worked at low normal stresses. He found that the friction coefficient for nominally 0.32 mm sand under low normal stress , up to 7 kN/m^2 (1 lbf/in^2) was almost twice the value obtained for the same material under similar conditions at somewhat higher normal stress , 14 to 124 kN/m^2 (2 to 18 lbf/in^2). The friction coefficient as defined by Equation 3.40 is inherently independent of the absolute values of the stresses, as indeed has been shown by many investigators. If this effect shown by Cumoliŏglu is a real physical effect, predominant under low normal stresses, it is most important. However, it is more likely to be an artifact of the experimental apparatus. Under low normal stress with small grains the shear stress tends to be unsteady

due to excessive *stick slip* of the top part of the shear box over the base plate; this is shown in the wide variation in the results of the above author (19, Figure 5.2.1). The upper part of the shear box tends to *ride up* and trap sand grains between it and the base plate. These sand grains then cause additional friction, which cannot be accounted for in calibration experiments. Although there is significant scatter in the above results there is a sufficiently clear trend to see that the friction coefficient tends to decrease with decreasing solids concentration.

The value of the angle of friction predicted by Rowe's experimental plot have been used in this investigation as input to the model, since they are the only results giving the dependence upon particle size for a flooded granular mass. As the foregoing discussion has shown there is much scope for research into this important variable.

Rowe's results satisfactorily explain the trend of the experimental results with particle size for the three sands investigated, as can be seen most clearly in Figure 3.4. The horizontal lines lie in fairly good agreement with the experimental points.

The horizontal flow model was found to produce values of the *in situ* and delivered solids concentration essentially the same as the experimentally measured values when the *actual* solids concentration in the bed, C_2 was taken as the freely settled value for the particular sand.

3.5.2 Low velocity results

At low velocities, while a gravity bed of solids is still clearly evident in the pipe, the value of the fluid friction factor associated with the lower layer has little effect on the model. This well stratified flow régime is shown in Figure 3.13. At these velocities the predominating frictional contribution arises from particle-wall contact. The fluid wall shear stress becomes increasingly more important as the velocity is increased above 1 m/s. The use of the equivalent diameter of the flow area of the lower layer, as the length scale for the evaluation of the Reynold's number, for use in Equation 3.24, does not give

a sufficiently high fluid contribution. It may be more appropriate to take the length as the particle diameter, or a fraction thereof, as suggested by Televantos et al. (69). The continuation of the horizontal lines in Figures 3.10, 3.11 and 3.12 are based on one particle diameter. Decreasing this to 0.5d did not have a significant effect on the position of the line. By making this length scale arbitarily small the predicted losses could be made to look more like those shown by the experimental points.

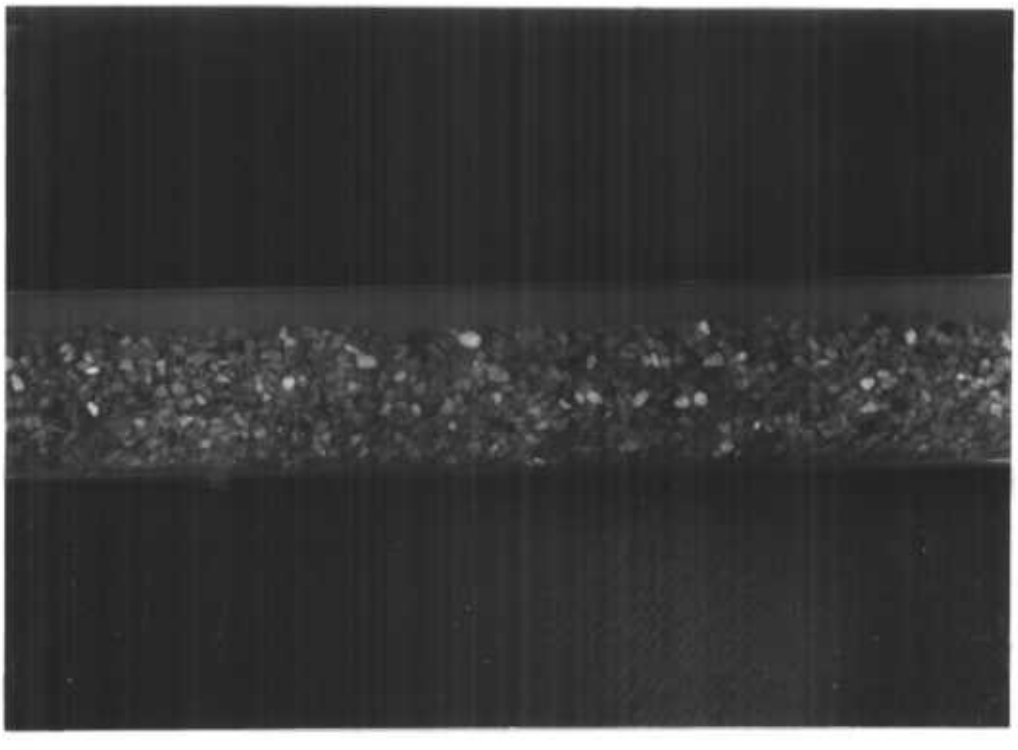


Figure 3.13

Photograph of the flow pattern of coarse sand at a mean velocity around 0.5 m/s reproduced actual size

3.5.3 High velocity results

The effect of increasing the velocity above the maximum which exists in the horizontal part of the curves is that the interfacial shear stress tends to loosen the surface of the bed. As the pressure gradient across the deposit increases the shear stresses within the granular bed increase disproportionately to the normal pressure. Thus Equation 3.40 can no longer be read as an equality. In practice this means that the bed of particles and the interstitial fluid begin to shear. Whilst no measurements of velocity profiles have been made in this investigation, Bantin's work (6), with radioactive tracers in a high concentration glass ballotini system, shows the existence of distinct velocity profiles in both phases. For shear to take place within a granular mass of solids some degree of dispersion or dilation of the mass must take place, to allow for the relative movement of the particles. This was demonstrated many years ago by Reynolds (56) who showed that if a mass of loose particles are

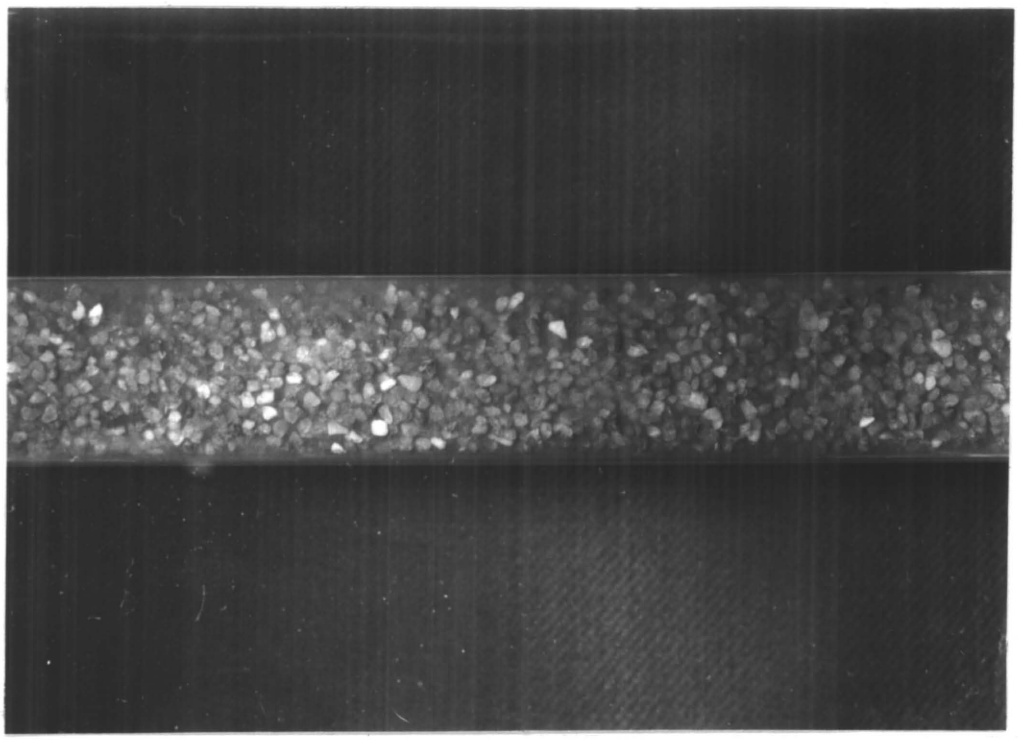


Figure 3.14

Photograph of the flow pattern of coarse sand at a mean velocity around 2.5 m/s

reproduced actual size

prevented from dilating they behave as a rigid body. The result of this dispersion of the particles associated with high flow velocities is to make the pipe appear full of solids as can be seen in Figure 3.14.

Mechanical forces are transmitted to the dispersion of particles either by the fluid or by other particles. Momentum can be transferred from one mass of fluid to another and then to unsupported particles. In anisotropic shear turbulence such a mechanism would lend to the support of the particles, once a certain threshold value of the shear turbulence had been exceeded. Momentum can also be transmitted from particle to particle by continuous or intermittent contact. In laminar flow, Bagnold (4) has shown that a granular mass can be dispersed in a fluid under conditions when shear turbulence is extremely weak or even non-existent. Under these conditions the particles are supported by the impulse of momentum from the previous particle contact. Over a period of time the weight of the particles supported in this manner would equal the mean upward flux of momentum per unit time. The solid transmitted stress arises from the shearing of the particles over one another, similarly the fluid transmitted stress arises from the shearing of the fluid, for this maintains the necessary internal turbulent motion. Both are maintained by the applied pressure force. Bagnold used similar reasoning to show that particles which were not suspended by fluid turbulence and which were not in continuous contact could transmit particulate stresses to the bottom of an open channel. For the case of a sheared deposit in a pipe this particulate stress will be transmitted to the wall of the pipe in the same manner as that previously considered for a gravity bed of particles which are in contact. There will also be a normal stress at the pipe wall arising from the knocking or jostling of the particles within the flow field.

Many relations have been proposed to determine the conditions required for the onset of turbulent suspension of solid particles. The vast majority of these have been developed for unpressurised, open channel flow, and are not strictly applicable to pipeline conditions. Wilson & Watt (84) suggest a method for calculating the velocity needed to initiate turbulent suspension

V which is an exponential function of the particle to pipe diameter.

$$V = 0.6\, w \left(\frac{2}{f}\right)^{\frac{1}{2}} \exp\left(\frac{45d}{D}\right) \qquad (3.42)$$

Here f is the fanning friction factor for an equal discharge of clear fluid, and w is the particle fall velocity. Their formula appears to be in good agreement with the results from several laboratories although the range of particle to pipe diameters tested was relatively small (0.01 to 0.03). Applying this equation to the three sands investigated indicates no suspension, even at the maximum velocity.

As the particles would appear not to be suspended by fluid turbulence they may still be considered as constituting a bed-load.

The results of subtracting the particulate wall stress, associated with the bed, from the total wall stress at different velocities are presented in Table 3.1. For convenience the wall stresses are expressed in terms of frictional hydraulic gradient. The hydraulic gradient obtained for the flow of an equal discharge of clear water at the same velocity is also shown. In all instances these mixture losses are higher than for the flow of clear water alone.

Table 3.1

The difference between the total head loss and that attributable to the bed-load at various velocities

MATERIAL	MEAN VELOCITY / (m/s)		
	1.4	2	3
FINE SAND	0.12	0.25	0.7
MEDIUM SAND	0.12	0.27	0.7
COARSE SAND	0.09	0.24	0.67
CLEAR WATER	0.087	0.17	0.35

These results have been obtained for each of the three sands, by subtracting from the smoothed value of the total loss, the *bed-load value* predicted by extending the horizontal line in Figures 3.10 to 3.12. A very small error is introduced by neglecting the small increase in bed depth due to the whole of the pipe being filled with the bed-load.

From a first glance at these results in the above table it may be concluded that there is a small particle size dependence between the finer two sands and the coarsest. However, it must be remembered that the input concentration for the coarsest sand was somewhat lower than that for the other two sands. This accounts for the small difference seen in the above sets of results. It is found that at the higher velocities this extra loss, which is independent of particle diameter, can be taken into account by using a pseudo-homogeneous type of correction (ρ_m/ρ_f), to the clear water loss.

3.5.4 The pseudo-homogeneous correction

Recently Savage & Cowin (63) have proposed a constitutive equation for the flow of cohesionless granular materials. Their equation is intended to represent the flow behaviour of the two-phase system under relatively low normal stress at high shear rates corresponding to Bagnold's so-called *grain inertia* region. Here the fluid in the interstices plays a minor rôle in comparison to the dominant energy dissipating effects arising from particle-particle interactions. The theory is not intended to represent the stresses when the rate of deformation tends to zero. Their work should, therefore, be applicable to the high velocity results obtained in this current investigation.

The authors propose that the total shear stress $\underline{\tau}_t$ has components which can be expressed in terms of an equilibrium stress $\underline{\tau}_o$ and contributions due to the presence of concentration and velocity profiles within the flow field. Their expression has the form;

$$\underline{\tau}_t = \underline{\tau}_o + a_1 \underline{I} + a_2 \underline{D} + a_3 \underline{M} + a_4 (\underline{M}\cdot\underline{D} + \underline{D}\cdot\underline{M}) \qquad (3.43)$$

where the rate of deformation tensor $\underline{D}$ necessarily contains elements relating to the local velocity gradient, and $\underline{M}$ describes the local solids concentration gradients within the flow field.

The coefficients a_1 to a_4 are functions of both local concentration and velocity.

At low velocities where $\underline{D}$ tends to zero, $\underline{\tau}_t$ approaches the equilibrium value, where $\underline{\tau}_o$ arises from the hydrostatic inter-particulate stress due to the weight of particles. At higher velocities $\underline{D}$ is large enough to enable the term $a_2\underline{D}$ to make a significant additional contribution to the total wall stress. Since the term a_2 depends upon the local velocity gradient, $a_2\underline{D}$ will be proportional to the square of the velocity gradient. This will lead to a shear stress for the two-phase system which should lie parallel to the water curve, but displaced from it. Equation 3.43 is therefore a mathematical statement of the findings in the previous section -- namely that at high shear rates the total stress consists of a bed-load component plus a contribution to take into account the momentum transfer by particle-particle interactions. Equation 3.43 accounts for the non-Newtonian nature of the flow as evidenced by Bagnold's (3) experiments, whilst also satisfying the traditional Mohr - Coulomb condition.

The authors propose the use of Equation 3.43 for the prediction of the behaviour of simple two-dimensional flow examples. Difficulty was experienced by them in making a direct comparison with experimental evidence due to certain experimental problems. Their experiments did, however, reflect the general trends of the analysis in the shapes of the velocity profiles.

The direct application of this theory to the three-dimensional case of pipeline flow would require much more information pertaining to the local solids concentration and velocity profiles than is currently available. Accurately making these measurements without unduly disturbing the flow is in itself a difficult task.

The result of adding the frictional loss, approximated by the pseudo-homogeneous adjustment to the clear-water loss, to the bed-load component for the three sands is given in Figures 3.15 to 3.17. The computational results are in excellent agreement with the experimental points in all three cases.

3.5.5 Comparison with results from another laboratory

Televantos et al. (69) used a stratified model to analyse some interesting high concentration slurry results obtained in a 78.7 mm (3.1 in.) line. The hydraulic behaviour of the closely sized coarse gravel, - 7.9 + 3.3 mm (- 5/16 in. + 4 BSS mesh) is shown in Figure 3.18 and the *in situ* concentration in Figure 3.19. The co-ordinate of both figures is mean slurry velocity. The clear water line is given by a smooth pipe relation. It can be seen that at low velocities, below 1 m/s, when a bed of solids was reported to be visible in the line, the pressure loss tends to rise to high values. This is unlike the results obtained in the current investigation where the low velocity losses were independent of velocity. Televantos' low velocity results can be explained in part by the *in situ* concentration increasing rapidly (and hence the value of $((\tau_p)_2)$ and partly by a *stick slip* effect of the gravel against the ABS plastic pipeline. Rabinowicz (55, p. 97) has shown that such an effect can occur at low velocities when the static value of the coefficient of friction is much larger than the dynamic value. As the velocity increases above 1 m/s the frictional losses again increase. In order to explain this hydraulic behaviour Televantos et al. found it necessary to make the coefficient of sliding friction μ_p, velocity dependent. The magnitude of μ_p follows a similar trend to the hydraulic characteristic. This has the effect of making the character of the particle wall stress more like that exhibited by fluids. This type of approach may be satisfactory at low velocities to provide an approximation to the time dependent phenomena of *stick slip*. However, the increase in the value of μ_p after about 1 m/s seems unlikely. Using this approach for design has the inbuilt complication that the models predictions are highly dependent upon the velocity dependence of μ_p and as yet there is no way of predicting this previously unreported behaviour. The hydraulic characteristic of the gravel can be partly explained, at velocities above the minimum, by the analysis proposed here.

The coefficient of sliding friction is evaluated by a small extrapolation of Equation 3.41. The contact-load component is then added to the mixture density correction of the clear-water hydraulic gradient, to obtain the total loss given by the solid line in Figure 3.18. Other data presented by the same author (68) are less amenable to analysis, because in one case, the *in situ* concentration appears to go above the packed settled value, and in the other a wide-size-range material was used. The use of such a material poses a problem for the selection of μ_p as the number of particle contacts per unit area are inconsistant with the use of a mean particle diameter. There is also a likelihood of particle suspension under the reported conditions.

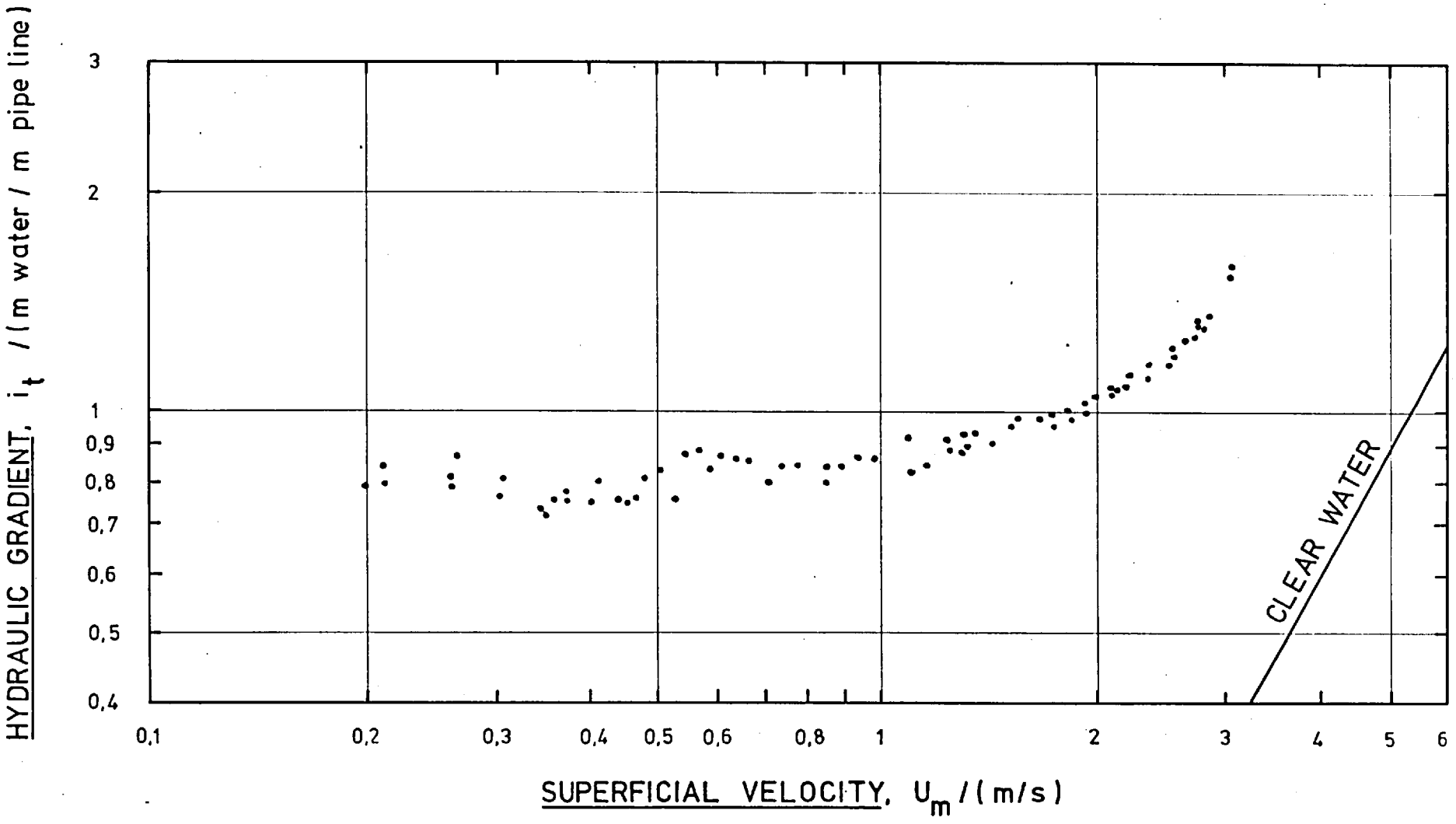


Figure 3.1

The experimental points describing the hydraulic characteristic of the fine sand in horizontal flow

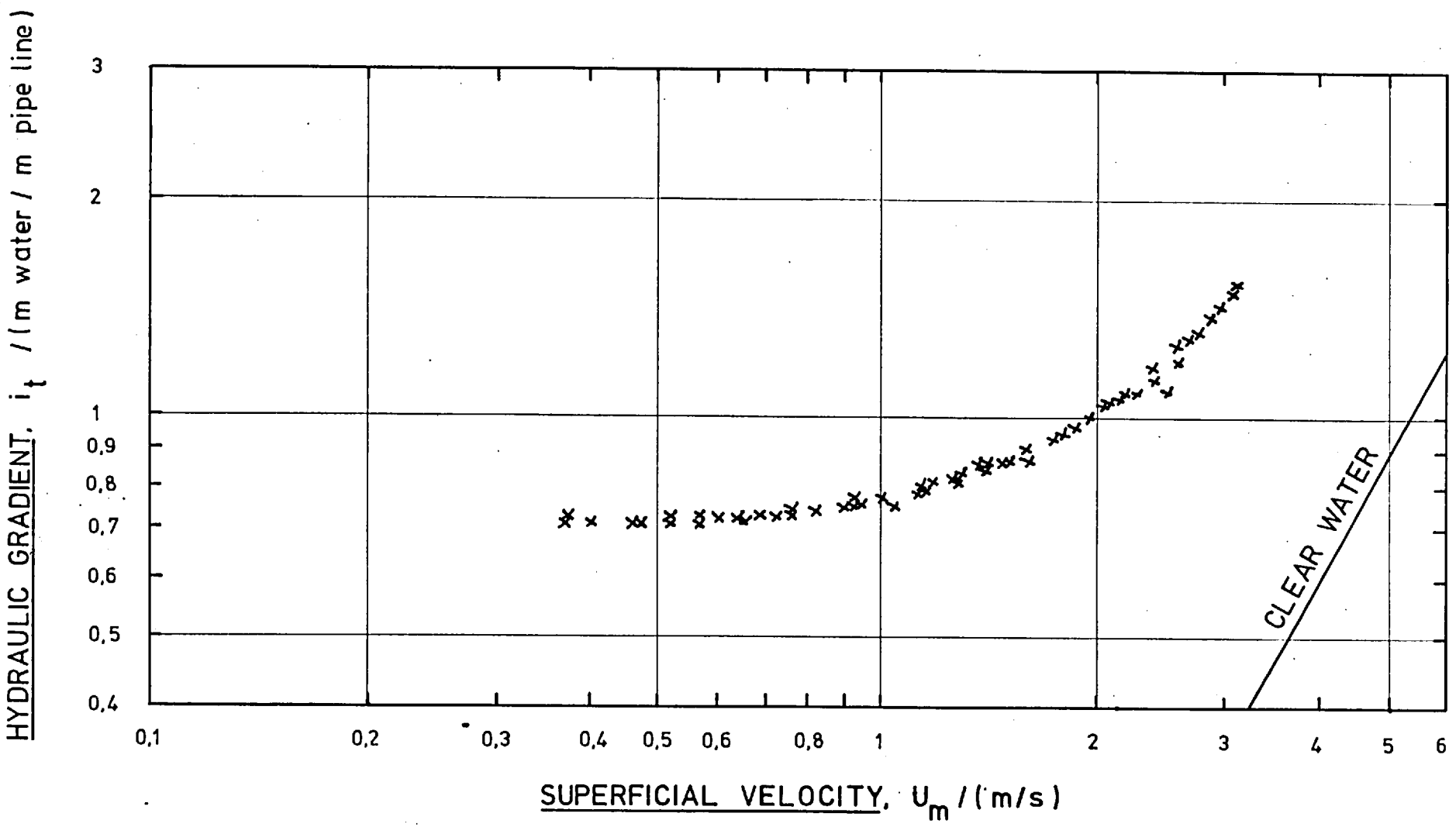


Figure 3.2

The experimental points describing the hydraulic characteristic of the medium sand in horizontal flow

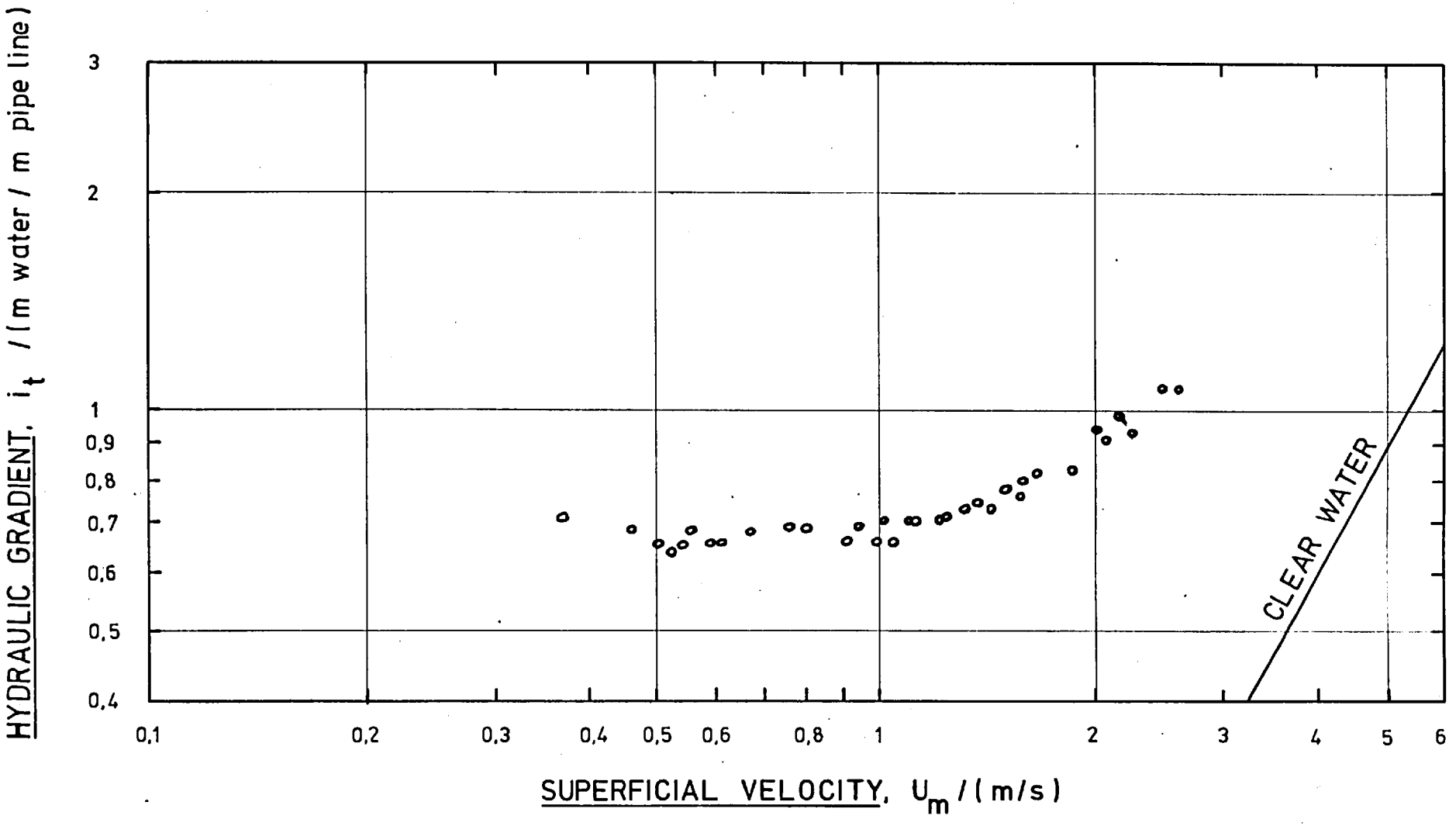


Figure 3.3

The experimental points describing the hydraulic characteristic of the coarse sand in horizontal flow

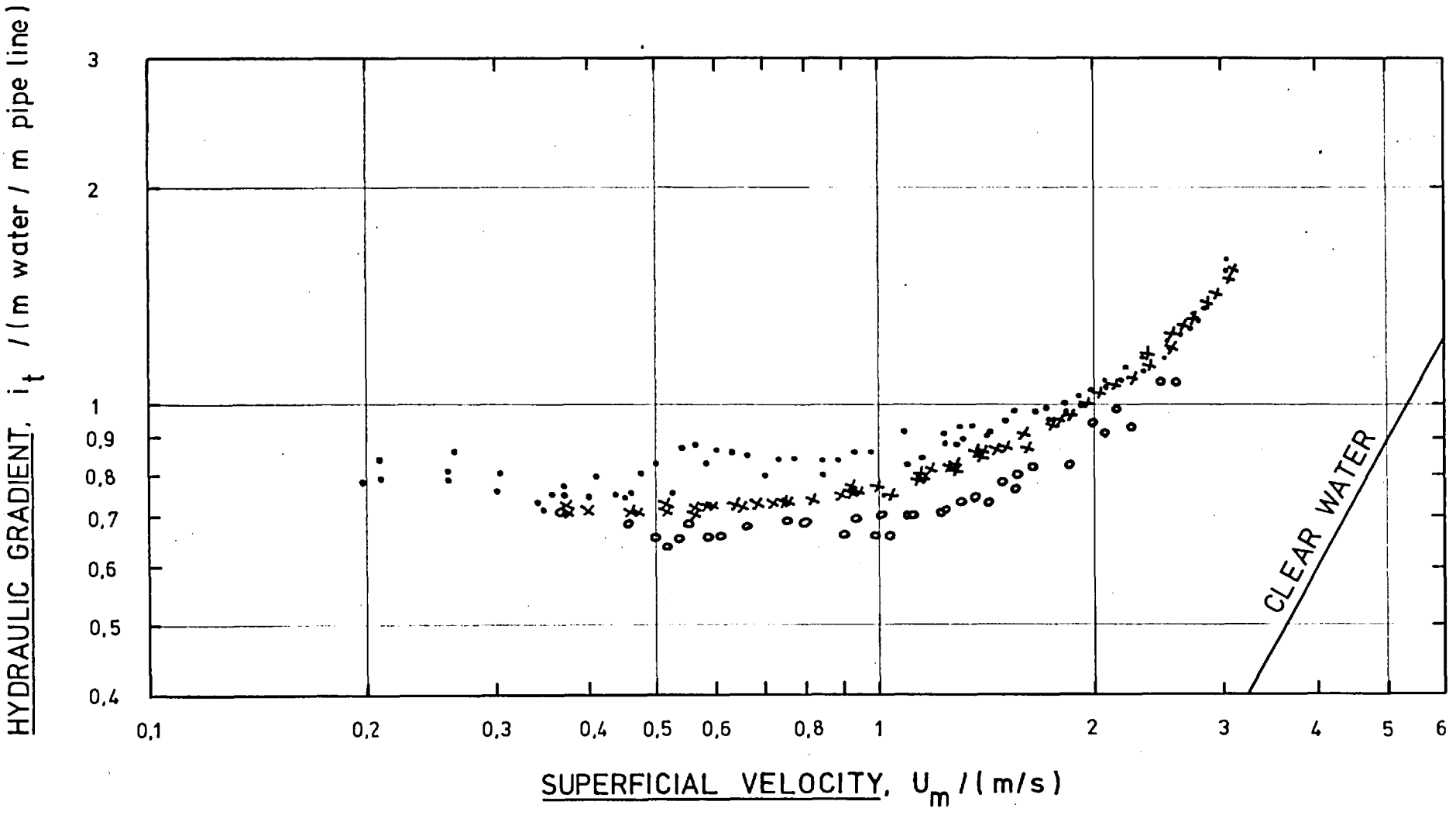


Figure 3.4

Overlay of the experimental points describing the hydraulic characteristic of all three sands

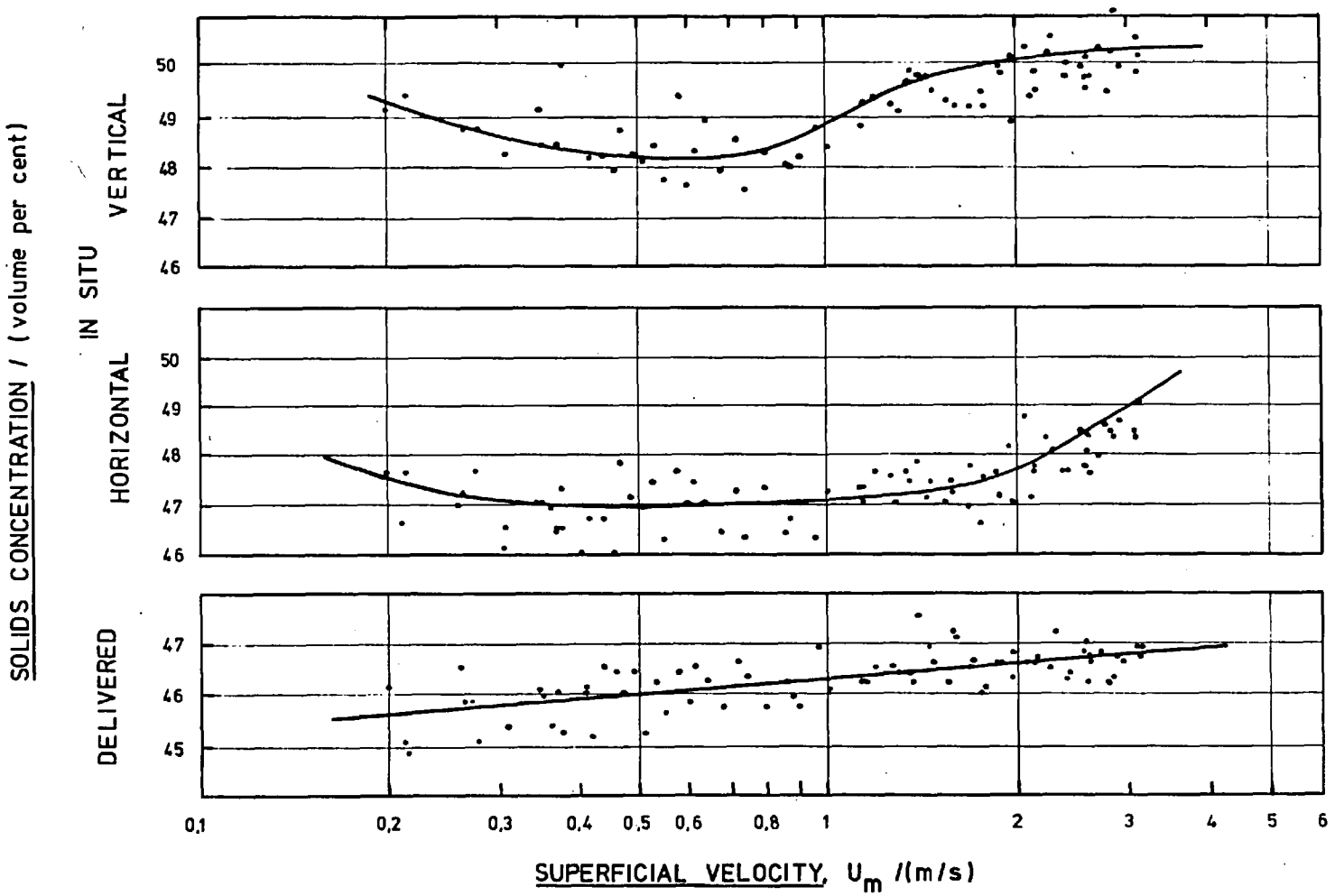


Figure 3.5

The horizontal and vertical in situ and delivered solids concentration as a function of mean velocity for the fine sand

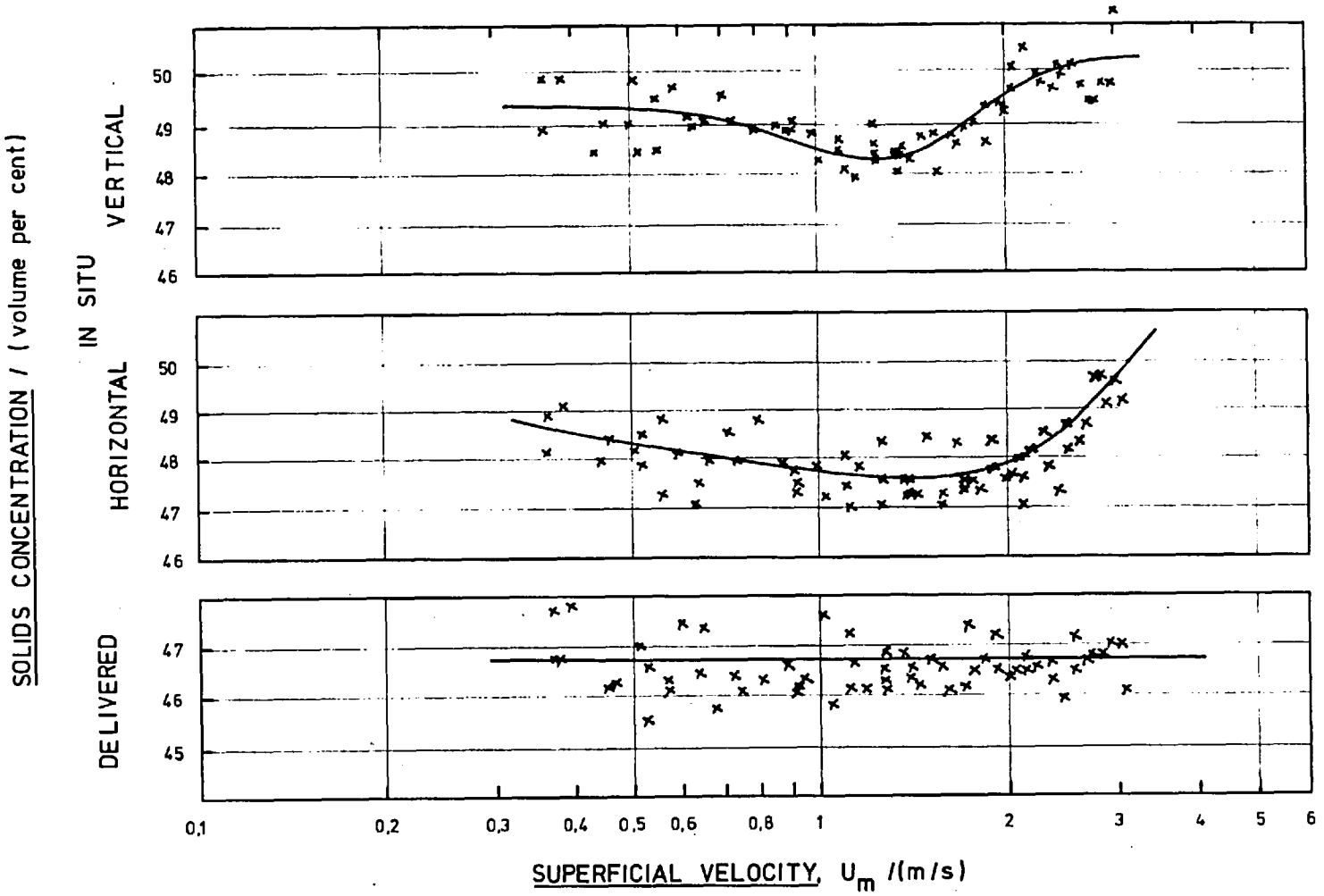


Figure 3.6

The horizontal and vertical in situ and delivered solids concentration as a function of mean velocity for the medium sand

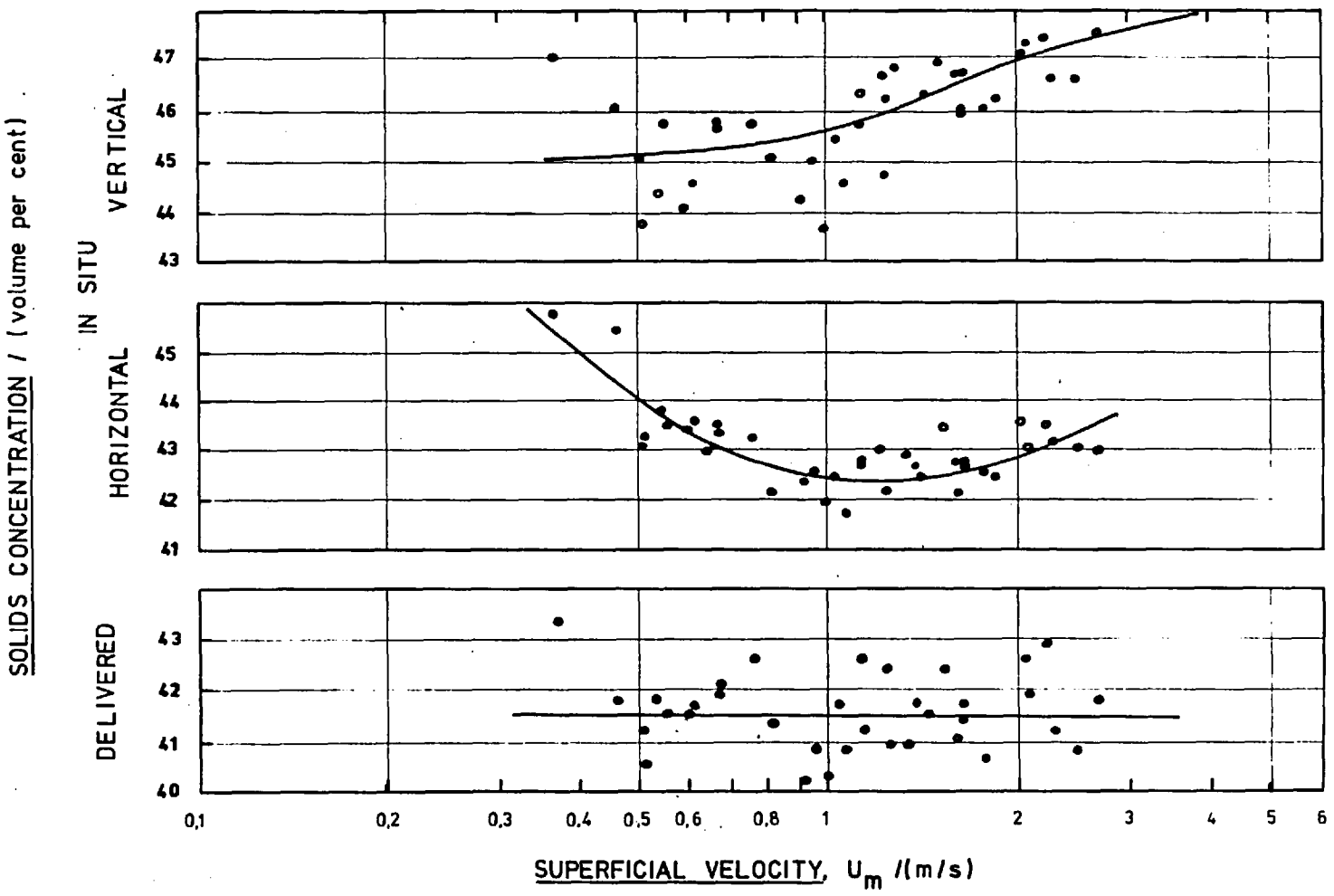


Figure 3.7

The horizontal and vertical in situ and delivered solids concentration as a function of mean velocity for the coarse sand

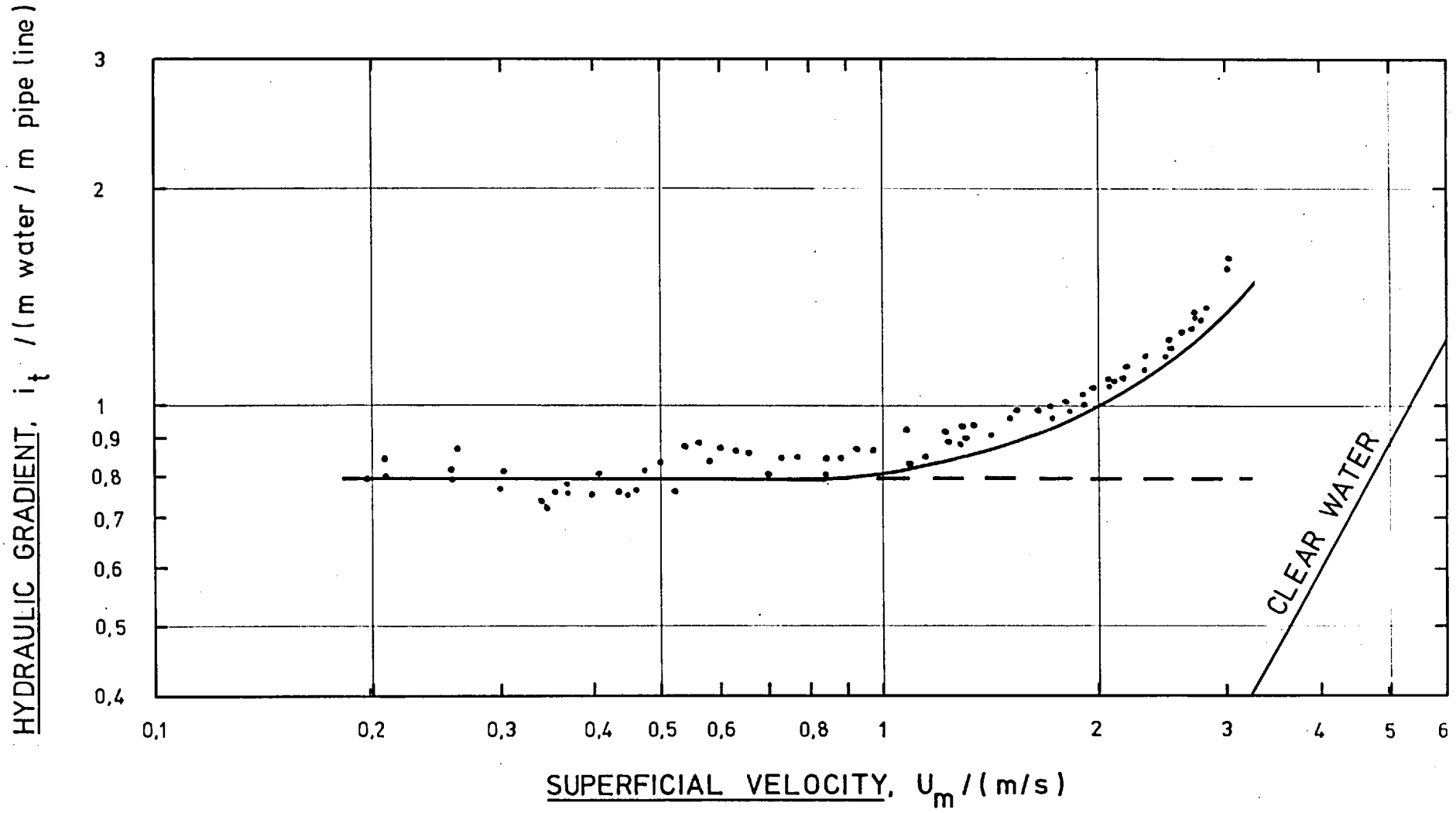


Figure 3.10

Results of the two-layer analysis overlaid on the experimental points for the fine sand

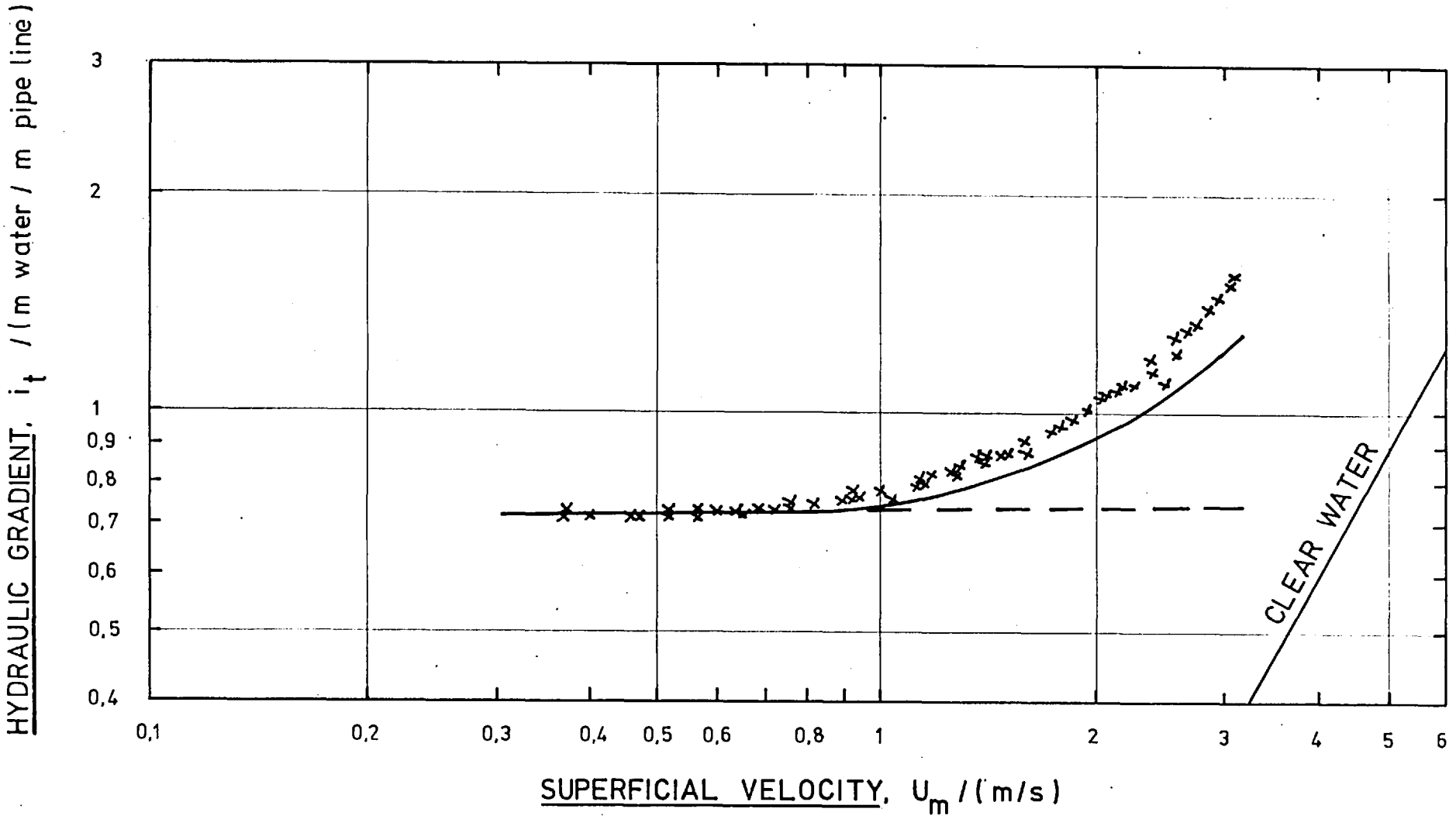


Figure 3.11

Results of the two-layer analysis overlaid on the experimental points for the medium sand

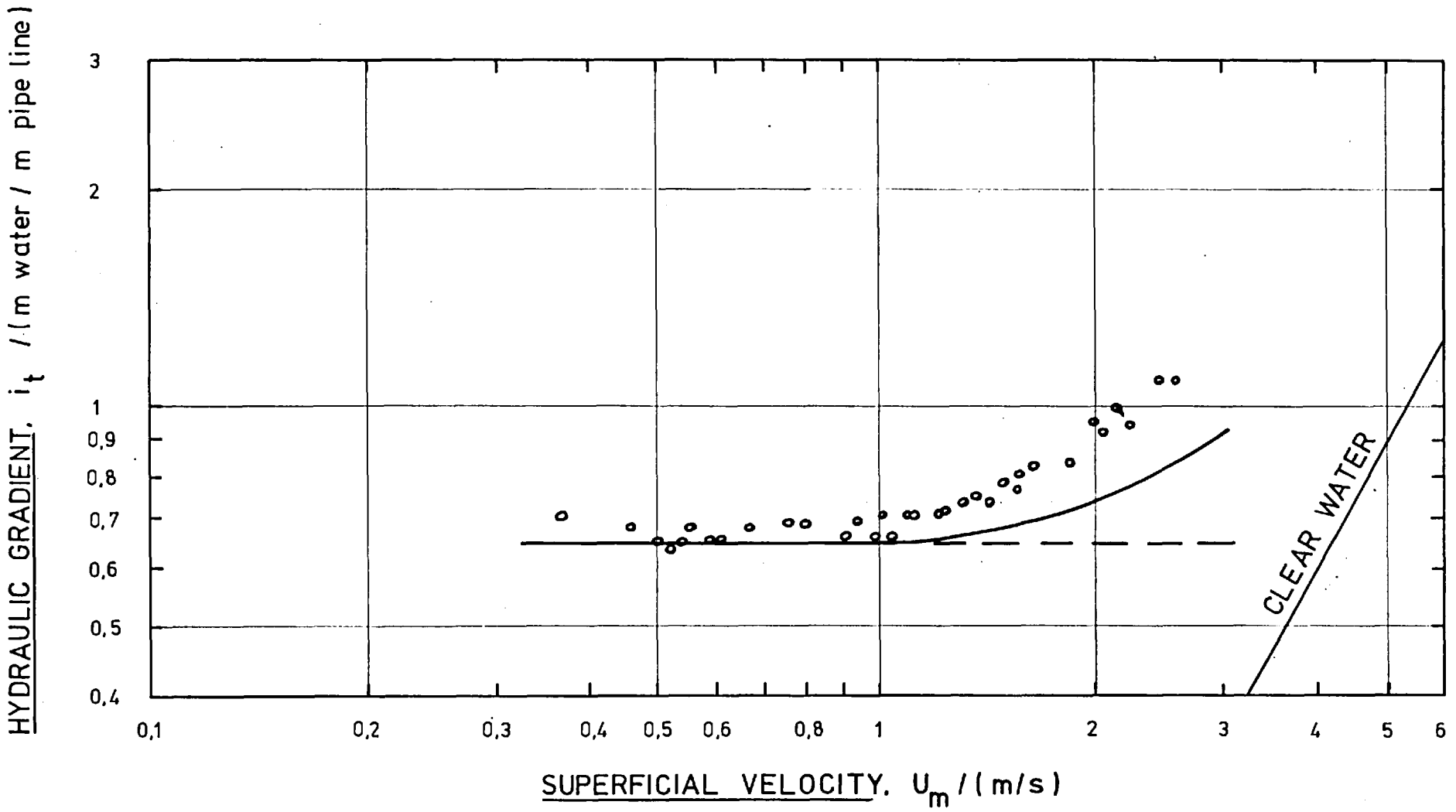


Figure 3.12

Results of the two-layer analysis overlaid on the experimental points for the coarse sand

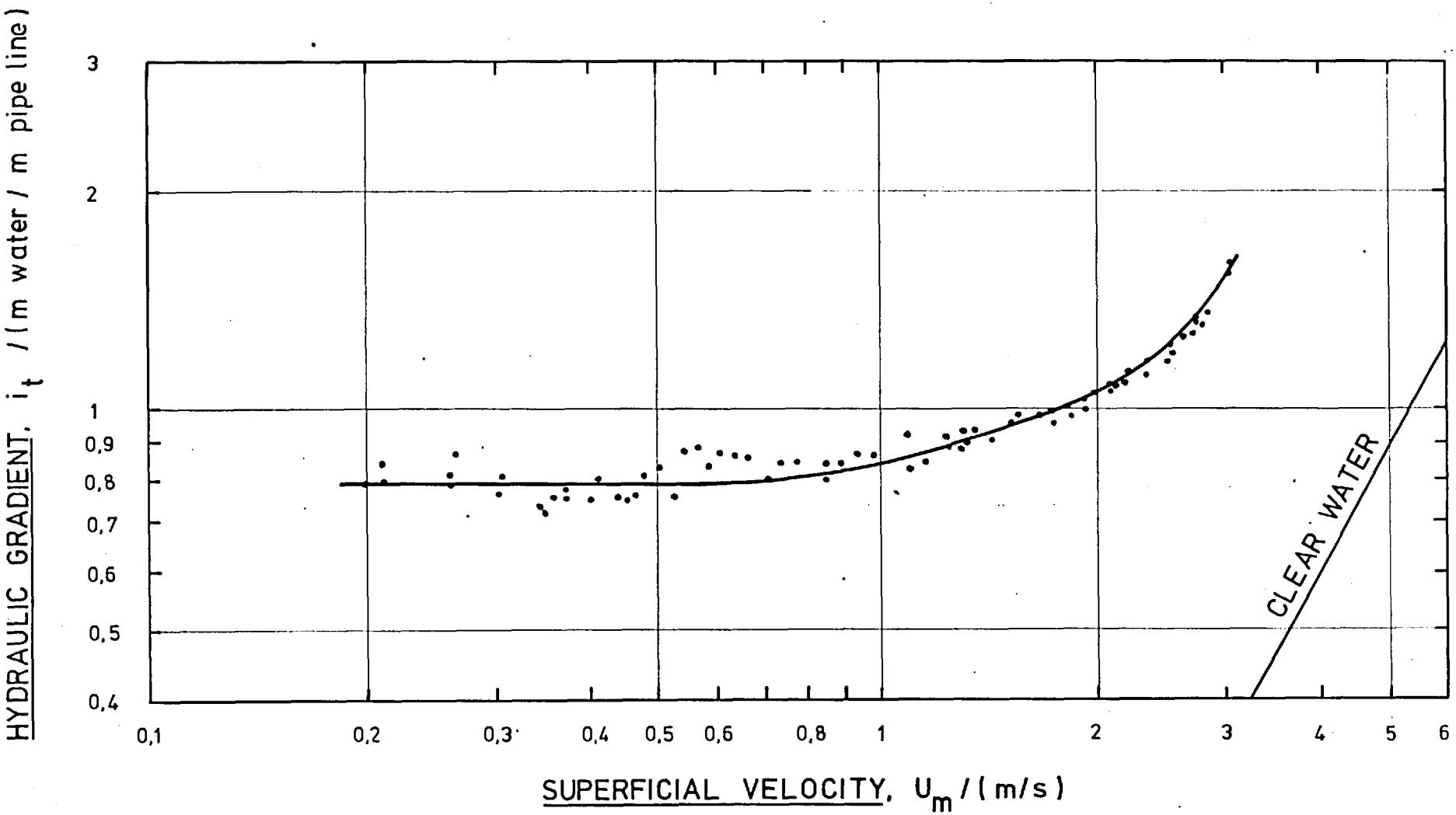


Figure 3.15

Results of the modified two-layer analysis for fine sand overlaid on the experimental points

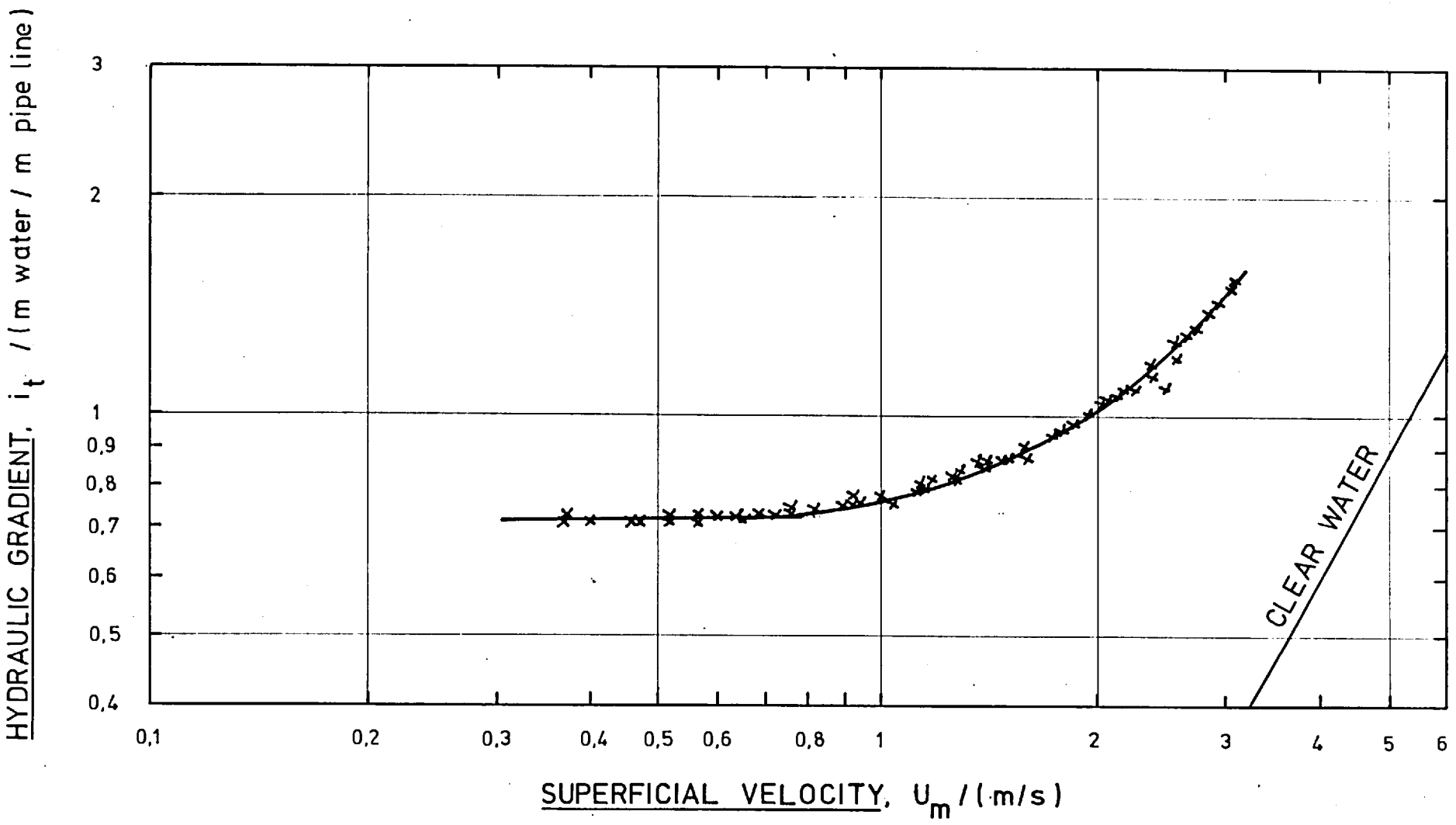


Figure 3.16

Results of the modified two-layer analysis for medium sand overlaid on the experimental points

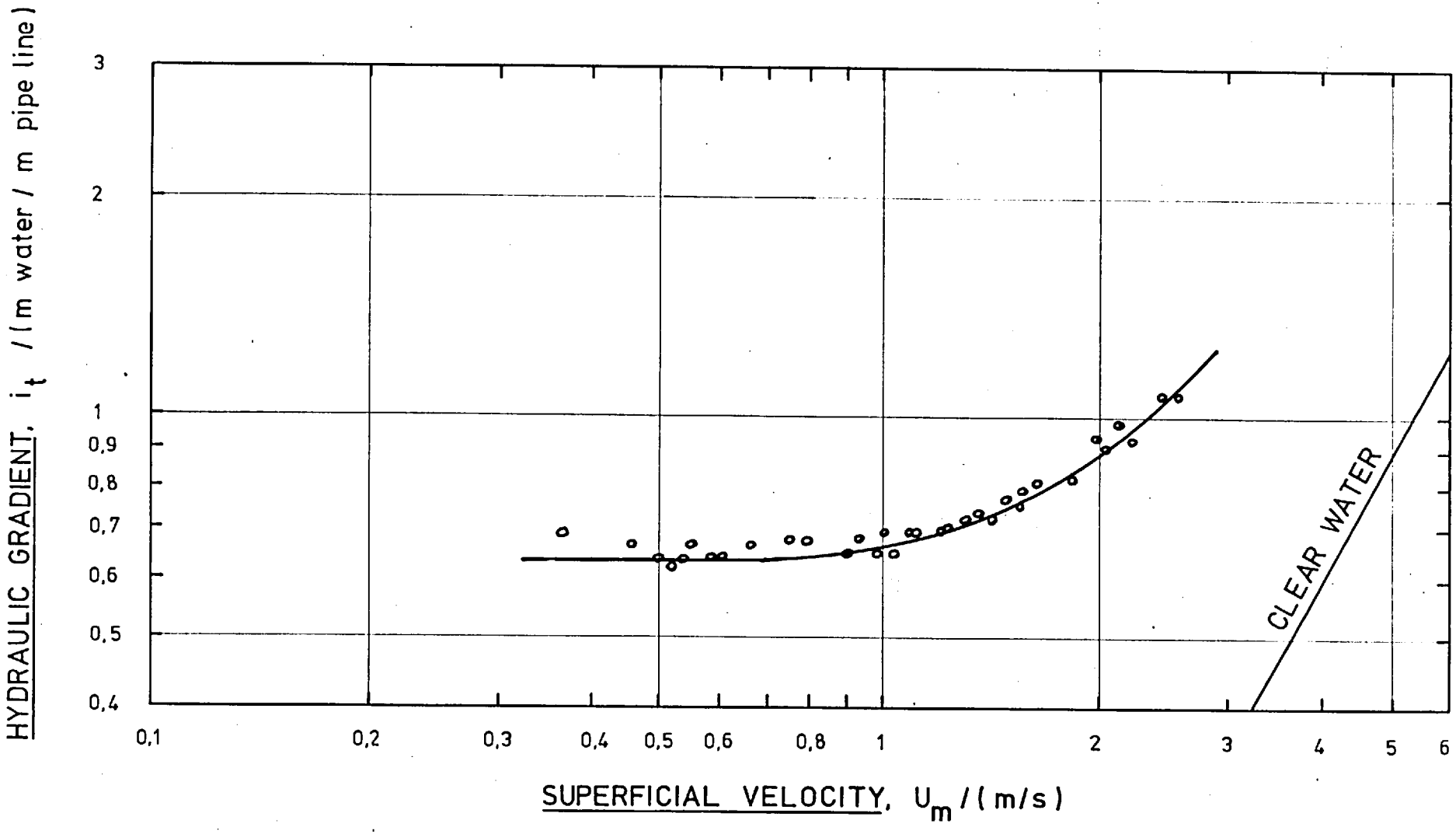


Figure 3.17

Results of the modified two-layer analysis for coarse sand overlaid on the experimental points

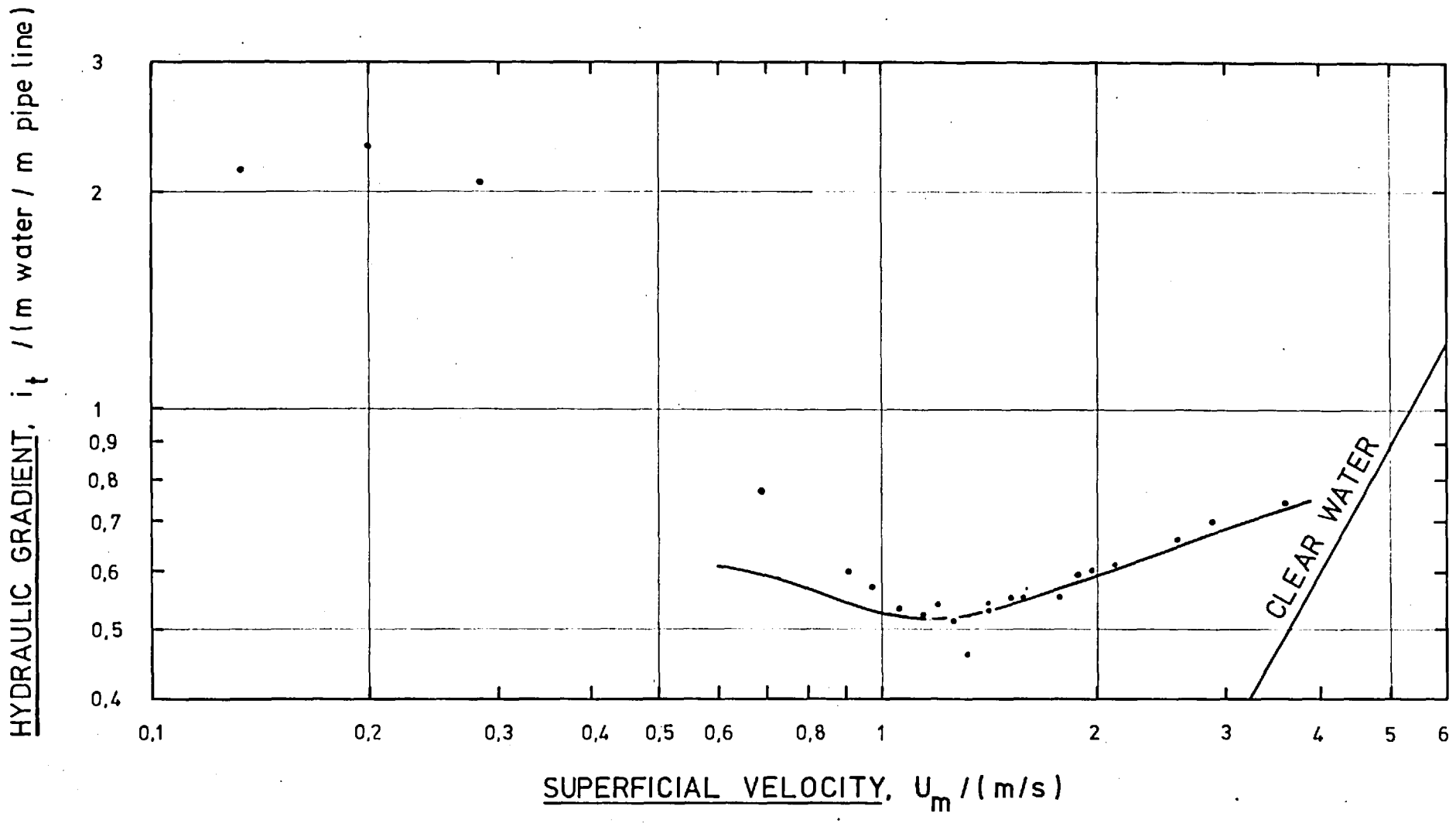


Figure 3.18

Results of the modified two-layer analysis for -5/16 in. + 4 BSS gravel from Reference 68

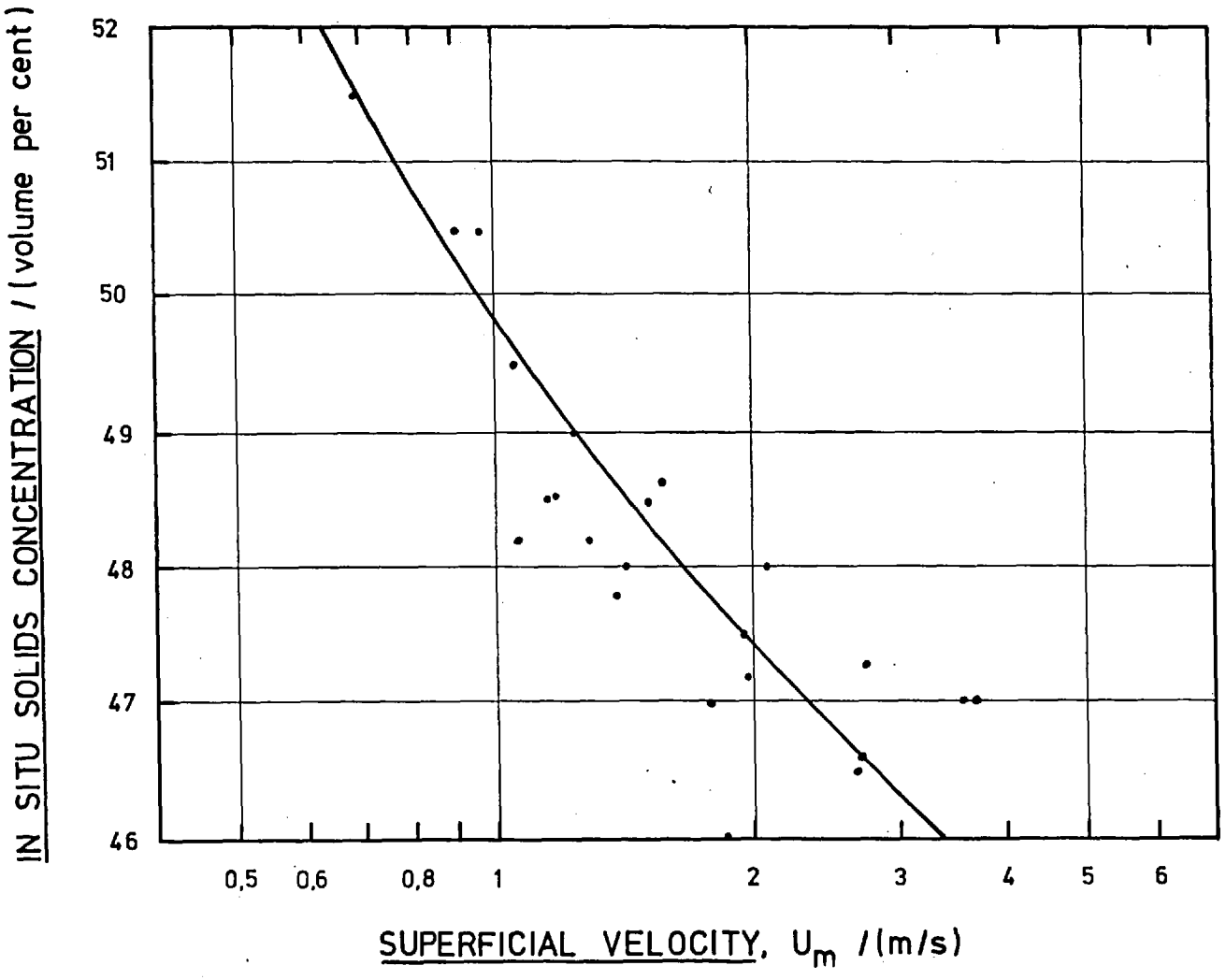


Figure 3.19

In situ solids concentrations as a function of mean velocity for the -5/16 in. + 4 BSS gravel, plotted from Reference 68

4. VERTICAL RISING FLOW

4.1 Introduction

It is important to first consider what happens in a non-flowing solid-liquid system when fluid is passed upwards through an initially stationary bed of granular material. At low liquid flowrates, the fluid flows through the tortuous paths created by the interstices of the *porous media*. The frictional pressure drop across a porous bed in which the solids are supported by particle-particle contact is dependent upon the flow régime of the fluid. The Kozeny equation (18, p. 4) can be used to estimate the frictional pressure drop i_f under streamline conditions - whilst a more widely applicable formula is given by Ergun (18, p. 9):

$$i_f = 150 \frac{C^2}{(1 - C)^3} \frac{\nu_f U_f}{d^2 g} + 1.75 \frac{C}{(1 - C^3)} \frac{U_f^2}{d\, g} \qquad (4.1)$$

The first term accounts for the losses due to viscous drag which dominate at low velocities whereas the second term is only significant as the kinetic losses predominate at high velocities.

As the fluid flowrate is increased the unrestrained bed of solids starts to expand. The pressure drop is then equal to the buoyant weight of solids per unit area of bed:

$$i_f = C \quad (S - 1) \qquad (4.2)$$

In this *particulately fluidised* state the solids are supported by fluid drag. Above the point of incipient fluidisation, the bed expansion - fluid velocity relationship can be predicted by the Richardson-Zaki correlation if the free-fall velocity of the particles at infinite dilution is known (31).

When the fluid velocity exceeds that of the smallest particle, solids transport begins -- the solids are carried away with the fluid stream. In hoisting, involving particles having a greater density than the fluid carrier, the solids velocity will in general be less than the fluid velocity due to the tendency of the particles to settle. This is reflected by the *in situ* solids concentration

being greater than the delivered solids concentration. In co-gravity flow the reverse is true. At low solids concentration, if the fluid velocity is decreased below that necessary to support the solids, it is likely that the system will eventually choke due to accumulation of solids.

Before dealing with hoisting at high solids concentration it is important to consider some of the work of previous investigators in leaner concentration transport.

4.2 The work of earlier investigators

Durand (20) performed large scale experiments with slurries made of sands of mean diameter 0.18, 1.00 and 4.36 mm flowing at velocities between 3 and 6 m/s in a 150 mm diameter pipe. The maximum solids concentration in these experiments was 8% by volume. The pressure drop was measured both in the rising and falling legs of a vertical test loop. By summing the results of such measurements he was able to remove the head attributable to the solids, assuming that the slip between the particles and water was negligible. He found that the frictional loss could not be distinguished from that of clear water flowing at the same velocity in his apparatus. The manometric head loss of the slurry i_t could be described as the sum of the fluid friction i_o and that due to the head of solids.

$$i_t = i_o + C\,(S - 1) \qquad (4.3)$$

Velocity profiles of the fluid in the rising section of the transport line, with the medium size sand at solids concentrations around 6% by volume, were indistinguishable from that of clear-water at the same velocity. Concentration profiles made at the same solids fraction showed essentially that the concentration was very nearly uniform across the pipe diameter. The solids concentration measurements were made starting 20 mm away from the wall.

The flow of coarse gravel and coal at sizes up to 19 mm (0.75 in.) was studied by Worster (85) and Worster & Denny (86) in pipe sizes up to 150 mm (6 in.). They did not present any experimental results, though, they did indicate that the frictional pressure

losses were of the same order as those for water alone.

A detailed experimental programme was undertaken by Newitt et al. (49). They studied the flow of closely sized sand in sizes between 0.1 and 3.8 mm, 0.11 mm zircon, 1.4 mm manganese dioxide and 1.2 mm perspex in a rising section of 25.4 mm (1 in) pipework. They found for the coarser materials that the frictional losses were either identical with the frictional water pressure drop or were slightly higher at low velocity, tending to the water friction line as the velocity increased. The maximum solids concentration of the slurries was about 20% by volume. The fluid velocity profile of the slurries was measured in a 51 mm (2 in) vertical line. Their observations were similar to those of Durand and confirmed that a solids concentration of 5% by volume of either perspex or 1.3 mm sand had no noticeable effect on the velocity profile. However, when the sand concentration was increased to 10% at a mean velocity of 1.8 m/s (6 ft/s) the maximum flow velocity had decreased by around 10%. They also mention that the near wall velocity was higher than if no solids were present. Upon increasing the sand concentration to 15% the effect was enhanced so that the central area was almost flat with a steep velocity gradient near the wall. High speed flash photographs showed the presence of a high concentration of solids flowing in a central core surrounded by an annulus of almost clear water. This flow pattern explains the closeness of the frictional gradient to that of clearwater. Newitt et al. mention that this core is formed by a Magnus type force acting on the particles, though they do not apply quantitative analysis to to the case of slurry pipeline flow. The same effect must have been present in Durand's work but his velocity profiles were not started close enough to the wall for this effect to become apparent. Newitt et al. proposed a small correction to the solids head term in Equation 4.3 to account for the slightly higher fluid velocity.

$$i_t = i_o + C\,(S - 1)\,\frac{U_m}{U_f} \qquad (4.4)$$

The velocity ratio approaches unity for particles with a small settling velocity. The *coring* effect was not noticed with smaller

particles, the frictional pressure drop diverged from the corresponding water friction curve as the velocity increased. This was attributed to the fact that the particle diameter was approximately the same as the thickness of the laminar sublayer which influenced the rate of shear at the pipe wall. The results of the smaller particle experiments could be satisfactorily described by an empirical correlation.

Bhattacharya & Roy (7) investigating 40 - 80 μm clay suspensions in kerosene found that in the velocity range 0.3 to 0.76 m/s (1 to 2.5 ft/s) the frictional pressure drop could not adequately be described by that of a single component Newtonian fluid. They present a correlation for their data.

Odjoe and Buchanan (52) attained solids concentrations of up to 41% by volume, by entraining the solids directly into the vertical transport line with a high velocity jet of water in their Hydrolift apparatus. However, the inline solids concentration was not measured directly but obtained by a method outlined by previous investigators (49) from the delivered solids concentration, mean slurry velocity and particle settling velocity. The hindered particle settling velocity was not used and at delivered solids concentrations around 30% it is likely that the inline concentration was somewhat lower than the authors reported. The majority of the experimental work was done with coarse materials in the size range 13 mm to 19 mm (0.5 in to 0.75 in) flowing in pipes of 51, 76 and 102 mm (2, 3 and 4 in) diameter at velocities up to 2 m/s (6.6 ft/s). The authors suggest that it is more appropriate to base the fluid wall friction on the water velocity in the slurry rather than the mean velocity of the slurry. They point out, however, that the fluid-wall friction is small compared with the solids head term, the correction making little difference to the overall pressure drop.

The flow behaviour of high concentration metal pastes was extensively investigated by Cairns & Lawther (10) as a possible method of fuelling a nuclear reactor. They measured the concentration profile in a vertical pipe containing rising flow of a slurry consisting of 2 micron tungsten particles. No evidence of core formation was found in the velocity range 0.91 to 4.1 m/s.

Work of a similar nature was conducted by Calvert & Miller (11) who studied paste flow in a hairpin pipe system. They investigated sand, copper shot and glass ballotini in the size range 40 to 300 μm at *creeping* velocities of up to 7×10^{-5} m/s, flowing close to the loosely settled solids concentration. The pressure gradient in their system was found to depend upon the exit conditions, especially when the slurry was free to fall into an open collecting vessel or when the exit was washed with water. If the fluid is allowed to drain from a high concentration slurry the resulting plug of drained material restrains the bulk flow and tends to block the exit. A similar experience was encountered while commissioning the sliding plate flow sampler at Imperial College. Frictional losses in the rising leg were estimated from viscometric data. The viscometric work gave results with wide scatter, characteristic of excessive stick slip experienced on the cylinder of the viscometer at very high solids concentrations.

Miller (47) studied the flow of sand and ballotini of about the same nominal size (300 to 400 μm) in 13 and 19 mm (0.5 and 0.75 in) lines. The sand was introduced into the line using a pressurised lock hopper feeder. This resulted in a high inline solids concentration for both materials, and measured values were typically above the freely settled concentration at velocities up to 3.4 m/s (11 ft/s). A gamma photon attenuation device was used to measure the inline solids concentration axially along a short length of pipework containing two right angled bends. Measurements of the pressure drop on a section of pipework containing rising flow indicated a change in friction mechanism at about 0.6 m/s (2 ft/s). Below this value Miller found that the friction loss could be attributed to water flowing at the same velocity in the line. Some of Miller's experimental results were published jointly with Cloete & Streat (17).

In an attempt to elucidate the flow mechanism of high concentration vertical flow Leung et al. (45) suggested that the flow could be described within the régimes encountered in a particulately fluidised bed or a moving packed bed. Their analysis did not prove an entirely satisfactory explanation of Miller's results.

Using a liquid radioactive tracer technique Bantin (6) measured the fluid velocity profile in a vertically flowing slurry of 300 μm ballotini at concentrations near the freely settled value in a 27 mm glass line. The velocity profiles suggested the presence of steep fluid velocity gradients in the vicinity of the pipe wall; elsewhere the fluid velocity profile was flat.

Bantin concluded that the particles were supported by the fluid, with negligible particle-particle interaction. However, the solids concentration remained almost constant with increasing mean slurry velocity. This was thought to be due to the solids being prevented from expanding due to downstream constraints. At high velocity, Bantin attributed the irreversible losses to liquid wall friction, though this was greatly influenced by the presence of particles and could not be predicted with any accuracy from the clear water friction gradient. This was contrary to Miller's conclusions.

Hill (35) reports that when pumping 300 μm and 1.8 mm sand in the same apparatus as used by Bantin there was no discernible difference in hydraulic gradient or solids concentration for the two materials.

Working with 300 μm closely graded sand in a 25.4 mm line at solids concentrations near that of the freely settled material Televantos (68) was unable to detect any longitudinal stress in the flowing slurry. This would be present if the solids were constrained as Bantin put forward. Televantos found that the slurry pressure gradient could be described by adjusting the fluid wall loss by an amount proportional to the mean slurry density.

$$i_t = i_o \ (C \ (S - 1) + 1) \ + \ C \ (S - 1) \qquad (4.5)$$

This pseudo-homogeneous correction is the same as that used in earlier work by Einstein (25).

4.3 Description of experimental results

The hydraulic characteristics of the three sands conveyed in upward vertical flow are presented in Figures 4.1 to 4.3. Data for all the sands are overlaid on Figure 4.4 for comparison. The abscissa on

these figures is mean slurry velocity and the ordinate is the manometric gradient which has been measured by a differential pressure transducer. The general expression for manometric gradient is $(\Delta P/\rho_f g - \Delta z)/\Delta x$, where Δx is the distance along the pipe and Δz the vertical rise, which is equal to Δx for hoisting. This point is being clarified at this stage as there is much confusion in the literature as to whether the reported hydraulic gradient is measured with two separate devices or with a differential device -- the difference between the two methods is unity, when expressed as a hydraulic gradient. The variation of inline and delivered solids concentration with slurry velocity is presented in Figures 3.5 to 3.7.

The delivered volumetric solids concentration was higher for the two finer sands (d = 0.32 mm, C = 0.465 and d = 0.68 mm, C = 0.467) than for the coarsest (d = 1.7 mm, C = 0.415). For the coarser sands the delivered concentration was found to be invarient with velocity (Figures 3.6 and 3.7), however, a slight velocity dependence could be detected (Figure 3.5) in the case of the finest sand. In the aforementioned Figures it can be seen that the *in situ* spatial concentration has a slight dependence on velocity. As the solids are fed into the transport system at almost constant concentration there is a distinct tendency for the particle concentration to adjust, to take into account changes in energy dissipation. For the case of the two finer sands a distinct minimum is seen, whilst the coarsest sand tends to follow the high velocity trend of the two finer sands. As the *in situ* spatial concentration is always higher than the input concentration there is a relative interphase velocity, this relative velocity of the two phases u_r can be calculated from:

$$u_r = U_m (C - C_d)/((1 - C)C) \qquad (4.6)$$

which is obtained from a material balance on the particles and fluid in the pipe on the assumption of flat velocity profiles in both cases. The value of the relative velocity was about 10% of the mean slurry velocity throughout the experimental range. The experiments were performed at mean velocities between about 0.2 and 3.1 m/s.

Frictional losses can be obtained from the smoothed hydraulic and inline concentration values from these Figures, by subtracting from the manometric gradient the head attributable to the solids. These results are presented in Figures 4.5 to 4.7 as points, the solid upper line represents the average values of the total manometric gradient -- the other lines will be dealt with at a later stage. Plots of the two smaller particle size sands are of similar shape characterised by two rising lines separated by a well defined minimum. The plot for the coarsest material consists of a continuously rising line. At high velocities the lines for all three materials coincide. The plots for the two finer sands would suggest that there are two different frictional mechanisms, one dominating at low velocity and one at very high velocity. Results for the coarse sand would seem to suggest only one dominant mechanism, namely that associated with the high velocities for the other two sands.

Classification of the slurry as an equivalent fluid cannot be fully valid unless certain conditions are satisfied. For turbulent flow these require the particle size and associated time scale be smaller than the smallest length and time scales of the turbulence (46). With aqueous pipeline flow this only occurs for small particles, typically less than 100 μm in diameter. Particles in excess of this size will span the viscous sublayer and will come into periferal contact with the wall and yet will never be fully submerged in the sub layer. As a result the fluid-particle interactions of the equivalent fluid hypothesis cannot take place (71).

A pseudo-homogeneous modification can be made to the clear water friction as is given by Equation 4.5. This is an attractive computational short cut. With foresight, such an approximation would give reasonable design results for the largest sand, however, it would not account for the frictional behaviour of the two finer sands throughout the velocity range investigated.

4.4 Theoretical flow model

4.4.1 The dispersive force

As the frictional losses are always greater than the losses attributed to the clear fluid there must be a component in the

wall stress due to the presence of the particles. Particulate systems, like fluids exhibit a resistance to flow, this can be likened to an apparent viscosity which is representative of the energy dissipated by the interaction of the particles and the fluid. In this situation the stress at the wall can be considered as the sum of two components, one based on the carrier fluid alone, $(\tau_f)_w$ the other, $(\tau_p)_w$ representing particle-wall contact.

The second particulate stress component was investigated by Bagnold (3). He considered the influence of the particles upon the resistance of the two-phase mixture to shear. The particles must knock or push each other out of the way according to whether or not their inertia outweighs the fluid viscosity, both kinds of encounter must involve displacement of the particles normal to the planes of shear. As this *dispersive* stress is not present when a Newtonian fluid is sheared he proposed that it was due to the interaction of the particles. He investigated his hypothesis on mixtures of neutrally buoyant spheres of diameter 1.3 mm sheared in Newtonian fluids of varying viscosity in the annular space between two concentric cylinders. The volume concentration of the grains was varied between 13 and 62%.

Both tangential and normal stresses were measured, and a calculated clear-fluid value was subtracted from the tangential stress to obtain the particle-associated shear stress, τ_p. On the basis of experimental results τ_p was found to be proportional to the velocity gradient dU/dy at low strain rates, whereas at high strain rates it varies as $(dU/dy)^2$.

To account for the two components the transition region between these extremes a simple summation has been found to be adequate, giving:

$$\tau_p = \tau_{p1} + \tau_{p2} \tag{4.7}$$

where

$$\tau_{p1} = \mu_f f_1(c) \frac{dU}{dy} \tag{4.7a}$$

$$\tau_{p2} = f_2(c) \left(\frac{dU}{dy}\right)^2 \tag{4.7b}$$

Here $f_1(c)$ and $f_2(c)$ represent functions of concentration and μ_f is the viscosity of the fluid. The first term is directly comparable to the viscous stress of fluid alone (μ_f (dU/dy)) and thus $f_1(c)$ can be regarded as an adjustment to viscosity which accounts for the presence of the particles. Bagnold suggested two alternate formulations for $f_1(c)$, and many additional possibilities exist. A large number of viscosity correction equations have been proposed in the literature (73), and each of them is equivalent to some function $f_1(c)$. For example, the viscosity correction of van Dijck and Eilers (23) gives:

$$f_1(c) = \left(1 + \frac{1.25\ c}{(1 - c/c_*)}\right)^2 - 1 \qquad (4.8)$$

where C_* is the maximum volumetric concentration of the particles - usually referred to as the packed settled concentration.

The most important part of Bagnold's work concerns the second term in Equation 4.7, the *inertial* term. He presents this term as a function of relative solids concentration:

$$f_2(c) = B\left[\left(\frac{C_*}{c}\right)^{1/3} - 1\right]^{-2} \qquad (4.9)$$

where the coefficient B will be discussed later.

For the case of hoisting low concentrations of large particles at moderate velocities, it has already been shown that a large body of experimental evidence exists for the formation of a particle-lean annulus in the region of the pipe wall. It is proposed here that for the case of high solids concentration hoisting the same mechanism can lead to the formation of a dense core of solids flowing axially in the pipe.

In the mechanics of non-cohesive solids, the ratio between the shear stress at failure and the normal inter-granular stress is denoted by tan ϕ and Bagnold used essentially the same relation in his work. However, further analysis of his data shows that only the term $(dU/dy)^2$ is significant in relation to the normal particulate stress σ_p (this is reflected in the noticeable difference in the slopes shown on Figures 3 and 4 of Reference 3). The result can be expressed in terms of an inequality, the

generality of this expression will be considered during subsequent application:

$$\sigma_p \tan \phi > \tau_{p2} \qquad (4.10)$$

The total shear stress $(\tau_f + \tau_p)$ has a maximum value of $\rho_f g j D/4$ at the wall and decreases linearly to zero at the centre line of the pipe. Thus:

$$\tau_f + \tau_p = \rho_f g i_f \frac{D}{4} \left(1 - \frac{2y}{D}\right) \qquad (4.11)$$

where i_f is the frictional loss and y is a radial length measured inward from the wall of the pipe. Although the value of τ_p will be small near the pipe axis, substantial values of σ_p can exist

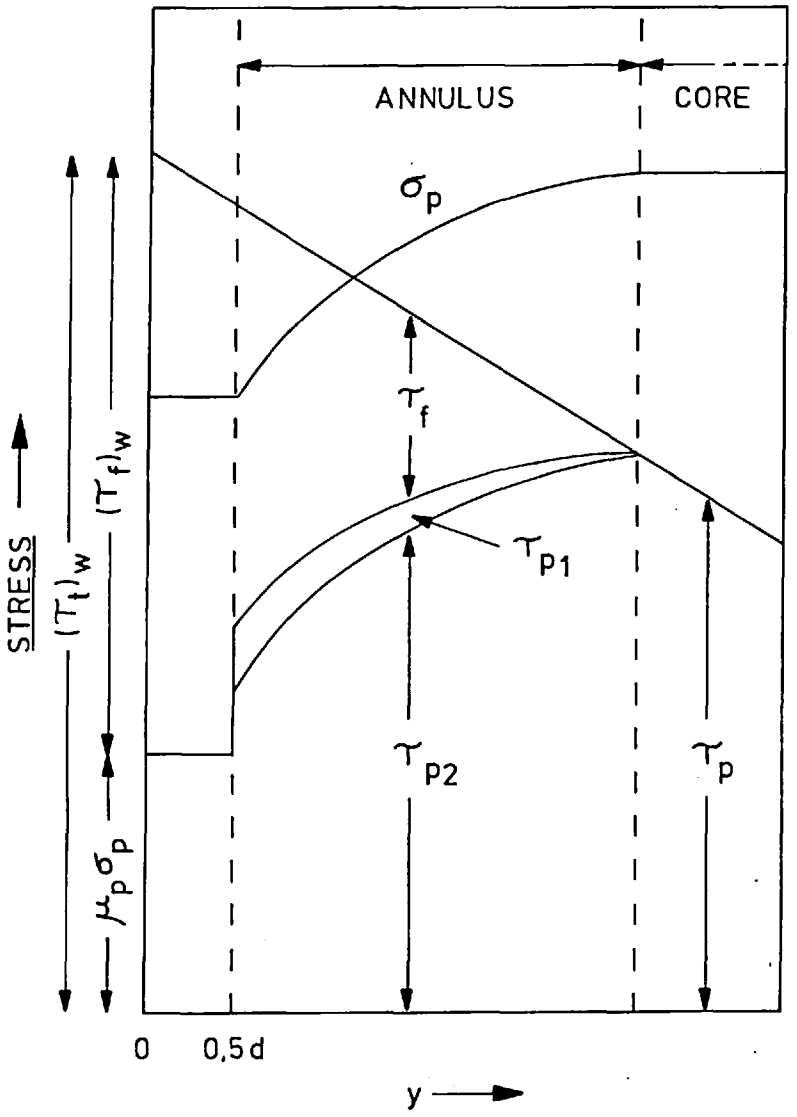


Figure 4.8

Schematic representation of the stresses in vertical rising flow near the pipe wall

in the core. Specifically as the concentration approaches C_* the core can resist a shear stress in the absence of a velocity gradient, provided adequate inter-granular pressure is maintained. Moreover, for flow with no bends and no cross-pipe gravitational component, both σ_p and c must remain constant throughout a region of zero velocity gradient. This region of constant high concentration, constant velocity and constant normal stress will be called the *core*. Here stress is transmitted solely by particle-particle contact in the absence of a fluid velocity gradient. Within the core $\sigma_p \tan \phi$ will exceed τ_{p2} whereas at the outer edge of the core, and in the surrounding annulus, Equation 4.10 must read as an equality. These stress relations for the core are illustrated in Figure 4.8, which also indicates that within the annulus σ_p and hence τ_{p2}, may vary with distance from the wall.

4.4.2 The Magnus force

This variation in σ_p can be linked to a *lift force* on the particles often referred to as a Magnus force. This *lift force* F_m results in the axial migration of particles away from the pipe wall. This force arises from the influence of a steep fluid velocity gradient on the particles, such as that found in the vicinity of the pipe wall. The forces acting on the particle are given below in Figure 4.9. The magnitude of this lift force may be expressed in general terms as $\rho_p \times \Gamma \Delta u$, where Γ is the circulation around the object, referred to the plane of the flow, which in the present case is any plane passing through the pipe axis. The length x is the dimension of the object perpendicular to this plane, and Δu is the difference between the velocity of the object and that of similarly-placed fluid a considerable distance away (53, 59). For particles in vertical flow Δu equals the fall velocity, w, and x is taken as the length of a cylinder with the same volume and diameter as the particle, i.e. d/1.5, where d is the diameter of a spherical particle. The circulation Γ can be evaluated as $(du_f/dy)\ \pi\ d^2/4$, where u_f represents fluid velocity in the absence of localized particle effects. Thus the force F_m acting on the particle can be written:

$$F_m = \rho_f w \frac{\pi d^3}{6} \frac{du_f}{dy} \qquad (4.12)$$

The fall velocity employed in this expression should be corrected for the effect of particle concentration, using, for example, the

method of Richardson & Zaki (31). To be consistent, a particle velocity u_p is also to be defined. This equals $(u_f - w)$, and its differential with respect to y will thus be virtually the same as du_f/dy.

For the present case, with substantial particle concentrations, the sum of the Magnus-effect forces on the particles in a unit volume gives a direct evaluation of the normal stress gradient $d\sigma_p/dy$. As the number of particles per unit volume is simply $c/(\pi\, d^3/6)$, one obtains:

$$\frac{d\sigma_p}{dy} = c\,\rho_f\, w\, \frac{du_f}{dy} \qquad (4.13)$$

Leaner mixtures, for which a high-concentration core may not exist, require an alternate approach linking Magnus force to concentration

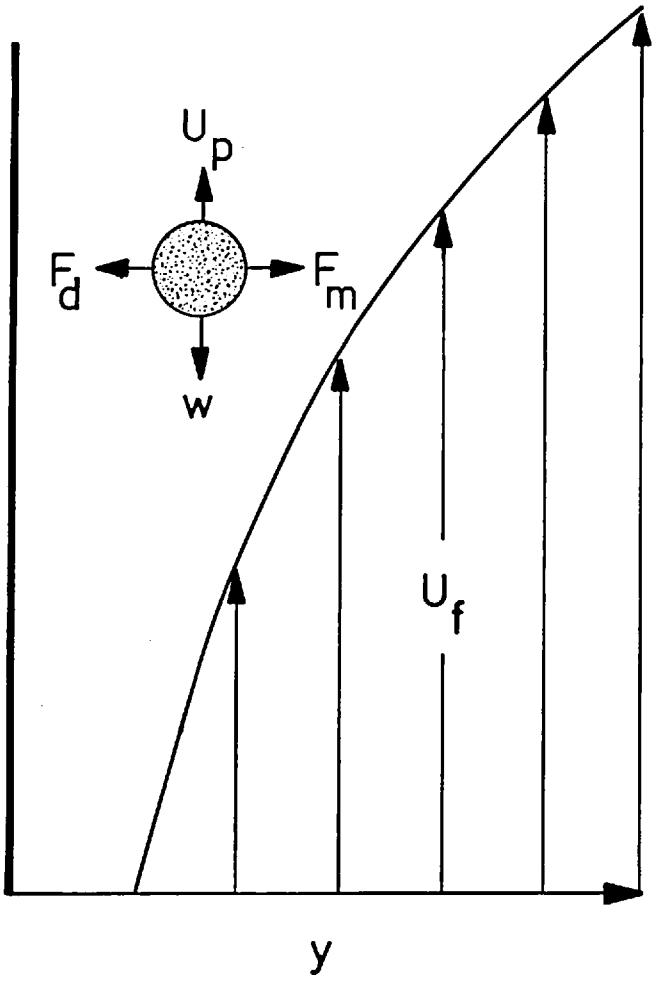


Figure 4.9

Schematic representation of the forces on a particle in a steep fluid velocity gradient

via the dispersive properties of turbulent flow. Engelmann (26) used a relation involving the turbulent dispersive force in his analysis of large particles flowing at low concentrations. Such an indirect approach may be dispensed with in the present case, although change of c across the annulus is still expected, as shown in Figure 4.10. This change can be determined from the variation of σ_p expressed by Equation 4.13, using the fact that the associated value of τ_{p2} from Equation 4.10 must agree with that obtained by means of Equation 4.7b., the latter equation is then solved for concentration.

Analysis of the near wall zone of the annulus is complicated due to the finite size of the sand grains. Particle velocities are

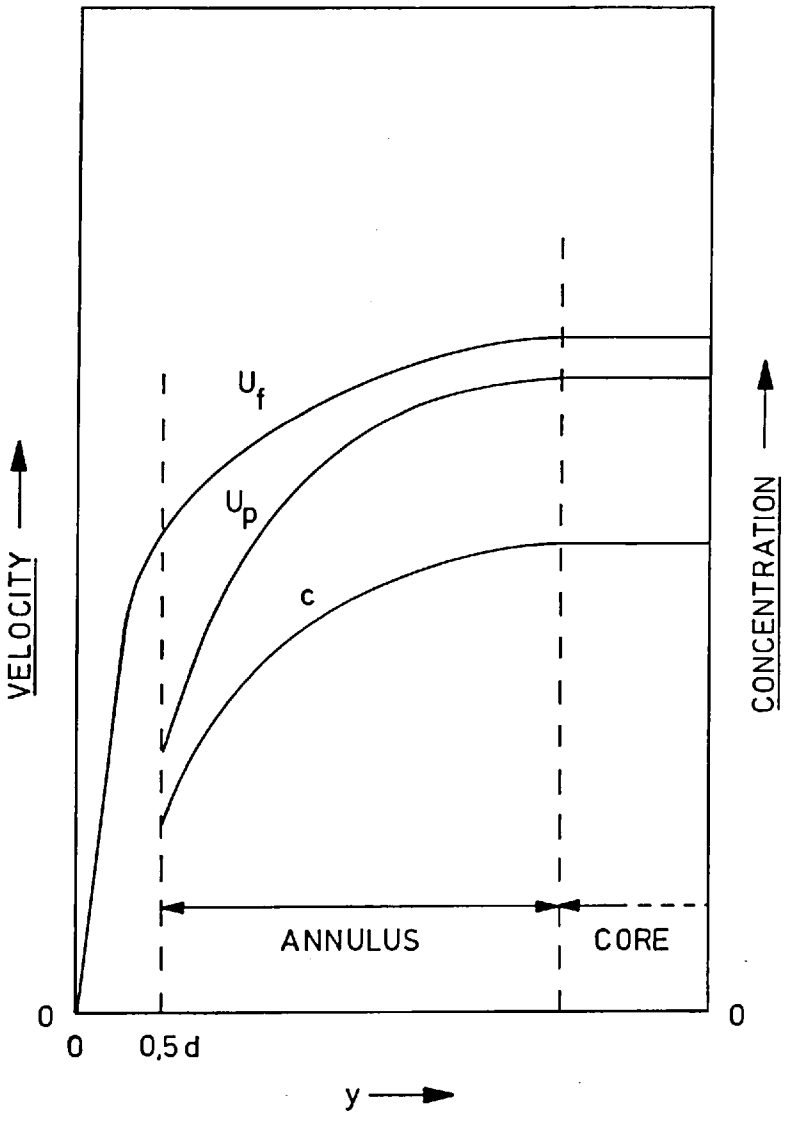


Figure 4.10

Schematic representation of the velocity and solids concentration profiles in vertical rising flow near the pipe wall

meaningless in the range $0 \leq y \leq d/2$ and concentration of particles difficult to describe. Fluid velocity gradients are obtained from the basic turbulent similarity equation using a shear velocity, u_*, based on the fluid stress component τ_f:

$$\frac{du_f}{dy} = \frac{(\tau_f/\rho_f)^{\frac{1}{2}}}{\kappa y} \qquad (4.14)$$

Here κ is the Von Karman coefficient, it has been suggested that (87, p. 187, 90) the value of 0.4, generally used for single-phase flow may not be applicable to slurries, but in the absence of experimental results to quantify this effect the accepted value has been used in this work. As it is expected that the particle radius will generally exceed the thickness of the laminar sublayer, especially at high shear rates, that case will be dealt with here.

4.4.3 Computational producure

4.4.3.1 High velocity results

Trial values of the solids concentration and fluid shear stress at a distance $y = d/2$ from the wall are treated as input. Conditions at the wall must first be estimated before calculations can proceed stepwise into the body of the flow. The total wall shear stress $(\tau_t)_w$ can be estimated from the shear stress at a distance $y = d/2$ from the wall, and used to calculate the frictional gradient i_f:

$$i_f = \frac{(\tau_t)_{d/2}}{(1 - d/D)} \quad \frac{1}{g\rho_f D/4} \qquad (4.15)$$

In the immediate vicinity of the wall ($0 \leq y \leq d/2$) the Magnus force is assumed negligible and a starting value of the normal wall stress can be obtained by reading Equation 4.10 as an equality:

$$\sigma_p = \tau_{p2}/\tan \phi \qquad (4.16)$$

this value will be constant in the region of $0 \leq y \leq d/2$. The normal stress is transmitted through the laminar sublayer to the wall. Multiplication of this normal stress by the mechanical friction coefficient between the particles and the wall surface (denoted μ_p and generally less than $\tan \phi$, see Appendix 1) gives the particle-associated component of the wall shear stress:

$$(\tau_p)_w = \tau_{p2} \frac{\mu_p}{\tan \phi} \qquad (4.17)$$

This allows the fluid velocity at y = d/2 to be obtained from the logarithmic velocity law (70), where u_* is the shear velocity:

$$(u_f)_{d/2} = u_* \left[2.5 \ln \left(\frac{0.5d}{\nu_f} u_* \right) + 5.5 \right] \qquad (4.18)$$

Once conditions in the near wall zone have been established it is then possible to move out towards the pipe axis in successive increments of y. This procedure is performed by a computer algorithm. The value of σ_p at each increment is determined by Equation 4.9 and the matching values of τ_{p2} (from Equation 4.7b) and c, noting the remarks made after Equation 4.10. From the value of τ_f, obtained from Equation 4.11, a new value of du_f/dy is obtained from Equation 4.14 and hence u_f and u_p can be determined.

The core is reached when c closely approaches the limiting value C_*, and the fluid and particle velocity gradients approach zero. The values of u_p, u_f and c are summed to obtain mean slurry velocity U_m, and *in situ* and delivered concentration (denoted C and C_d respectively).

The computations can be repeated with a range of input values of c and τ_f (at y = d/2), with each run giving a new set of values for U_m, i_f, C and C_d.

The results of this analysis of frictional loss are overdrawn on the experimental points on Figures 4.5 to 4.7 by the lines closest to the clear water line. This analysis takes account of the frictional losses where a particle lean annulus occurs in the flow.

4.4.3.2 Low velocity results

At low velocities it is unlikely that the lift force experienced by the particles would be sufficient to create a particle-lean annulus. Under these conditions, provided the particle concentration is high enough, it could be envisaged that the core would extend to the outer layer of particles at y = d/2. As shown in Figure 4.8 the stress τ_{p2} coincides with the total stress at the edge of the core. For limiting cases a good estimate of τ_{p2} will be $(\tau_t)_w$ $(1 - {}^d/D)$, this expression together with Equation 4.16 and

and the definition of the total stress gives the following:

$$(\tau_f)_w = (\tau_t)_w \left[1 - \left(1 - \frac{d}{D} \right) \frac{\mu_p}{\tan \phi} \right] \qquad (4.19)$$

The total wall shear stress is obtained from Equation 4.11, Equation 4.19 can then be used to calculate u_*:

$$u_* = \left(g \; i_f \; \frac{D}{4} \left[1 - \left(1 - \frac{d}{D} \right) \frac{\mu_p}{\tan \phi} \right] \right)^{\frac{1}{2}} \qquad (4.20)$$

Further, with the core occupying virtually the whole pipe, the velocity at $y = d/2$ will correspond to the mean velocity U_m. Neglecting a minor correction for the differences between u_f and u_p, this implies that substitution of Equation 4.20 into Equation 4.18 will give the mean velocity directly. The results of this analysis for the finer two sands is also overlaid on Figures 4.6 and 4.7, being represented by the rising lines on the far left of these Figures.

Before considering these results in detail it is worth examining the parameters used in the calculations. There are many relations available for $f_1(c)$ in the literature. The form of the relation used in this work reduces (as $c \to o$) to the well known formulation derived by Einstein (24) which gives results agreeing with the experiment for low concentrations. The model was found to be insensitive to the form of $f_1(c)$; not entirely surprising as the value of the concentration given to start calculations was often very small. The form of B in Equation 4.9 was given by Bagnold as $0.013 \; d^2 \; \rho_p$. Bagnold performed his experiments at one particle diameter and density, the only justification for his formulation would have come from a dimensional-analysis approach. In earlier work (82) B was taken as 10^{-2}, in SI units, invarient of both d and ρ_p -- upon reflection this was perhaps unjustified.

It was recognised that the Magnus force for the real three-dimensional flow around particles might differ considerably from the two-dimensional approximation incorporated into Equations 4.12 and 4.13. To test for possible influence of this effect, calculations were re-run with these equations multiplied by various constants. It was found that the effect was negligibly small even for a factor of two in either direction.

4.5 Comparison of the analysis with experimental results

4.5.1 Low velocities results

At low fluid shear stress, the particles tend to be uniformly distributed, so that the core virtually fills the whole pipe. For the two finer sands the solids concentration was sufficiently high, as a result there was a high level of grain - wall contact, and the particulate portion of the wall shear stress was large.

In Figure 4.5 the low-velocity calculated line does not lie parallel to the water line. This occurs because the radius of the smaller particles is less than the thickness of the viscous sub-layer (which is calculated from $11.6\ \nu_f/u_*$). In this region the value of the mean velocity, U_m which corresponds to the velocity from y = d/2 outwards, has been obtained from the viscous flow relation:

$$U_m = \frac{d\ u_*^2}{2\ \nu_f} \qquad (4.21)$$

The fit of the lower- velocity calculations to the appropriate portion of the experimental data appears to be fully satisfactory for both the finer sands, including the grain-diameter effect which shifts both the experimental and calculated lines slightly to the right for the medium particles. For the low velocity runs there is good agreement, the computations falling within the experimental scatter.

The coarsest sand does not appear to have two distinct types of frictional mechanism, although there is an indication of a change occuring below 0.9 m/s as can be seen in Figure 4.7. The reason for this behaviour is probably the inter relation of two effects. The coarse sand was fed into the transport line at a slightly lower concentration resulting in a lower *in situ* concentration. The larger particles, with diameter just over double that of the medium sized sand, would tend to enhance the lift force produced by the Magnus effect. The theoretical prediction of the experimental results is exceptionally good throughout the velocity range investigated.

4.5.2 High velocity results

The calculated high velocity lines for the two finer sands are shown in Figures 4.5 and 4.6. These are seen to have somewhat larger divergence from the experimental data than has been found in previous cases but nevertheless reasonably good agreement has been found. The experimental results appear to follow a line of somewhat greater slope than that of the calculated lines, which lie parallel to the clear fluid line. The calculations also show a very slight difference between the two particle diameters which is not found in the high velocity experimental results. The thickness of the particle-lean annulus was found to be quite small in comparison to that observed in leaner concentration conveying, its thickness was found to vary from five particle diameters for the finest sand to two particle diameters for the coarsest sand investigated. The calculated high velocity lines lie very close to the simple mixture-density relation of Equation 4.5. A direct comparison of the theoretical predictions with the experimental points can be obtained by adding to the calculated frictional loss the static head attributable to the solids. This is represented by the solid lines overlaid on the experimental results in Figures 4.12 to 4.14. The agreement is good for the high and low velocity regions, however, the theory fails to predict the transition.

The results obtained from the computational procedure using the Magnus effect to estimate the frictional loss for hoisting iron ore (S = 4.5) of the same particle size as the coarse sand is in excellent agreement with the prediction of Equation 4.5. The results of this analysis are shown in Figure 4.11 with a dashed line. Runs with constand d and varying pipe diameter tend to indicate that the constant composition lines move closer to the water line as pipe diameter increases. Predictions from Equation 4.5 under these conditions tend to be significantly higher than those obtained from the axial model.

The smooth rising curve on the i_m, U_m plane reported for the coarse sand is of a similar shape to those reported by Bantin (6) and Televantos (68), for finer sands. The low velocity friction mechanism reported here for the two finer sands may have been unrecognised by the previous investigators as the instrumentation of the apparatus now in use is more sophisticated.

Hoisting at high solids concentration may be attractive under certain circumstances. For the fine-sand cases studied, the simple mixture-density approach would underestimate the energy requirements by about 20% at 1 m/s. The dashed line on Figure 4.12 represents the losses calculated by the mixture-density approach of Equation 4.5. The friction mechanisms exhibited by the finer two sands undergo a smooth transition as the fluid component of the wall shear stress increases with velocity. Only the two extreme conditions have been dealt with here, the prediction of the value of σ_p at which the transition occurs may not be particularly amenable to analysis.

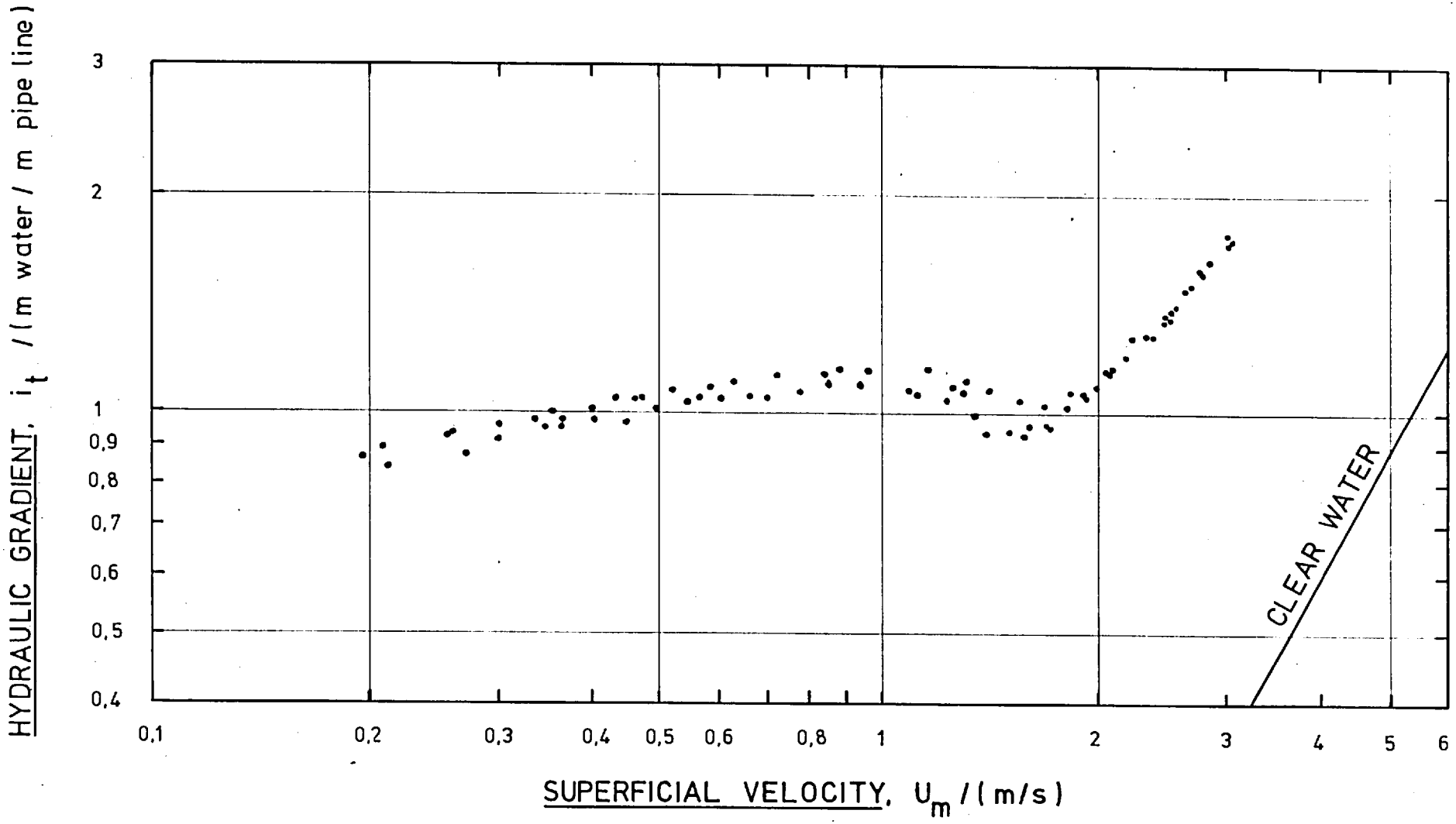


Figure 4.1

The experimental points describing the hydraulic characteristic of the fine sand in vertical rising flow

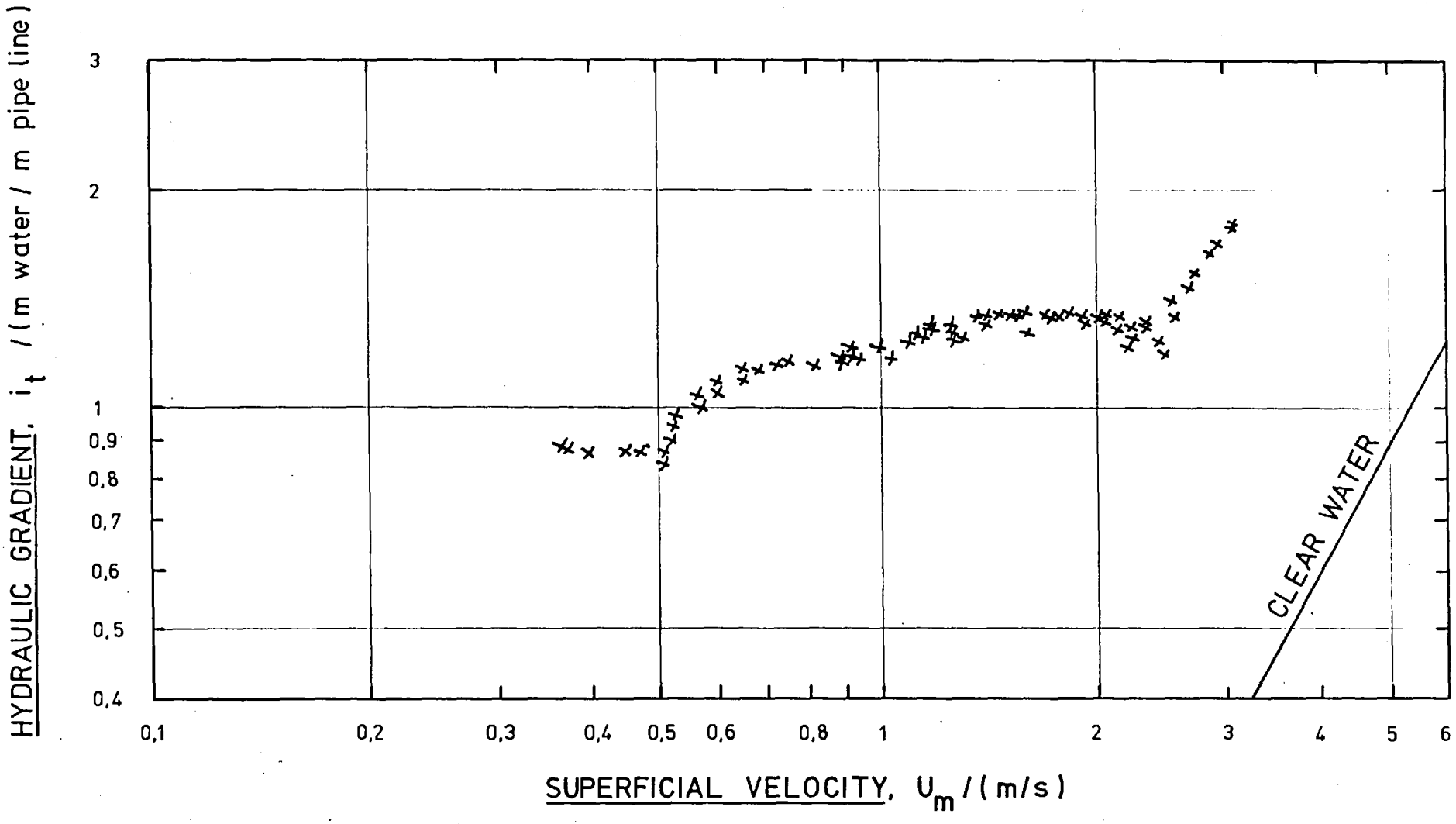


Figure 4.2

The experimental points describing the hydraulic characteristic of the medium sand in vertical rising flow

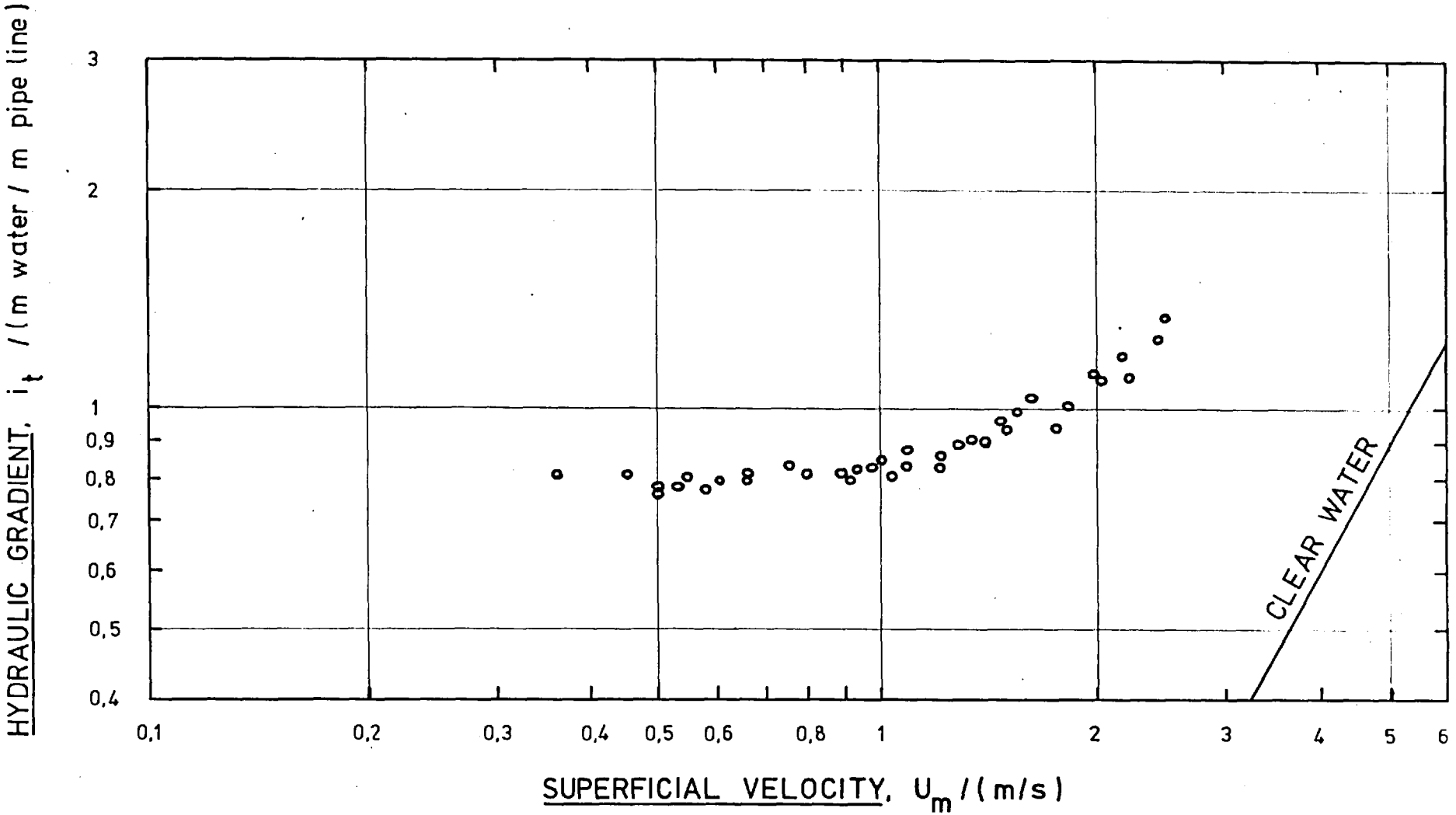


Figure 4.3

The experimental points describing the hydraulic characteristic of the coarse sand in vertical rising flow

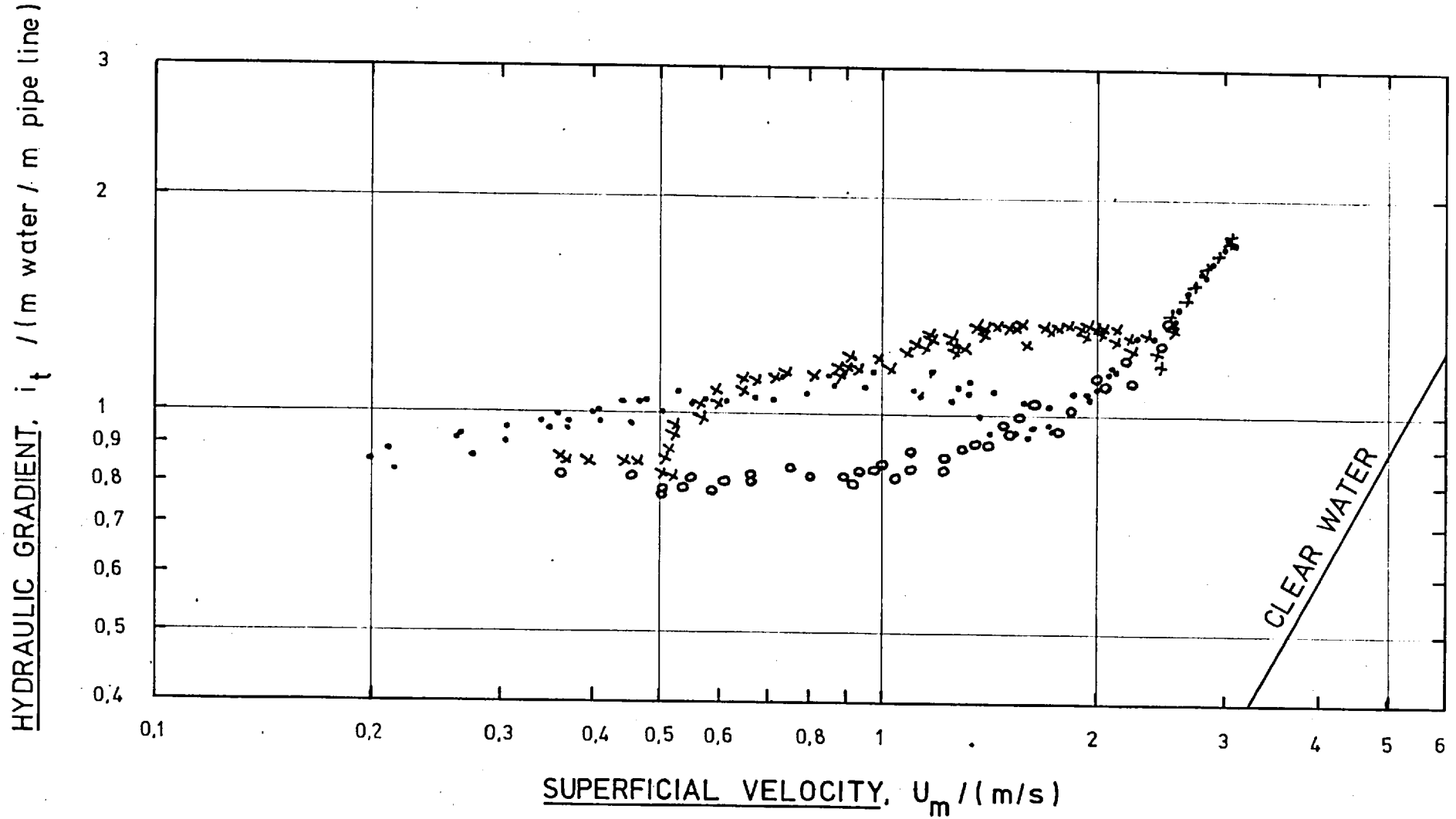


Figure 4.4

Overlay of the experimental points describing the hydraulic characteristics of all three sands in vertical rising flow

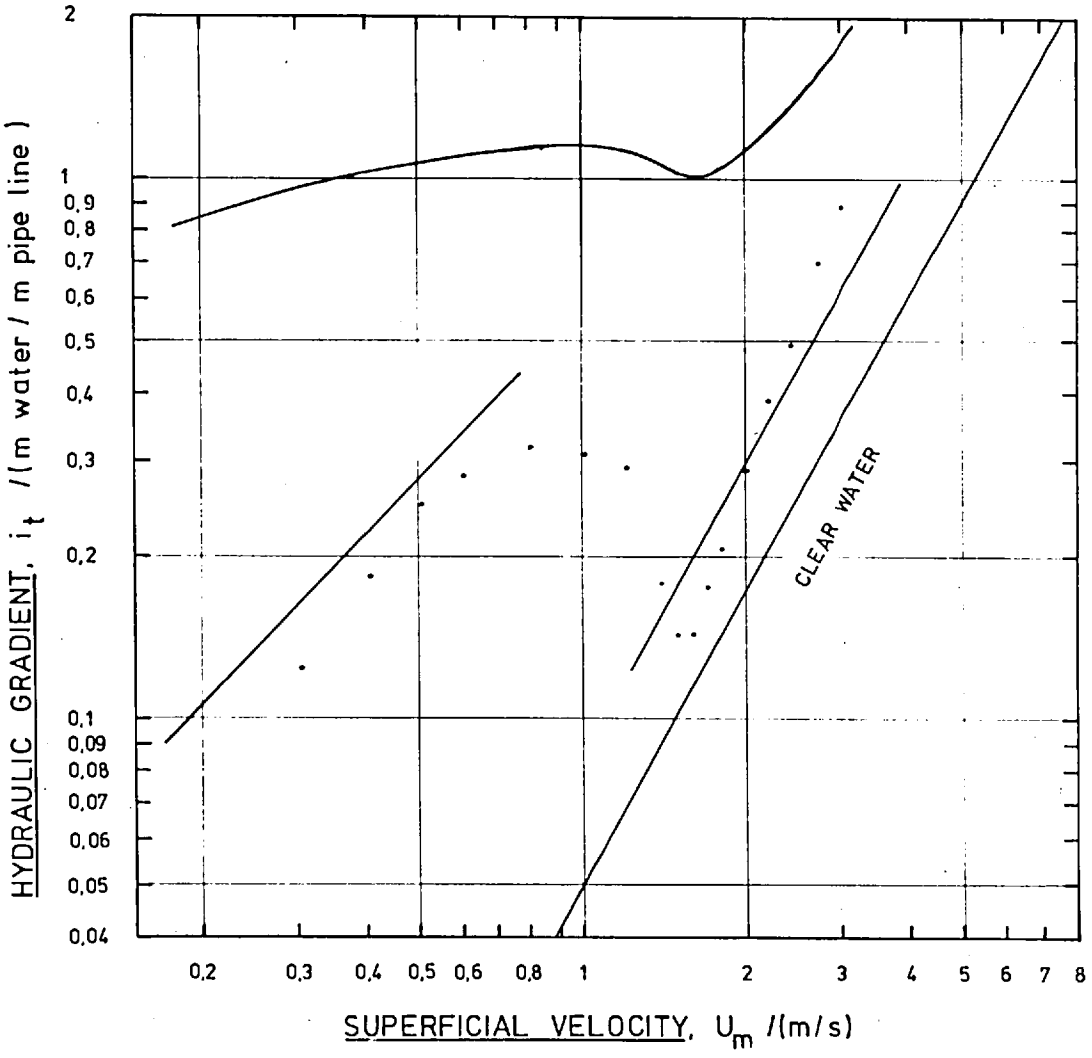


Figure 4.5

The experimental and calculated frictional losses for fine sand

The upper solid line gives the average total loss. The points represent experimental data and the associated solid lines are theoretical predictions

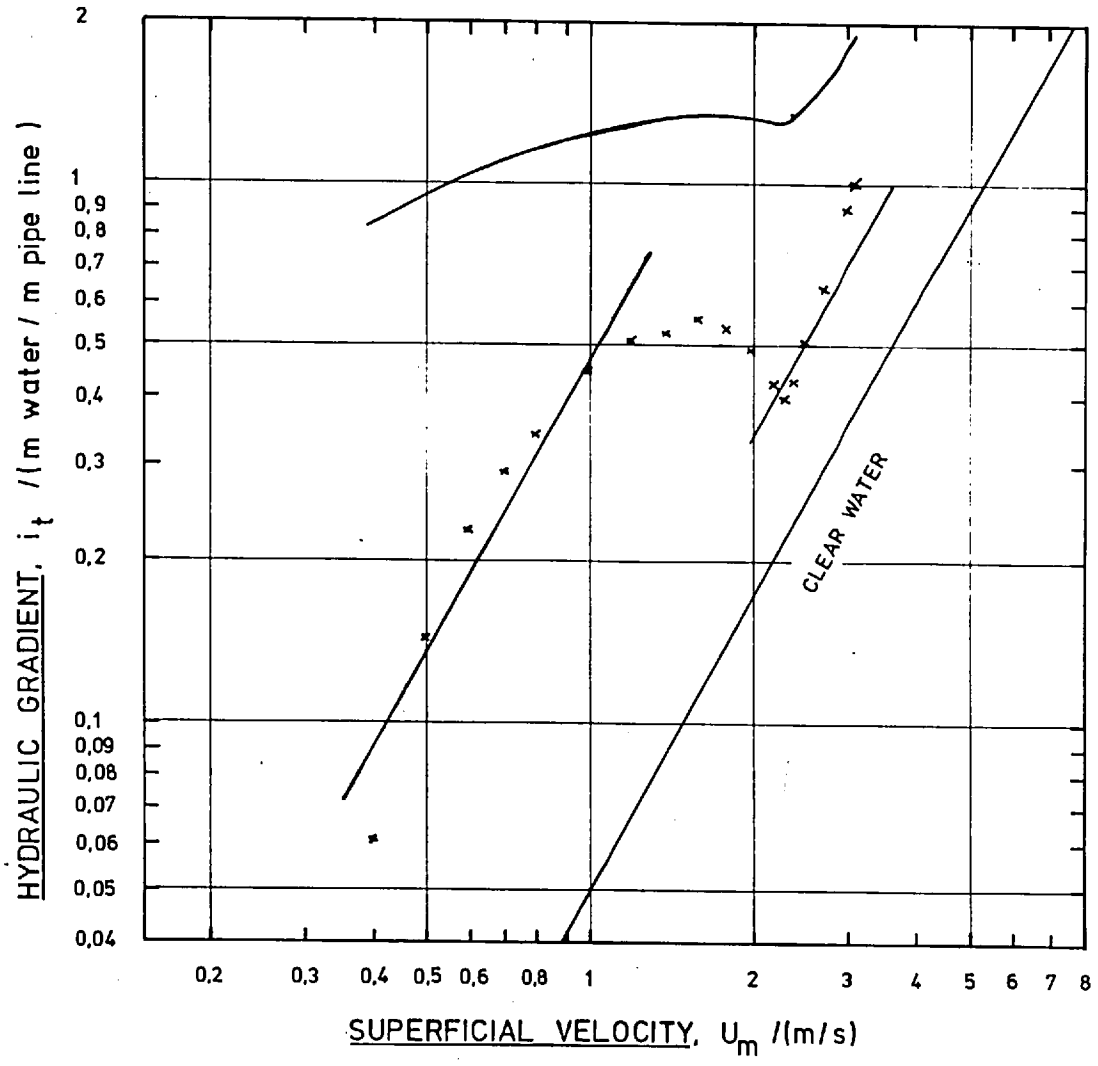


Figure 4.6

The experimental and calculated frictional losses for medium sand

The upper solid line gives the average total loss. The points represent experimental data and the associated solid lines are theoretical predictions

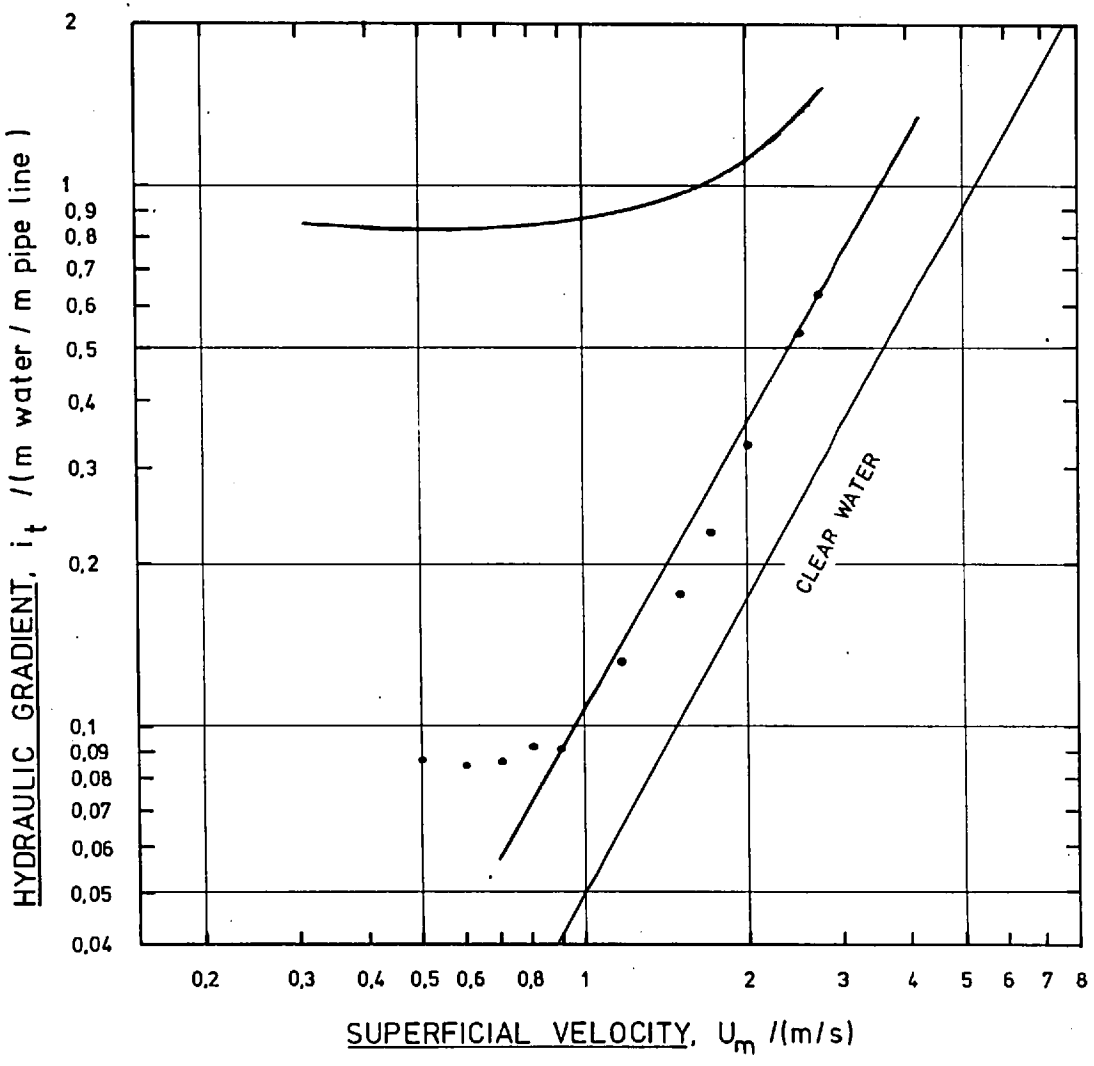


Figure 4.7

The experimental and calculated frictional losses for coarse sand

The upper solid line gives the average total loss. The points represent experimental data and the associated solid lines are theoretical predictions

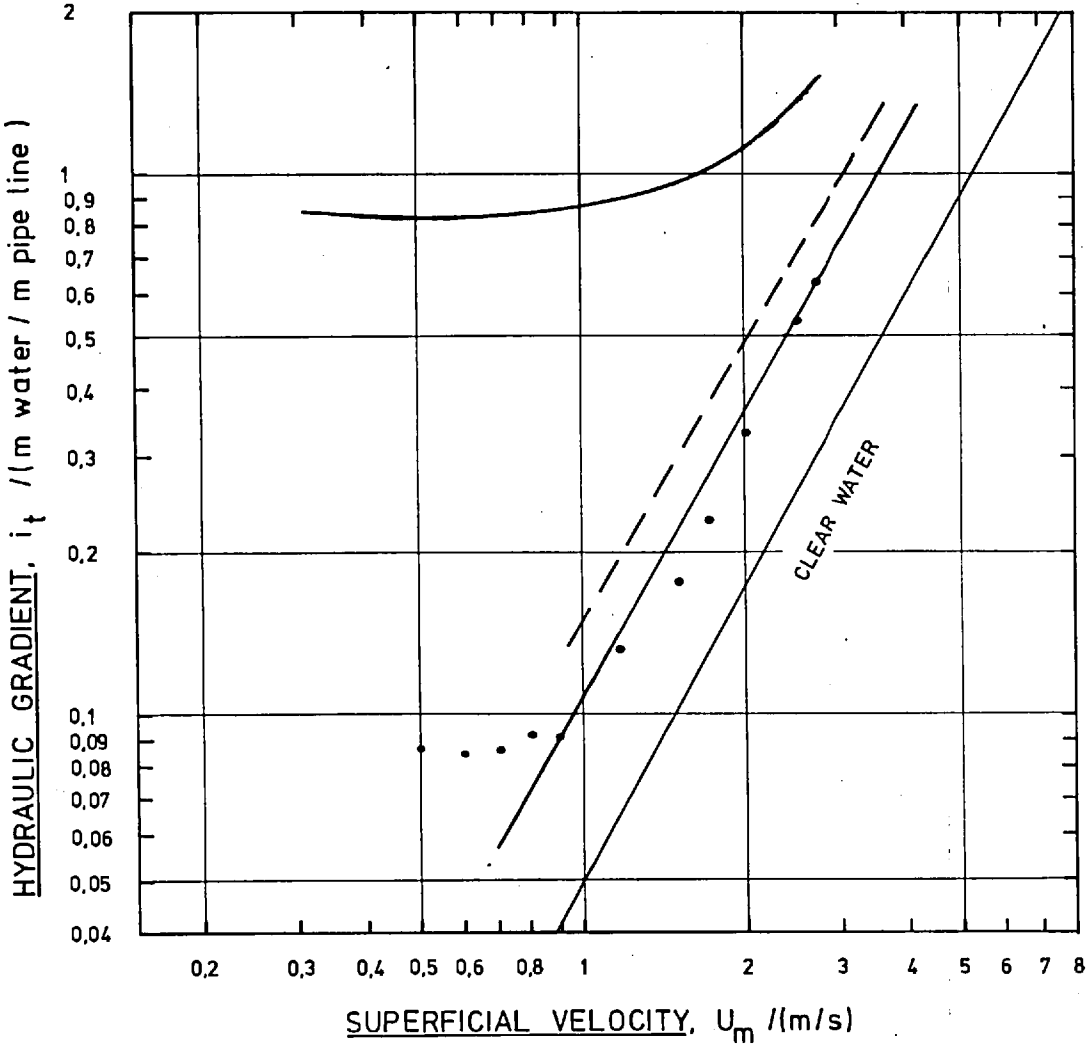


Figure 4.11

Predicted frictional loss (broken line) for iron-ore (S = 4.5) of the same diameter as the coarse sand

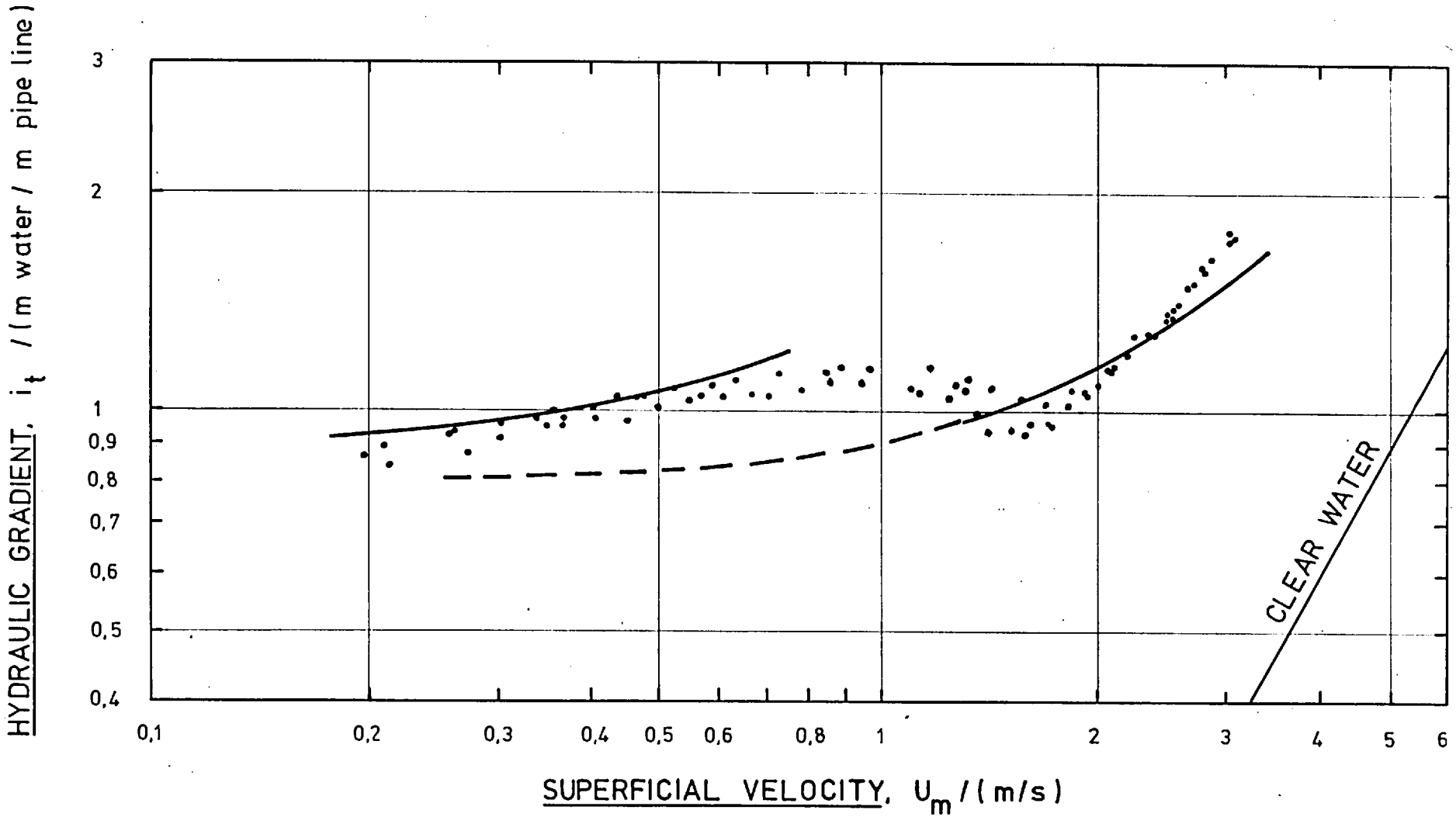


Figure 4.12

Predicted total loss overlaid on the experimental points for the fine sand

The broken line represents Equation 4.5

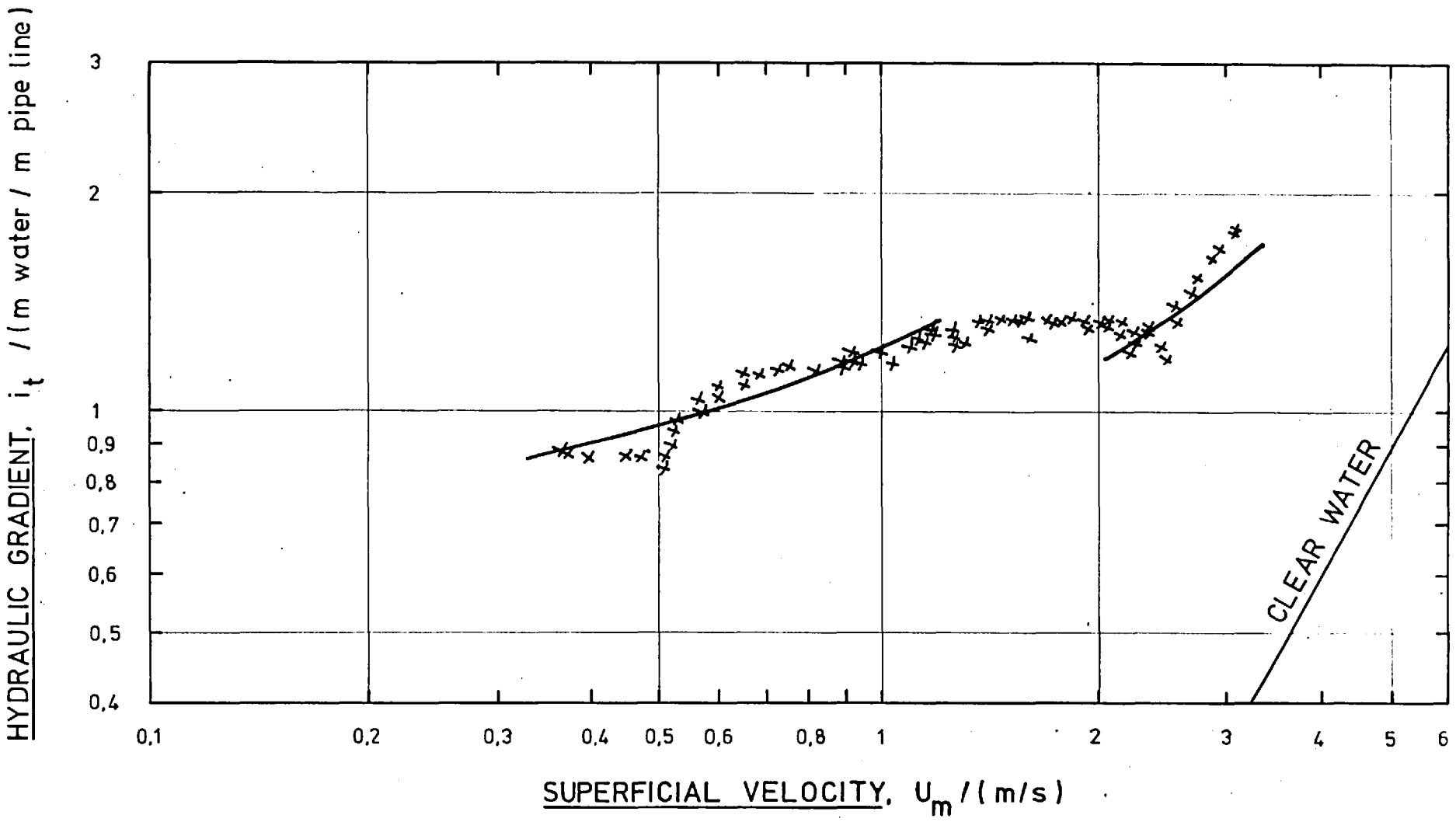


Figure 4.13

Predicted total loss overlaid on the experimental points for the medium sand

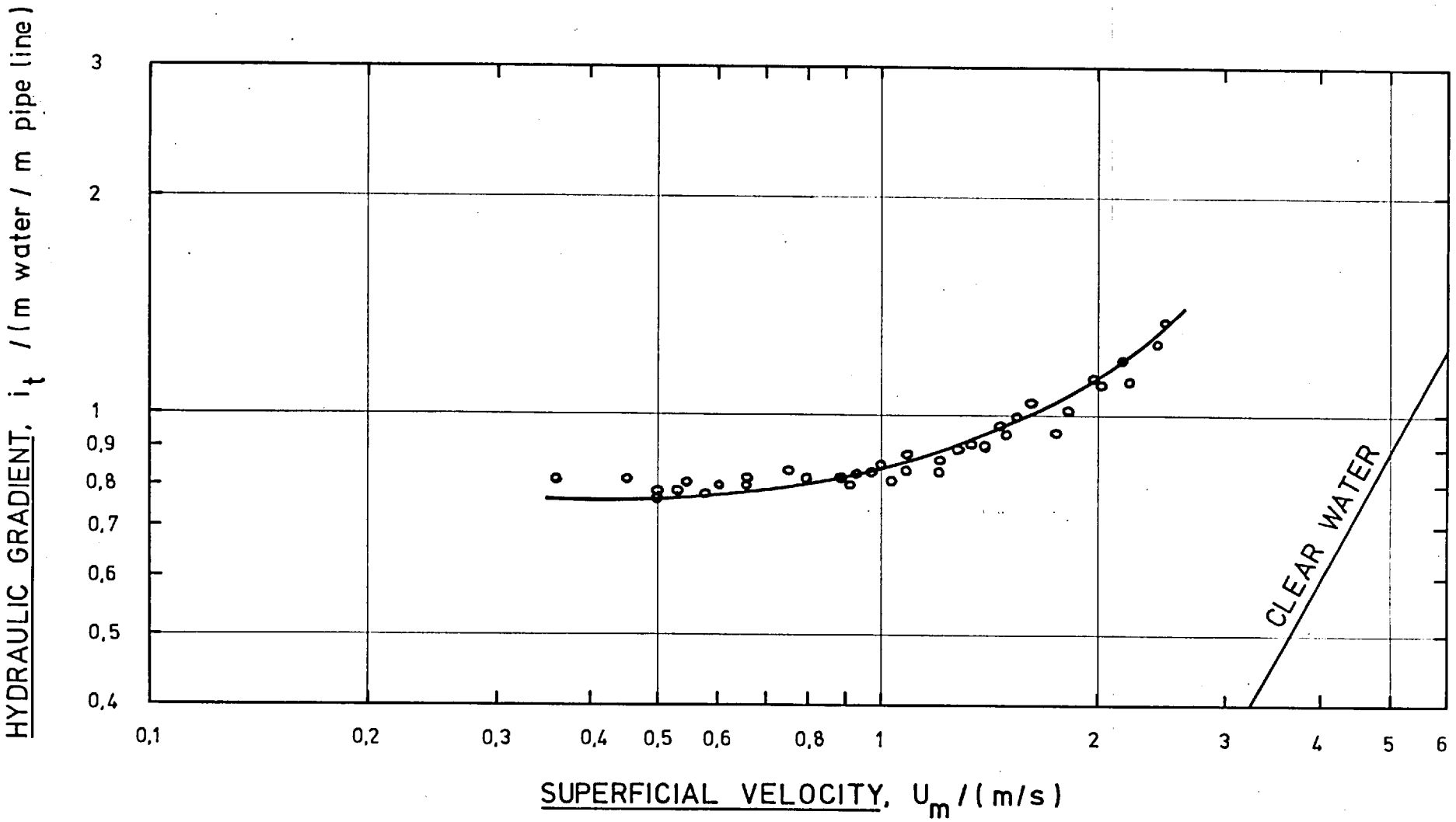


Figure 4.14

Predicted total loss overlaid on the experimental points for the coarse sand

5. CONCLUSIONS

5.1 Horizontal flow

The horizontal flow of high concentration sand-water slurries can be interpreted using a discrete two-layer flow model. At low velocities, typically below 1.5 m/s, when a bed of solids is evident in the pipe the flow can be analysed in terms of a gravity bed of solids moving *en bloc* in the pipe with a clear waterway above. As the velocity is increased, up to about 3 m/s, the bed of solids tends to shear, with the result that the bed dilates to virtually fill the entire cross-section of the pipe. In this high-shear-rate flow regime it appears that the mixture pressure loss for sand-density particles tends to approach the clear water losses multiplied by the mixture density. This may be fortuitous since the non-Newtonian behaviour brought about at the high solids concentration by particle-particle interaction, in addition to a bed-load contribution, is far more complex than a simple mixture density effect. For particles of a different density experimental work should be undertaken to verify or disprove this approach.

5.2 Rising vertical flow

The upward flow of high concentration slurries has been interpreted by using an axial flow model. This model postulates that in the vicinity of the pipe wall a particle-lean annulus will be created by the interaction of a Magnus type of lift force tending to drive the particles inward towards the pipe axis and a dispersive Bagnold type force. The rest of the flow area is filled by a high solids concentration core. Under the conditions of low slurry velocity, typically less than 1.0 m/s, and high solids concentration, approaching the freely settled value, it is believed that the core will extend to the pipe wall. This satisfactorily explains the very high frictional energy losses experienced under these flow conditions. At higher velocities the theory is based upon a Bagnold type of dispersive force which is prevalent under conditions of high shear rates in solid-fluid mixtures. The results suggest that the accepted approach of regarding the frictional mixture loss

as equivalent to a mixture density correction to the clear water line appear to be approximately correct for sand-density particles at higher velocities. However, this mixture density correction lacks theoretical justification and should not be applied to particles of other densities without prior experimental verification.

5.3 General conclusions

The use of mathematical models to interpret the flow of solid-fluid mixtures gives better insight into possible scale-up of small diameter pipe experiments than would otherwise be obtained by data correlation techniques. In solid-fluid flows at moderately high solids concentration the predominant energy dissipative mechanisms are manifested in solid - solid interactions. In horizontal flow the choice of the value of the particle boundary coefficient of friction is of prime importance. When the particles are closely sized this does not appear to be difficult. For wide size range materials, the selection of the coefficient of friction and assessment of the effect of particle suspension are difficult and thus the prediction of energy consumption is rather more complicated.

NOMENCLATURE

A	area normal to the velocity or cross-sectional area of pipe	L^2
A	constant	-
A_1	area of water-way in the two-layer analysis	L^2
A_2	area of bed in two-layer analysis	L^2
a	coefficient	-
B	constant	-
C	*in situ* or transport volumetric solids concentration = $V_p/(V_p + V_f)$	-
C_D	drag coefficient	-
C_b	solids concentration of bed assuming $u_r = 0$	-
C_d	delivered or input volumetric solids concentration	-
C_2	actual concentration in the bed of the stratified model	-
C_*	pack settled or maximum concentration of particles	-
c	local volumetric concentration of particles	-
D	internal diameter of pipe	L
$\underline{D}$	Rate of deformation tensor	LT^{-1}
De	equivalent diameter = 4A/wetted perimeter	L
d	particle diameter (mm)	L
F	force per unit volume of entire flow field	$ML^{-2}T^{-2}$
F_d	dispersive force on particles	$ML\ T^{-2}$

$(F_f)_p$	drag force on the fluid by the particles	$ML^{-2}T^{-2}$
$(F_f)_w$	drag force on the fluid by the wall	$ML^{-2}T^{-2}$
F_m	Magnus force on particle	$ML\ T^{-2}$
F_n	normal force	$ML\ T^{-2}$
$(F_p)_f$	drag force on the particles by the fluid	$ML^{-2}T^{-2}$
$(F_p)_w$	drag force on the particles by the wall	$ML^{-2}T^{-2}$
f	single-phase Fanning friction factor $= \tau_w/0.5\ \rho_f\ U_f^2$	-
$f_{1,2}$	interfacial friction factor used in the two-layer	-
g	acceleration due to gravity	LT^{-2}
I	intensity of gamma radiation	T^{-1}
$\underline{I}$	unit tensor	-
I_e	intensity of gamma radiation transmitted through an empty pipe	T^{-1}
I_f	intensity of gamma radiation transmitted water	T^{-1}
I_m	intensity of gamma radiation transmitted through a two phase mixture	T^{-1}
I_o	intensity of incident gamma radiation	T^{-1}
i	hydraulic pressure gradient expressed as $= \Delta P/\rho_f\ \Delta x$ (m water/m pipeline)	-
i_f	frictional manometric gradient	-
i_o	manometric gradient for clear water flowing in the pipe at U_m	-
i_t	total manometric gradient	-

K	constant	-
k	measure of pipe roughness, height of relatively uniform sized sand grains that would give the roughness effect experienced in pipe flow	L
L	length of pipe	L
L_v	volumetric liquid throughput	L^3T^{-1}
l	length	L
ln	natural logarithm to the base e	-
$\underline{M}$	stress tensor	$ML^{-1}T^{-2}$
n	exponent	-
P	pressure (m water)	$ML^{-1}T^{-2}$
r	radial co-ordinate	-
S	wetted pipe perimeter	L
S_v	volumetric solids throughput	L^3T^{-1}
S_1	wetted perimeter associated with upper layer	L
S_2	wetted perimeter associated with lower layer	L
$S_{1,2}$	length of interface in two layer model	L
t	time	T
U	superficial velocity = total volumetric discharge/flow area	LT^{-1}
U_f	superficial velocity of fluid	LT^{-1}
U_m	superficial velocity of two-phase mixture	LT^{-1}
U_p	superficial velocity of particles	LT^{-1}
U_1	superficial velocity of upper layer	LT^{-1}

U_2	superficial velocity of lower layer	LT^{-1}
u	local axial velocity	LT^{-1}
u_f	local fluid velocity	LT^{-1}
u_p	local particle velocity	LT^{-1}
u_r	relative or local slip velocity defined by Equation 3.36	LT^{-1}
u_*	shear velocity defined as = $((\tau_f)_w/\rho_f)^{0.5}$	LT^{-1}
$(u_f)_{d/2}$	local fluid velocity at distance y = d/2 from wall	LT^{-1}
$(u_f)_2$	local fluid velocity in lower layer	LT^{-1}
$(u_p)_2$	local particle velocity in lower layer	LT^{-1}
V	volume	L^3
W	mass	M
w	fall velocity of particle in an infinite medium	LT^{-1}
X	numerical value proportional to an electrical signal	-
x	thickness or depth of material	L
x_w	pipe wall thickness	L
y	distance from pipe wall measured radially	L
z	axial cylindrical co-ordinate; defined as being positive in the direction of bulk flow	-
β	half angle subtended by bed deposit defined by Figure 3.8	radian
Γ	circulation around an object	L^3T^{-1}
Δ	increment	-

δ	thickness of laminar sublayer	L
η	dynamic fluid viscosity	$ML^{-1}T^{-1}$
θ	angular co-ordinate	radian
κ	Von Karman constant ($\simeq$ 0.4)	-
μ	linear attenuation coefficient	L^{-1}
μ_f	linear attenuation coefficient of fluid	L^{-1}
μ_p	linear attenuation coefficient of particles	L^{-1}
μ_p	coefficient of sliding friction between a granular mass and a solid boundary	-
μ_w	linear attenuation coefficient of pipe wall material	L^{-1}
ν_f	kinematic viscosity of fluid	L^2T^{-1}
π	natural constant	-
ρ	density	ML^{-3}
ρ_f	fluid density	ML^{-3}
ρ_m	mixture density	ML^{-3}
ρ_p	average particle density	ML^{-3}
σ	normal stress	$ML^{-1}T^{-2}$
σ_p	normal stress due to particles	$ML^{-1}T^{-2}$
τ	shear or tangential stress	$ML^{-1}T^{-2}$
τ_f	fluid shear stress	$ML^{-1}T^{-2}$
$(\tau_f)_w$	fluid shear stress at the wall	$ML^{-1}T^{-2}$
$(\tau_f)_1$	fluid shear stress at wall in upper layer	$ML^{-1}T^{-2}$
$(\tau_f)_2$	fluid shear stress at wall in lower layer	$ML^{-1}T^{-2}$

τ_p	particulate shear stress	$ML^{-1}T^{-2}$
$(\tau_p)_w$	particulate shear stress at the wall	$ML^{-1}T^{-2}$
$(\bar{\tau}_p)_2$	average particulate shear stress in lower layer	$ML^{-1}T^{-2}$
τ_{p1}	*viscous* component of particle shear stress defined by Equation 4.7	$ML^{-1}T^{-2}$
τ_{p2}	*inertial* component of particle shear stress defined by Equation 4.7	$ML^{-1}T^{-2}$
$(\tau_t)_w$	total wall shear stress	$ML^{-1}T^{-2}$
$(\tau_t)_{d/2}$	total wall shear stress at distance y = d/2 from wall	$ML^{-1}T^{-2}$
$(\bar{\tau}_t)_2$	Average total shear stress at wall in lower layer	$ML^{-1}T^{-2}$
τ_1	wall shear stress associated with upper layer	$ML^{-1}T^{-2}$
τ_2	wall shear stress associated with lower layer	$ML^{-1}T^{-2}$
$\tau_{1,2}$	interfacial shear stress in stratified model	$ML^{-1}T^{-2}$
ϕ	angle of internal friction of a granular material	Degree
ϕ	dependent Durand variable	-
ψ	independent Durand variable	-

DIMENSIONLESS GROUPS

Re	Reynolds number the characteristic length is given in the text	
S	density ratio ρ_p/ρ_f	

SUBSCRIPTS

b	bed
d	delivered or input dispersive

e	empty pipe
f	fluid frictional
k	index
m	mixture
n	normal
p	particle
r	relative
t	total
v	volume
w	wall
o	incident initial
1	upper layer of two-layer model
2	lower layer of two-layer model
1,2	interface of two-layer model
-	signifies the quantity as a three-dimensional stress tensor (Section 3.5.4)

SUPERSCRIPTS

-	a bar above a quantity indicates an average value

The nomenclature given above has been used in the text, except in instances where an expression has been taken directly from a reference, in which case a full redefinition of the symbols used is given. As far as is possible symbols have been used to represent only one quantity, in instances where this is not the case the context should make the distinction clear.

REFERENCES

1. BABCOCK H.A. The sliding bed flow régime. First Int. Conf. on the Hydraul. Transp. of solids in pipes. BHRA Bedford Eng. paper H1, (1970)

2. BABCOCK H.A. Heterogeneous flow of heterogeneous solids. Advances in solid liquid flow in pipes and its application. Ed. by Zandi I, paper 8, p.125, (1971)

3. BAGNOLD R.A. Experiments on a gravity-free dispersion of large solid spheres in a Newtonian fluid under shear. Proc. R. Soc. A 225, p.49, (1954)

4. BAGNOLD R.A. The flow of cohensionless grains in fluids. Philos. Trans. R. Soc. A 249, p.235, (1956)

5. BAGNOLD R.A. The nature of saltation and of 'bed-load' transport in water. Proc. R. Soc. A 332, p.473, (1973)

6. BANTIN R.A. Hydraulic transportation of solids-water mixtures at high volumetric concentrations. PhD Thesis Univ. London (1972)

7. BHATTACHARYA A., & Roy A.N. Flow of solid-liquid suspension in vertical columns. Ind. & Eng. Chem. 47, p.268, (1955)

8. BOSLEY J., SCHOFIELD C., & SHOOK C.A. An experimental study of granule discharge from hoppers. Trans. Inst. Chem. Eng. 47, p.T147, (1969)

9. BUTTERFIELD R., & ANDRAWS K.Z. On the angles of friction between sand and plane surfaces. J. of Terramechanics 8(4) p.15, (1972)

10. CAIRNS R.C., & LAWTHER K.R. Studies of small particle suspensions for LMFR. Part 4. Concentration profiles across a bend and vertical pipe. Aust. At. Energy. Comm. Res. Establ. Lucas Heights AAEC/E37, (1958)

11. CALVERT S., & MILLER R.H. Flow of dense pastes in vertical tubes. Ind. & Eng. Chem. 50 , p.1793, (1958)

12. CARLTON A.J., & CHENG D.C-H. Design velocities for hydraulic conveying of settling suspensions. Third Int. Conf. on the Hydraul. Transp. of solids in pipes. BHRA Bedford Engl. paper E5, (1974)

13. CARLTON R.A., FRENCH R.J., JAMES J.G., BROAD B.A., & STREAT M. Hydraulic transport of large particles using conventional high concentration conveying. Fifth Int. Conf. on the Hydraul. Transp. of solids in pipes. BHRA Bedford Engl. paper D2, (1978)

14. CARSTENS M.R. A theory for heterogeneous flow of solids in pipes. Proc. of the ASCE. J. of the Hydraul. Div. 95, p.275, (Jan. 1969)

15. CHENG D.C-H. A design procedure for pipeline flow of non-newtonian dispersed systems. First Int. Conf. on the Hydraul. Transp. of solids in pipes. BHRA Bedford Engl. paper J5, (1970)

16. CHENG D.C-H. Application of the Warren Spring Laboratory pipeline design method to settling suspensions. Second Int. Conf. on the Hydraul. Transp. of solids in pipes. BHRA Bedford Engl. paper C3, (1972)

17. CLOETE F.L.D., MILLER A.I. & STREAT M. Dense phase flow of solids water mixtures through vertical pipes. Trans. Inst. Chem. Eng. 45, p.T392, (1967)

18. COULSON J.M., & RICHARDSON J.F. Chemical Engineering 2, Second Ed. Pergamon Press (1968)

19. CUMALIOĞLU I.M. An experimental study of the coefficient of friction between flooded granular particles and solid surfaces. M.Sc. Theses Univ. of London (1975)

20. DURAND R. Ecoulements de mixture en conduites verticales - influence de la densité des matériaux sur les caractéristiques de refoulement en conduite horizontale. La Houille Blanche. 8, p.124, (1953) (In French)

21. DURAND R., & CONDOLIOS E. The hydraulic transport of coal and solid materials in pipes. Proc. of a Colloq. on the Hydraul. Transp. of Coal. Nat. Coal Board London. Paper 4, (1952)

22. DURAND R., & CONDOLIOS E. Expperimental study of the transport of solids in pipes. Second Conf. Soc. Hydrotec. de France, Grenoble. (June 1952)

23. EILERS H. Die Viskosität von emulsionen hochviskoser stoffe als funktion der konzentration. Kolloid Zeitschritft 97, p.313, (1941) (In German)

24. EINSTEIN A. Eine neue Bestimmungder Molekül-dimensionen Ann. der Physik. 19, p.286, (1906) (In German)

Bewichtigung zumeiner Arbeit: Bestimmungder Molekül - dimensionen. Ann. der Physik 34, p.591, (1911) (In German)

25. EINSTEIN H.A. Loop system for measuring sand-water mixtures Proc. of the ASCE. J. of the Hydraul. Div. 92, p.1, (1966)

26. ENGELMAN H.E. Vertical hydraulic lifting of large solids - a contribution to marine mining. Offshore Technol. Conf. Texas (1978)

27. ERCOLANI D., & FERRINI F. Electric and thermic probes for measuring the limit deposit velocity. Sixth Int. Conf. on the Hydraul. Transp. of solids in pipes. BHRA Bedford Engl. paper A3, p.27, (1979)

28. FOWKES R.S. & WANCHECK G.A. Material handling research: hydraulic transport of coarse solids. U.S. Dep. of the Interi. Bur. of Mines Rep. 7283. (1963)

29. FRANCIS J.R.D. Experiments on the motion of solitary grains along the bed of a water stream. Proc. R. Soc. A 332, p.443, (1973)

30. GAESSLER H. Experimentelle und theoretische Untersuchungen über die Stromungsvorgänge beim Transport von Feststoffen in Flussigkeiten durch horzontal Rohrleitungen. PhD Thesis Technische Hochschule, Karsruhe, W.Ger. (1967) (In German)

31. GODDARD K., & RICHARDSON J.F. Correlation of data for minimum fluidising velocity and bed expansion in particulately fluidised systems. Chem. Eng. Sci. 24, p.363, (1969)

32. GOVIER G.W. & CHARLES M.E. The hydraulics of the pipeline flow of solid-liquid mixtures. Eng. J. 44, p.50, (Aug. 1961)

33. GRIMLEY A. The hydrodynamic behaviour of settling suspensions flowing in a horizontal circular pipeline. PhD Thesis Loughborough Univ. of Technol. (1973)

34. HAYDEN J.W., & STELSON T.E. Hydraulic conveyance of solids in pipes. Advances in solid-liquid flow in pipes and its applications. Ed. by Zandi I. paper 9, p.149, (1971)

35. HILL A. Hydraulic transport of solids-water mixtures at high volumetric concentrations MSc Thesis Univ. London (1973)

36. HISAMITSU N., SHOJI U., & KOSUGI S. Effect of added fine particles on flow properties of settling slurries. Fifth Int. Conf. on the Hydraul. Transp. of solids in pipes. BHRA Bedford Engl. paper D3, (1978)

37. HOLLAND J., MILES J.E.P., SCHOFIELD C., & SHOOK C.A. Fluid drag effects in the discharge of granules from hoppers. Trans. Inst. Chem. Eng. 47, p.T154, (1969)

38. HUBBELL J.H. Photon cross-section attenuation coefficients and energy absorption coefficients from 10 keV to 100 GeV. Nat. Stand. Ref. Data Syst. Nat. Bur. Stand. 29. Washington (1969)

39. JENIKE A.W. Quantitative design of mass-flow bias. Powder Technol. 1, p.237, (1967)

40. KAO T., & WOOD D.H. Incipient motion of solids in solid liquid transport system. Soc. of Min. Eng. AIME. 255, p.39, (1974)

41. KAZANSKIJ I., BRUHL H., & HINSCH J. Influence of added fine particles on the flow structure and pressure losses in sand-water mixtures. Third Int. Conf. on the Hydraul. Transp. of solids in pipes. BHRA Bedford Engl. paper D2, (1974)

42. KRUGER C.C. Hydraulic displacement of mud at No. 1 shaft Doornfontein Gold Mine. Hoisting Conf. South Afr. Inst. of Mech. Eng. Johannesburg. Paper 41, (1973)

43. KUHN M. Development for an improved system of vertical solids transportation. Sixth Int. Conf. on the Hydraul. Transp. of solids in pipes. BHRA Bedford Engl. paper F3, p.283, (1979)

44. LAUBSCHER B. A study of the hydro-lift feeder for introducing solids into a hydraulic hoisting installation. Hoisting Conf. South Afr. Inst. Mech. Eng. Johannesburg. Paper 38, (1973)

45. LEUNG L.S., WILES R.J., & NICHLIN D.J. Transition from fluidised to packed bed flow in vertical hydraulic conveying. Trans. Inst. Chem. Eng. 47, p.T271, (1969)

46. LUMLEY J.L. Two-phase and non-Newtonian flows. Turbulence Ed. by P. Bradshaw. Topics in applied physics 12, Springer Verlag (1976)

47. MILLER A.I. Hydrodynamic studies in solids liquid contacting. PhD Thesis Univ. London (1966)

48. NEWITT D.M., RICHARDSON J.F., ABBOTT M., & TURTLE R.B. Hydraulic conveying of solids in horizontal pipes. Trans. Inst. Chem. Eng. 33, p.93, (1955)

49. NEWITT D.N., RICHARDSON J.F. & GLIDDON B.J. Hydraulic conveying of solids in vertical pipes. Trans. Inst. Chem. Eng. 39, p.93, (1961)

50. NEWITT D.M., RICHARDSON J.F. & SHOOK C.A. Hydraulic conveying of solids in horizontal pipes. Part 2: Distribution of particles and slip velocities. Proc. of the Symp. on the interaction between fluids and particles. Inst. Chem. Eng. London p.87, (1962)

51. NIKURADSE J. Stroemungsgestze in rauhen Rohren. VDI Forschungsheft. 361, 4, (July/Aug. 1933) (In German)

52. OEDJOE D., BUCHANAN R.H. The pressure drop in the hydraulic lifting of dense slurries of large solids with wide size distribution. Trans. Inst. Chem. Eng. 44, p.T364, (1966)

53. PRANDTL L., & TIETJENS O.G. Applied hydro-and aeromechanics, Dover (1957)

54. PRZEWLOCI K., MICHALIK A., KORBLE K., & WOLSKI K. A radiometric device for the determination of solids concentration distribution in a pipe. Sixth Int. Conf. on the Hydraul. Trans. of solids in pipes. BHRA Cranfield Engl. paper B3, p.105, (1979)

55. RABINOWICZ E. Friction and wear of materials. John Wiley & Sons, New York (1965)

56. REYNOLDS O. On the dilatancy of media composed of rigid particles in contact. Philos. Mag. 5th Ser. 20, p.469, (1885)

57. ROSCOE K.H. The influence of strains in soil mechanics. Geotech 20(2), p.129, (1970)

58. ROSE H.E. & DUCKWORTH R.A. Transport of solid particles in liquids and gases. The Engineer 227, (5903) p.392; (5904) p.430; (5905) p.478, (1969)

59. ROUSE H. Ed. Advanced mechanics of fluids. Wiley (1959)

60. ROWE P.W. The stress-dilatancy relation for static equilibrium of an assembly of particles in contact. Proc. R. Soc. A 269, p.500, (1962)

61. SAKAMOTO M. Development of hydrohoists; slurry feeders without contamination. Third Int. Conf. on the Hydraul. Transp. of solids in pipes. BHRA Bedford Engl. paper A1, (1974)

62. SAKAMOTO M., UCHIDA K., & KAMINO Y. Vertical type hydrohoist for hydraulic transportation of fine slurry. Sixth Int. Conf. on the Hydraul. Transp. of solids in pipes. BHRA Bedford Engl. paper F1, p.257, (1969)

63. SAVAGE S.B. Gravity flow of cohesionless granular materials in chutes and channels. J. Fluid Mech. 92(1) p.53, (1979)

64. SCHRIEK W. Problem areas in the design of slurry pipelines. Canadian pipeline analysis control and design activity. Banff Alberta Can. (1973)

65. SINCLAIR C.G. The limit deposit-velocity of heterogeneous suspensions. Proc. of the Symp. on the interaction between fluids and particles. p.78, London, (1962)

66. SOO S.L., & REGALBUTO J.A. Concentration distribution in two-phase pipe flow. Can. J. of Chem. Eng. 38, p.160, (1960)

67. TAYLOR D.W. Fundamentals of soil mechanics. John Wiley & Sons

68. TELEVANTOS Y. The flow mechanism of hydraulic conveying at high solids concentration. PhD Thesis Univ. London, (1977)

69. TELEVANTOS Y., SHOOK C., CARLTON A., & STREAT M. Flow of slurries of coarse particles at high solids concentration. Can. J. of Chem. Eng. 57, p.255, (1979)

70. TENNUKES & LUMLEY. A first course in turbulence MIT (1972)

71. THOMAS A.D. Coarse particles in a heavy medium - turbulent pressure drop reduction and deposition under laminar flow. Fifth Int. Conf. on the Hydraul. Transp. of solids in pipes. BHRA Cranfield England. paper D5 (1978)

72. TSCHEBOTARIOFF G.P. Soil mechanics, foundations and earth structures. McGraw-Hill (1951)

73. VOCADLO J.J. Role of some parameters and effective variables in turbulent slurry flow. Fourth Int. Conf. on the Hydraul. Transp. of solids in pipes. BHRA Bedford Engl. D4, (1976)

74. WALLIS G.B. One-dimensional two-phase flow. McGraw-Hill, New York, (1969)

75. WASP E.J., REGAN T.J., WITHERS J., COOK P.A.C., & CLANCY J.T. Cross country coal pipeline: Hydraulics. Pipeline News. 35, p.20, (July 1963)

76. WASP J., KENNY J.P., & GANDHI R.L. Solid liquid flow slurry pipeline transportation. Trans. Technol. Publ. (1972)

77. WIEDENROTH W. A summary and comparison of known calculations of critical velocity of solids-water mixtures and some aspects of the optimisation of pipelines. Second Int. Conf. on the Hydraul. Transp. of solids in pipes BHRA Bedford Engl. paper E1, (1972)

78. WILSON K.C. Slip point of beds in solid-liquid pipeline flow. Proc. ASCE. J. of the Hydraul. Div. p.HY1, (1970)

79. WILSON K.C. Co-ordinates for the limit of deposition in pipeline flow. Third Int. Conf. on the Hydraul. Transp. of solids in pipes BHRA Bedford Engl. paper E1 (1974)

80. WILSON K.C. A unified physically based analysis of solid liquid pipeline flow. Fourth Int. Conf. on the Hydraul. Transp. of solids in pipes. BHRA Bedford Engl. paper A1, (1976)

81. WILSON K.C. Deposit-limit nomograms for particles of various densities in pipeline flow. Sixth Int. Conf. on the Hydraul. Transp. of solids in pipes. BHRA Bedford Engl. paper A1, (1979)

82. WILSON K.C., BROWN N.P., & STREAT M. Hydraulic hoisting at high concentration; a new study of friction mechanisms. Sixth Int. Conf. on the Hydraul. Transp. of solids in pipes BHRA Cranfield Engl. p.269, (1979)

83. WILSON K.C., STREAT M., & BANTIN R.A. Slip-model correlation of dense two-phase flow. Second Int. Conf. on the Hydraul. Transp. of solids in pipes. BHRA Bedford Engl. paper B1, (1972)

84. WILSON K.C., & WATT W.E. Influence of particle diameter on the turbulent support of solids in pipeflow. Third Int. Conf. on the Hydraul. Transp. of solids in pipes. BHRA Bedford Engl. paper D1, (1974)

85. WORSTER R.C. Hydraulic transport of solids. Coll. on the Hydraul. Transp. of Coal. Natl. Coal Board London. paper 1, (1952)

86. WORSTER R.C., & DENNY D.F. Hydraulic transport of solid material in pipes. Proc. Inst. Mech. Eng., 169, p.563, (1955)

87. YALIN M.S. Mechanics of sediment transport. Pergamon Press (1972)

88. ZANDI I. The hydraulic transport of bulky materials. Advances in solid-liquid flow in pipes and its application. Ed. by Zandi I., p.1, (1971)

89. ZANDI I., & GOVATOS G. Heterogeneous flow of solids in pipelines. Proc. of the ASCE. J. of the Hydraul. Div. 93, p.145, (1967)

90. ZISSELMAR R., & MOLERUS O. Investigation of solid-liquid pipe flow with regard to turbulence modification. Chem. Eng. J. 18, p.233, (1979)

APPENDICES

APPENDIX 1

A1 Physical properties of the sands

The physical properties of the three sands are presented in Table A1.1. The sands all originate from the gravel pits around the Leighton Buzzard area of England. Samples of the materials are shown in Figure A1.1, from which it can be seen that they are all naturally rounded.

A1.1 Particle size

A screen analysis for the three sands is shown in Figure A1.2. These curves are the result of three separate screenings performed with about 0.5 kg material loaded onto a set of 203 mm (8 in) diameter sieves. The three sands are all closely sized and the d_{50} diameter has been used throughout in the computations and text as being representative of the material.

A1.2 Particle density

The average particle density has been measured using the standard technique with a glass density bottle.

A1.3 Limiting volumetric solids concentration

It is convenient to know the maximum concentration by volume of the particles, often referred to as the pack settled concentration C_*. This is measured by taking a flooded sample of the sand and vibrating it until no further volume reduction occurs. For equal sized spheres this corresponds to rhombohedral packing where $C = 0.741$, for most natural granular materials this limit is seldom reached, and the value of $C = 0.62$ is more commonly the upper limit to packing.

The loosest arrangement of particles that can be obtained under static conditions is referred to as the freely settled concentration. This was measured by placing a few grammes of sand into a 0.5 m long 25 mm diameter graduated tube, filled with water and closed at one end. The tube containing the sand and water was stoppered and abruptly turned upside down to cause the grains to fall the length

of the tube and settle gently at the bottom. The value of the freely settled concentration found in this manner is close to that obtained for spheres in the most open square packing where the theoretical value of the concentration is 0.524.

A1.4 Fall velocity

The average fall velocity of the grains has been determined under conditions approximating infinite dilution. A small pinch of particles was introduced axially into a 80 mm diameter vertical tube containing still water. The slight spread in particle diameters caused terminal velocity segregation to occur in the sedimentation tube. When the particles had obtained steady motion the successive times for the front and tail-ends of the small cloud of particles to pass over a given distance was measured. It can be seen from the results that there is a spread of some 20% in the terminal velocity either side of the average value which was used in calculations.

A1.5 Angle of repose

The angle of internal friction exhibited by a granular mass is slightly dependent upon normal stress (57). Under conditions of low normal stress the angle of internal dynamic friction offered by a granular mass is very closely approximated by the angle of repose, ϕ exhibited by the material. This can be measured as the residual angle at which the face of a heap of material will stand after an avalanche of grains has been made to pass down the face. This is readily measured using the perspex box arrangement shown in Figure A1.3, the residual angle is measured with an engineering protractor to within 0.5 degree. It can be seen from the results in Table A1.1 that there is very little difference in the angle from around 30 degrees, whether the tests are performed dry of flooded.

A1.6 Coefficient of sliding friction

The effect of particle size upon the coefficient of dynamic sliding friction has been obtained from the experimental plot given by Rowe (45), the equation describing the line in the above Reference is given in this text by Equation 3.41.

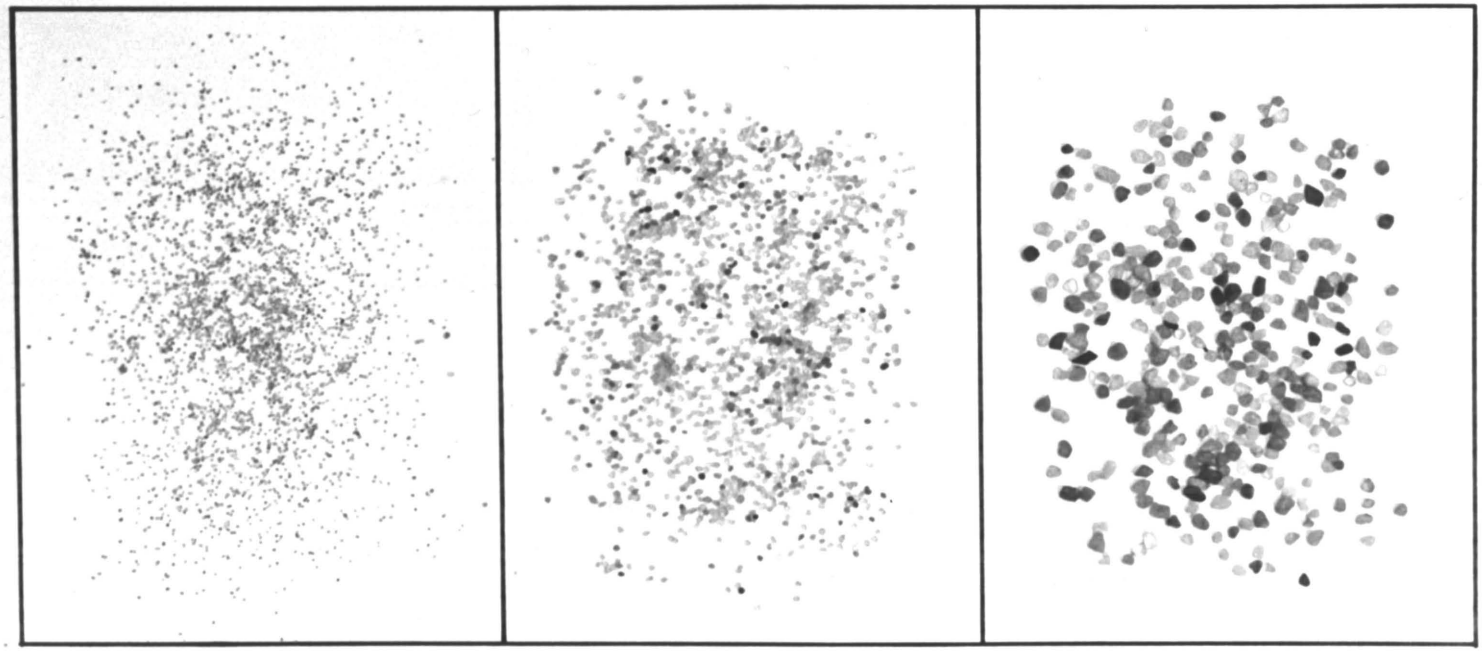


Figure A.1.1

Photograph of the three sands

reproduced actual size

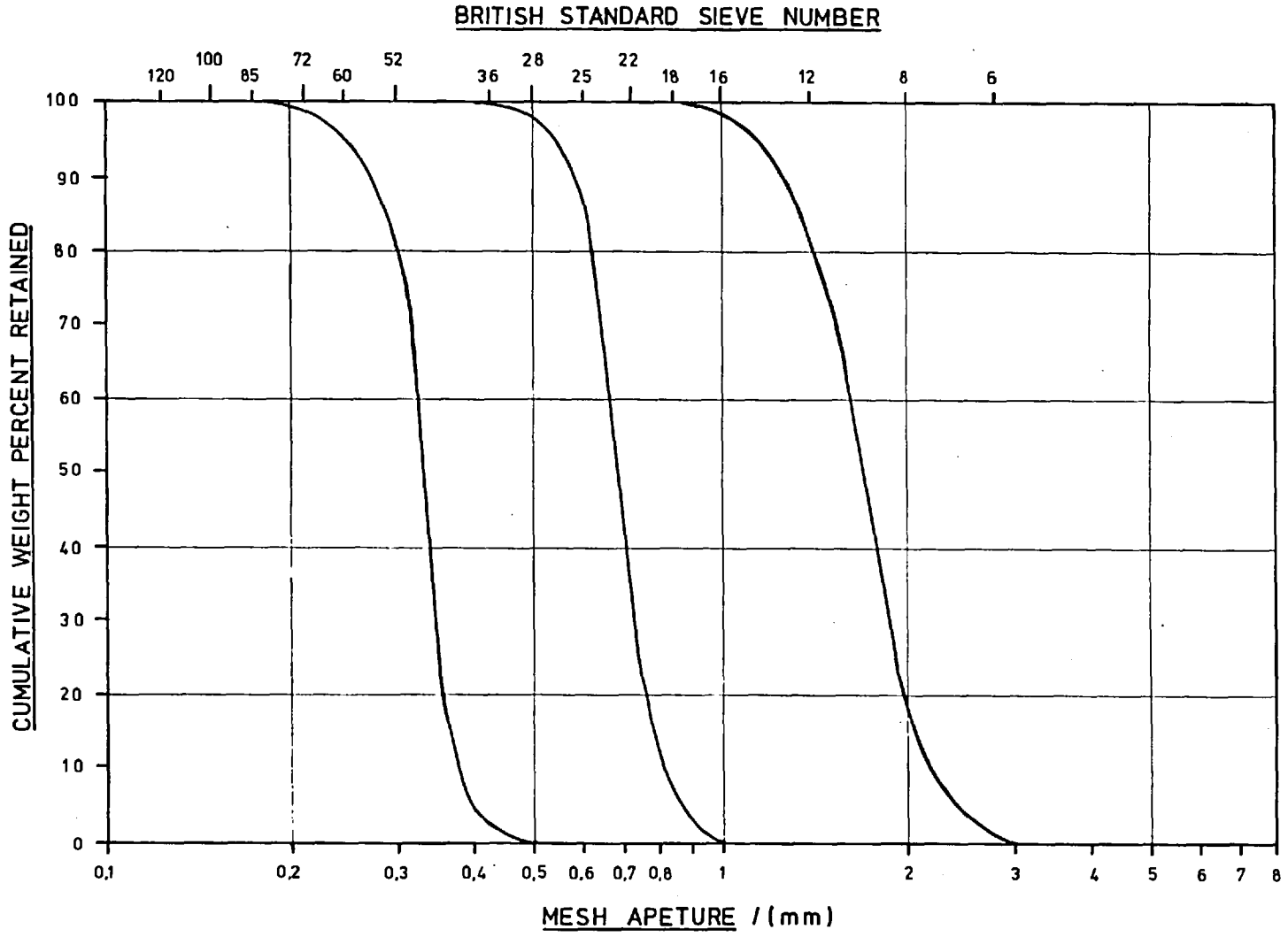


Figure A.1.2

Sieve analysis for the three sands

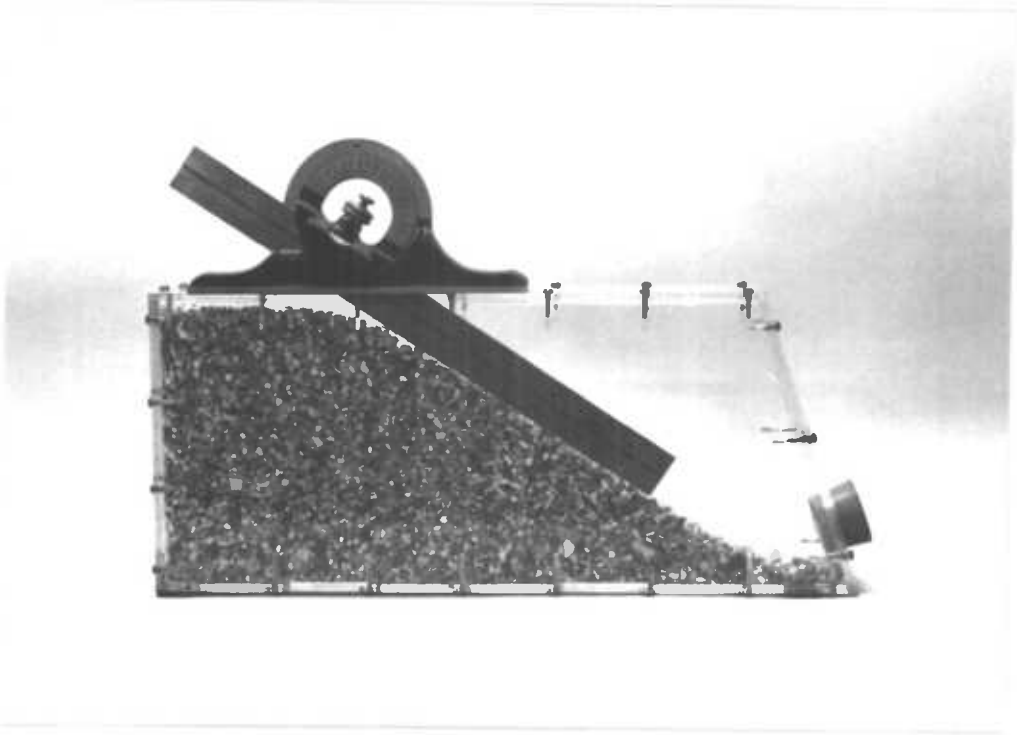


Figure A.1.3

Photograph of the apparatus used to measure the angle of repose

TABLE A1.1

P H Y S I C A L P R O P E R T I E S o f t h e S A N D S

SAND DESCRIPTION (BSS mesh number)	PARTICLE SIZE (/ 10^{-3} m)	PARTICLE DENSITY (/ ±0.003 10^3 kg/m^3)	SOLIDS CONCENTRATION (±0.005)		FALL VELOCITY (/ ±0.005 m/s)			ANGLE of REPOSE (/ ±0.5 Deg)		COEFFICIENT of SLIDING FRICTION (±0.02)
			PACK SETTLED	FREELY SETTLED	FRONT END	TAIL END	AVERAGE	DRY	FLOODED	
FINE (-36+60)	0.32	2.651	0.615	0.510	0.046	0.034	0.040	30.7	30.0	0.47
MEDIUM (-16+30)	0.68	2.647	0.632	0.533	0.108	0.066	0.087	30.5	30.3	0.43
COARSE (- 7+16)	1.7	2.654	0.618	0.512	0.2	0.135	0.168	31.8	30.9	0.39

(Density and viscosity of water at 20°C - ρ_f = 998.2 kg/m^3, μ_f = 1.002 x 10^{-3}kg/(ms))

APPENDIX 2

A2 Regression constants for the measuring devices

Table A2.1 contains the regression coefficients used in the experimental work; these are used in the calibration expressions developed in Chapter 2. The information necessary for the calibration of the density gauges can be obtained from Figures 2.10 and 2.11; noting for the horizontal device $I_e \simeq 84\ 700$, $I_f \simeq 53\ 700$ and for the vertical device $I_e \simeq 139\ 000$ and $I_f \simeq 90\ 400$.

TABLE A2.1

REGRESSION CONSTANTS OBTAINED FROM THE CALIBRATION OF THE MEASURING DEVICES

DEVICE (number)	REGRESSION CONSTANTS	
	A	B
PRESSURE TRANSDUCER		
(1)	-	0.912×10^{-3}
(2)	-	0.919×10^{-3}
(3)	-	0.130×10^{-2}
(4)	-	0.129×10^{-2}
LOAD CELLS	-105.2	0.142
FLOW METER	-	0.196×10^{-6}

The units of the regression constants are consistent with the equations of Chapter 2

EXPERIMENTAL RESULTS

LIST of TABLES

TABLE		PAGE
A3.1	Pressure-drop data for clear water	3
A3.2	Hydraulic data for the fine sand	4
A3.3	Frictional hydraulic data for the fine sand in rising vertical flow	7
A3.4	Hydraulic data for the medium sand	8
A3.5	Frictional hydraulic data for the medium sand in rising vertical flow	10
A3.6	Hydraulic data for the coarse sand	11
A3.7	Frictional hydraulic data for the coarse sand in rising vertical flow	13

ACCURACY of EXPERIMENTAL RESULTS

The values quoted for the accuracy of the experimental results have been obtained from a detailed consideration of the errors assosiated with the constituent measurements. The values are for typical mid-range results.

The measured manometric gradient is expected to have an accuracy better than 1%; in all cases the calibration lines fitted the experimental results with a regression coefficient of typically 0.998.

As mentioned in the text (Section 2.2.2.1) the values of *in situ* solids concentration are expected to have an accuracy better than 5%.

The accuracy of the delivered solids concentration is typically better than 2.5%.

The values of mean slurry velocity are expected to have an accuracy of better than 0.5%. The calibration of the flow-

meter over the experimental range of this variable was exceptionally good; the regression coefficient for the linear fit was better than 0.999.

TABLE A3.1

PRESSURE-DROP DATA for CLEAR WATER

FLUID VELOCITY /(m/s)	MANOMETRIC GRADIENT /(m water/ m pipeline)	
	HORIZONTAL	VERTICAL
4.02	0.604	0.650
3.24	0.404	0.432
2.88	0.324	0.346
2.45	0.237	0.252
2.07	0.178	0.189
1.89	0.150	0.160
1.62	0.107	0.119
1.4	0.091	0.093
1.21	0.061	0.070
0.98	0.046	0.052

TABLE A3.2

H Y D R A U L I C D A T A f o r t h e F I N E S A N D

SLURRY VELOCITY /(m/s)	MANOMETRIC GRADIENT /(m water/ m pipeline)		IN SITU SOLIDS CONCENTRATION -		DELIVERED SOLIDS CONCENTRATION -
	HORIZONTAL	VERTICAL	HORIZONTAL	VERTICAL	
3.06	1.43	1.70	0.492	0.502	0.467
3.05	1.40	1.70	0.484	0.499	0.469
3.04	1.40	1.72	0.485	0.506	0.469
2.87	1.32	1.60	0.487	0.500	0.466
2.80	1.28	1.53	0.484	0.511	0.467
2.79	1.29	1.54	0.485	0.503	0.463
2.71	1.24	1.48	0.486	0.495	0.462
2.66	1.23	1.46	0.480	0.504	0.468
2.57	1.17	1.38	0.477	0.498	0.466
2.54	1.19	1.37	0.484	0.502	0.467
2.53	1.15	1.32	0.478	0.498	0.462
2.51	1.14	1.35	0.481	0.496	0.470
2.50	1.14	1.33	0.485	0.500	0.468
2.37	1.12	1.26	0.477	0.510	0.464
2.35	1.09	1.26	0.477	0.498	0.463
2.23	1.09	1.25	0.481	0.506	0.472
2.20	1.06	1.17	0.484	0.503	0.465
2.10	1.03	1.12	0.478	0.499	0.467
2.10	1.03	1.13	0.477	0.495	0.467
2.09	1.04	1.12	0.472	0.494	0.466
2.01	1.01	1.07	0.488	0.504	0.466
1.92	0.899	1.03	0.471	0.502	0.468
1.92	0.972	1.04	0.482	0.489	0.463
1.84	0.951	1.05	0.472	0.499	0.466
1.83	0.987	0.996	0.477	0.500	0.466
1.73	0.933	0.971	0.476	0.492	0.461
1.72	0.958	0.943	0.467	0.495	0.460
1.69	0.966	1.00	0.478	0.454	0.466
1.68	0.956	0.953	0.470	0.492	0.465
1.58	0.938	0.908	0.473	0.492	0.471
1.57	0.956	1.01	0.475	0.460	0.472

TABLE A3.2

1.52	0.934	0.925	0.471	0.493	0.462
1.44	0.887	1.04	0.475	0.495	0.466
1.42	0.909	0.923	0.472	0.498	0.469
1.36	0.904	0.971	0.479	0.498	0.475
1.33	0.859	1.09	0.475	0.499	0.462
1.32	0.874	1.06	0.477	0.497	0.464
1.27	0.857	1.07	0.471	0.491	0.464
1.25	0.880	1.01	0.476	0.492	0.465
1.17	0.819	1.12	0.477	0.494	0.465
1.13	0.809	1.13	0.471	0.493	0.462
1.11	0.902	1.05	0.474	0.488	0.462
0.994	0.842	1.11	0.473	0.484	0.461
0.952	0.840	1.06	0.464	0.488	0.469
0.897	0.820	1.11	0.471	0.482	0.457
0.861	0.780	1.06	0.468	0.480	0.459
0.854	0.823	1.10	0.465	0.480	0.462
0.785	0.820	1.04	0.474	0.483	0.457
0.736	0.820	1.10	0.464	0.475	0.463
0.706	0.780	1.02	0.473	0.485	0.466
0.674	0.835	1.02	0.465	0.479	0.457
0.637	0.844	1.07	0.471	0.488	0.462
0.612	0.855	1.02	0.475	0.483	0.465
0.591	0.810	1.05	0.471	0.476	0.458
0.571	0.866	1.02	0.477	0.494	0.464
0.546	0.855	0.999	0.464	0.477	0.456
0.528	0.738	1.05	0.475	0.484	0.462
0.502	0.808	0.980	0.470	0.481	0.452
0.479	0.796	1.02	0.472	0.482	0.464
0.467	0.742	1.02	0.479	0.487	0.460
0.465	0.733	0.939	0.461	0.479	0.464
0.439	0.735	1.01	0.468	0.482	0.465
0.416	0.780	0.952	0.468	0.481	0.451
0.405	0.734	0.986	0.461	0.447	0.460
0.372	0.751	0.946	0.474	0.500	0.452
0.371	0,739	0.928	0.465	0.484	0.460
0.361	0.736	0.970	0.470	0.450	0.453
0.350	0.703	0.925	0.471	0.484	0.459
0.342	0.707	0.949	0.471	0.491	0.460

TABLE A3. 2

0.305	0.792	0.932	0.462	0.450	0.453
0.303	0.739	0.884	0.466	0.482	0.440
0.274	0.840	0.871	0.477	0.487	0.450
0.216	0.798	0.911	0.473	0.487	0.458
0.259	0.766	0.910	0.471	0.450	0.465
0.211	0.776	0.808	0.477	0.494	0.447
0.210	0.820	0.861	0.467	0.450	0.450
0.199	0.764	0.838	0.477	0.491	0.461

TABLE A3.3

FRICTIONAL HYDRAULIC DATA for the FINE SAND in RISING VERTICAL FLOW

SLURRY VELOCITY /(m/s)	MANOMETRIC GRADIENT /(m water / m pipeline)	SOLIDS CONCENTRATION -	MANOMETRIC GRADIENT due to SOLIDS /(m water / m pipeline)	FRICTIONAL MANOMETRIC GRADIENT /(m water / m pipeline)
3.0	1.68	0.502	0.831	0.849
2.7	1.50	0.501	0.829	0.671
2.4	1.30	0.501	0.829	0.471
2.2	1.20	0.501	0.829	0.371
2.0	1.10	0.500	0.827	0.273
1.8	1.02	0.499	0.826	0.194
1.7	0.99	0.498	0.824	0.166
1.6	0.96	0.498	0.824	0.136
1.5	0.96	0.497	0.822	0.138
1.4	0.99	0.496	0.821	0.169
1.2	1.09	0.492	0.814	0.276
1.0	1.10	0.487	0.806	0.294
0.8	1.10	0.482	0.797	0.302
0.6	1.06	0.481	0.796	0.264
0.5	1.03	0.481	0.796	0.234
0.4	0.97	0.483	0.799	0.171
0.3	0.92	0.486	0.804	0.116
0.25	0.9	0.489	0.809	0.091

The values of slurry velocity, manometric gradient and solids concentration were obtained from smoothing the experimental data.

TABLE A3.4

H Y D R A U L I C D A T A f o r t h e M E D I U M S A N D

SLURRY VELOCITY /(m/s)	MANOMETRIC GRADIENT /(m water/ m pipeline)		IN SITU SOLIDS CONCENTRATION -		DELIVERED SOLIDS CONCENTRATION -
	HORIZONTAL	VERTICAL	HORIZONTAL	VERTICAL	
3.09	1.53	1.78	0.491	0.512	0.461
3.07	1.48	1.74	0.495	0.509	0.470
2.93	1.42	1.65	0.490	0.498	0.470
2.86	1.39	1.61	0.496	0.494	0.468
2.71	1.31	1.50	0.487	0.497	0.468
2.64	1.28	1.45	0.483	0.501	0.466
2.57	1.19	1.32	0.486	0.500	0.465
2.54	.24	1.38	0.482	0.501	0.472
2.47	1.07	1.18	0.476	0.496	0.459
2.38	1.11	1.21	0.478	0.498	0.463
2.34	1.16	1.28	0.485	0.500	0.467
2.24	1.08	1.22	0.482	0.505	0.466
2.15	1.08	1.31	0.480	0.501	0.465
2.12	1.07	1.28	0.476	0.497	0.468
2.04	1.04	1.32	0.480	0.491	0.464
2.02	1.03	1.31	0.476	0.494	0.465
1.91	0.999	1.30	0.478	0.486	0.472
1.91	0.992	1.31	0.483	0.493	0.465
1.82	0.968	1.31	0.475	0.489	0.465
1.72	0.928	1.33	0.474	0.486	0.474
1.70	0.933	1.33	0.482	0.487	0.462
1.60	0.871	1.26	0.481	0.488	0.462
1.60	0.906	1.34	0.473	0.480	0.466
1.50	0.869	1.32	0.489	0.487	0.468
1.47	0.866	1.33	0.473	0.483	0.462
1.40	0.848	1.30	0.473	0.484	0.464
1.40	0.864	1.30	0.477	0.485	0.466
1.39	0.866	1.31	0.476	0.480	0.469
1.28	0.809	1.26	0.484	0.486	0.469
1.28	0.816	1.23	0.476	0.490	0.463
1.27	0.823	1.28	0.471	0.483	0.462

TABLE A3.4

1.27	0.805	1.25	0.476	0.484	0.466
1.18	0.881	1.26	0.479	0.479	0.462
1.14	0.800	1.25	0.471	0.481	0.467
1.13	0.794	1.25	0.481	0.485	0.473
1.11	0.786	1.21	0.475	0.487	0.462
1.04	0.758	1.16	0.472	0.483	0.459
1.00	0.770	1.20	0.479	0.488	0.477
0.940	0.761	1.17	0.476	0.490	0.464
0.919	0.768	1.18	0.474	0.489	0.462
0.916	0.767	1.20	0.478	0.489	0.462
0.808	0.744	1.13	0.484	0.489	0.464
0.752	0.735	1.14	0.480	0.491	0.462
0.724	0.736	1.23	0.486	0.496	0.465
0.684	0.729	1.10	0.480	0.491	0.458
0.649	0.723	1.08	0.476	0.490	0.475
0.642	0.726	1.08	0.472	0.492	0.466
0.603	0.729	1.06	0.482	0.498	0.475
0.573	0.721	0.988	0.474	0.485	0.462
0.572	0.715	1.04	0.489	0.496	0.464
0.527	0.727	0.969	0.486	0.499	0.467
0.525	0.716	0.866	0.480	0.485	0.456
0.519	0.731	0.870	0.483	0.491	0.471
0.469	0.715	0.884	0.485	0.492	0.464
0.456	0 716	0.865	0.481	0.485	0.463
0.401	0.719	0.888	0.492	0.500	0.480
0.375	0.730	0.879	0.490	0.500	0.479
0.375	0.732	0.873	0.483	0.490	0.469

TABLE A3.5

FRICTIONAL HYDRAULIC DATA for the MEDIUM SAND in RISING VERTICAL FLOW

SLURRY VELOCITY /(m/s)	MANOMETRIC GRADIENT /(m water / m pipeline)	SOLIDS CONCENTRATION -	MANOMETRIC GRADIENT due to SOLIDS /(m water / m pipeline)	FRICTIONAL MANOMETRIC GRADIENT /(m water / m pipeline)
0.4	0.88	0.495	0.819	0.061
0.5	0.96	0.494	0.817	0.142
0.6	1.04	0.493	0.816	0.224
0.7	1.10	0.492	0.814	0.286
0.8	1.15	0.491	0.812	0.338
1.0	1.24	0.486	0.804	0.436
1.2	1.30	0.483	0.799	0.501
1.4	1.32	0.483	0.799	0.521
1.6	1.35	0.485	0.803	0.547
1.8	1.34	0.489	0.809	0.531
2.0	1.30	0.493	0.816	0.484
2.2	1.24	0.498	0.827	0.393
2.3	1.22	0.500	0.827	0.392
2.4	1.25	0.500	0.827	0.423
2.5	1.30	0.500	0.827	0.473
2.7	1.46	0.497	0.822	0.636
3.0	1.70	0.495	0.819	0.985
3.1	1.80	0.494	0.817	0.985

The values of slurry velocity, manometric gradient and solids concentration were obtained from smoothing the experimental data.

TABLE A3.6

HYDRAULIC DATA for the COARSE SAND

SLURRY VELOCITY /(m/s)	MANOMETRIC GRADIENT /(m water/ m pipeline)		IN SITU SOLIDS CONCENTRATION -		DELIVERED SOLIDS CONCENTRATION -
	HORIZONTAL	VERTICAL	HORIZONTAL	VERTICAL	
2.64	1.10	1.35	0.420	0.476	0.418
2.48	1.10	1.35	0.421	0.467	0.408
2.26	0.948	1.16	0.422	0.467	0.412
2.20	0.99	1.43	0.426	0.475	0.429
2.08	0.925	1.14	0.421	0.474	0.419
2.01	0.965	1.16	0.425	0.472	0.426
1.84	0.840	1.06	0.415	0.463	0.426
1.78	0.753	0.912	0.426	0.446	0.417
1.65	0.845	1.07	0.418	0.468	0.417
1.62	0.784	0.985	0.412	0.461	0.414
1.58	0.817	1.03	0.418	0.468	0.410
1.52	0.800	1.01	0.425	0.470	0.424
0.989	0.671	0.848	0.410	0.437	0.403
1.37	0.759	0.948	0.421	0.469	0.417
1.43	0.754	0.947	0.419	0.464	0.415
1.32	0.754	0.928	0.419	0.468	0.409
1.24	0.733	0.898	0.420	0.463	0.409
1.24	0.726	0.861	0.412	0.448	0.424
1.12	0.727	0.876	0.417	0.458	0.412
1.12	0.738	0.909	0.418	0.464	0.426
1.06	0.675	0.857	0.408	0.446	0.408
1.02	0.720	0.880	0.415	0.455	0.417
0.989	0.671	0.848	0.410	0.437	0.403
0.946	0.715	0.864	0.416	0.451	0.408
0.910	0.677	0.830	0.414	0.443	0.402
0.813	0.704	0.847	0.412	0.451	0.413
0.760	0.712	0.870	0.423	0.458	0.426
0.670	0.700	0.846	0.425	0.458	0.419
0.668	0.701	0.855	0.424	0.457	0.421
0.612	0.670	0.829	0.426	0.446	0.417

TABLE A3.6

0.595	0.677	0.813	0.424	0.441	0.415
0.554	0.699	0.846	0.425	0.458	0.415
0.540	0.669	0.818	0.428	0.444	0.418
0.503	0.673	0.824	0.421	0.451	0.412
0.457	0.712	0.849	0.444	0.461	0.418
0.386	0.737	0.856	0.447	0.471	0.433

TABLE A3.7

FRICTIONAL HYDRAULIC DATA for the COARSE SAND in RISING VERTICAL FLOW

SLURRY VELOCITY /(m/s)	MANOMETRIC GRADIENT /(m water / m pipeline)	SOLIDS CONCENTRATION -	MANOMETRIC GRADIENT due to SOLIDS /(m water / m pipeline)	FRICTIONAL MANOMETRIC GRADIENT /(m water / m pipeline)
2.7	1.45	0.475	0.786	0.664
2.5	1.32	0.474	0.784	0.536
2.0	1.10	0.468	0.774	0.326
1.7	1.00	0.465	0.769	0.231
1.5	0.94	0.462	0.764	0.176
1.0	0.85	0.454	0.751	0.099
0.9	0.84	0.453	0.749	0.091
0.8	0.84	0.452	0.748	0.092
0.7	0.83	0.450	0.744	0.086
0.6	0.83	0.450	0.744	0.086
0.5	0.83	0.449	0.743	0.087

The values of slurry velocity, manometric gradient and solids concentration were obtained from smoothing the experimental data.